Department of Chemistry
Faculty of Science
University of Helsinki
Finland

Selective Miniaturized Sampling Systems for Nitrogen-Containing Compounds in Air

Eka Dian Pusfitasari

ACADEMIC DISSERTATION

To be presented for public examination with the permission of the Faculty of Science of the University of Helsinki, in Chemicum Auditorium A129, Department of Chemistry, on the 7th of July, 2023, at 12 o'clock

Helsinki 2023

ISBN (softcover): 978-951-51-9353-7

ISBN (PDF): 978-951-51-9354-4

http://ethesis.helsinki.fi

Publisher: University of Helsinki 2023

Supervisors

Professor Marja-Liisa Riekkola
Department of Chemistry
University of Helsinki
Finland

Docent Kari Hartonen
Department of Chemistry
University of Helsinki
Finland

Reviewers

Professor Jyrki Mäkelä
Faculty of Engineering and Natural Sciences
Tampere University
Finland

Docent Heidi Hellén
Finnish Meteorological Institute
Finland

Opponent

Associate Professor Marianne Glasius
Department of Chemistry
Aarhus University
Denmark

Abstract

A wide variety of nitrogen-containing compounds present in the air can contribute to air pollution, which in turn affects both human health and the climate. In this thesis, the applicability of two miniaturized air sampling techniques, solid-phase microextraction (SPME) Arrow and in-tube extraction (ITEX) was studied, for the selective collection of nitrogen-containing compounds in air samples. Different types of sorbent materials, including Mobil Composition of Matter No. 41 (MCM-41), titanium hydrogen phosphate-modified MCM-41 (MCM-41-TP), and zinc oxide-modified mesoporous silica microspheres, were used as sorbent materials in the ITEX sampling system. The adsorption and desorption behavior of gaseous nitrogen-containing compounds in passive SPME-Arrow and active ITEX sampling systems, coated and packed with different sorbent materials, was investigated. In addition, saturation vapor pressures of atmospheric trace gases were experimentally and theoretically estimated. The sampling systems with selected sorbent materials were applied to the determination of nitrogen-containing compounds in boreal forest SMEAR II station, indoor air, and cigarette smoke.

Adsorbent and adsorbate properties, such as hydrophobicity and basicity, were the major factors that affected sorbent selectivity towards nitrogen-containing compounds. Moreover, the pore volume and pore sizes of the sorbents were essential parameters for the adsorption performance, especially in the SPME Arrow system. The ITEX packing and the SPME Arrow coatings were reproducible and reusable. Due to the active sampling principle, the ITEX sampler with higher adsorption and desorption rates provided better results for the analysis, especially when quick injection was needed in gas chromatography. The selectivity of the ITEX sampling system was increased with the trap accessory, but further study is needed to prevent the loss of the targeted compounds. Whereas the ITEX's filter accessory was successfully employed to remove particles, enabling ITEX to collect only gas-phase samples. Vapor pressure results were achieved by laboratory experiments (by retention index approach) and by the COSMO-RS model.

An aerial drone was successfully employed as a platform to study vertical profiles of VOCs at high altitudes, from 50 to 400 m, for miniaturized SPME Arrow and ITEX atmospheric air sampling systems, along with portable devices for the real-time measurement of black carbon (BC) and total particle numbers. There was a clear distribution of the nitrogen-containing compounds collected at different altitudes at SMEAR II station, Finland, depending on their sources. In addition, other VOCs demonstrated the same trend.

Preface

This thesis is based on research carried out at the Department of Chemistry, University of Helsinki, from 2020 to 2023. The field campaigns were conducted at the Station for Measuring Ecosystem-Atmosphere Relations (SMEAR) II station in Hyytiälä, Finland. Funding for the work was provided by the Jane and Aatos Erkko Foundation and the Academy of Finland (the Atmosphere and Climate Competence Center "ACCC Flagship", Grant No. 337549). The Doctoral Program in Atmospheric Sciences (ATM-DP) is acknowledged for the travel and thesis completion grants. In addition, I thank the Orion Research Foundation for the young researcher grant in 2021.

First, I would like to express my deepest gratitude to my supervisor, Professor Marja-Liisa Riekkola, for providing me the opportunity to work under her supervision, which marked the beginning of my career in atmospheric sciences. Twice having surgery while doing my studies and during the COVID pandemic was a difficult moment. But I have been lucky to have a supervisor who always cares, not only about work but also about my health. Thank you very much for believing in me and patiently guiding me to learn from the very basics to become a young professional scientist. You not only taught me science, but also how to develop research, be an independent scientist, collaborate with other researchers, and enhance my writing skills. I will always be grateful for your strong support, insightful advice, and mentorship throughout my studies.

My warm gratitude is also addressed to my supervisor, Dr. Kari Hartonen, for his unwavering support during my studies. Having discussions with you was incredibly inspiring and always led me in the right direction. Your expertise in mass spectrometry and atmospheric sciences has always enlightened me and provided me with an exceptional learning experience. You also always generated outstanding ideas so that I could learn. Thank you also for your patience, especially when noticing the typos I made in the articles. It taught me to be more careful and continuously helped to improve the manuscript.

My sincere thanks are also delivered to my co-supervisor, Dr. Jose Ruiz-Jimenez, for his great encouragement and help throughout my studies. Your outstanding knowledge of chromatography and chemometrics is remarkable. I'm very grateful for the data discussion meeting, where you provided me with valuable guidance and feedback that helped me do data analysis and finish my research work on time. You always expressed a genuine interest in my work and motivated me to continue once I felt down. You also always pointed out that health is the most important of all. Your love and dedication to your family in Spain were also inspiring, reminding me of my family in Indonesia and teaching me to balance loving science with enjoying life.

I would like to extend my sincere gratitude to all my co-authors who contributed to my work. I am especially thankful to Professor Torgny Fornstedt and Dr. Jörgen Samuelsson from Karlstad University for their expert advice and for helping me work on the kinetics research. Dr. Jan-Henrik Smått and Saara Sirkiä from Åbo Akademi University are also acknowledged for their solid collaboration on the synthesis of new selective material presented in this thesis. I thanked Professor Tuukka Petäjä, Dr. Juha Kangasluoma, Jesse Haataja, and Yusheng Wu for making me learn more deeply about a condensation particle counter (CPC) for the first time. Dr. Krista Luoma and Tapio Elomaa are acknowledged for the fruitful discussion regarding black carbon data. Vitus Basel is thanked for his cooperation on vapor pressure research. Cristina Youngren is acknowledged for her friendship and for working together in the analytical chemistry laboratory.

Words cannot describe how I am indebted to Lic. Phil. Matti Jussila for the success of this thesis. Your extraordinary intelligence in building up new automated systems, such as the electronic controller used in the drone, the GC autosampler, the thermal desorption unit used for experiments both in the lab and for the field campaign, and many others, are very important parts of this thesis work. Your "magic touch" in repairing all the analytical instruments is also outstanding. In addition to that, your patience, great support, and kindness are always admirable.

I'm very grateful that I had the opportunity to be in the same laboratory with Karina Moslova, although only at the beginning of my doctoral studies. You were not only helping me with lab-related matters, but also continuously taught me how to maintain my good health, how to say "no", how to balance work and life, and always made me believe that I could finish my doctoral thesis in time, even when I felt it was impossible to.

To my un-biological Thai sister, Dr. Thanaporn Liangsupree, I thank you very much for always being there for me. I am very grateful to receive your bunch of love and support. Not only in scientific matters but also in life. Living far away from family did not make me feel so, for instance, when I was so scared before having my first ear surgery in 2020. You always tried to make me comfortable, sent me my favorite foods, and accompanied me. Your kindness as a human being is very inspiring.

I also wish to extend my sincere thanks to Professor Susanne Wiedmer for her kindness and support, especially when finishing this thesis. To Dr. Norbert Maier, thank you for our frequent discussions that helped to improve my research work. Arina Sukhova is warmly acknowledged for her massive help with lab-related matters and friendship. I always enjoyed it when we shared stories, especially about baby cheeks. I would also like to thank Vicky Fu for not only her scientific support but also the recreational activities we have done together. I am very glad that we shared the same office for 14 months. Eleanor Ash is also acknowledged for always cheering me up and helping to proofread part of this thesis. I thanked Dr. Evgen Multia not only for the friendship but also for letting me get points when playing badminton. Dr. Hangzhen Lan is thanked for helping me get started with the

research so that I could easily follow his path. I also thank other present and former staff members of the analytical chemistry laboratory for creating an enjoyable working atmosphere. To VERIFIN lab members, *e.g.*, Professor Paula Vanninen, Dr. Matti Kjellberg, Matti Kuula, Harri Kiljunen, Professor Anne Puustinen, and Dr. Karoliina Joutsiniemi, thank you for always supporting me in improving my capabilities in analytical chemistry. To Marja-Leena Kuitunen, thank you for the friendship and the great time we spent together since I was a trainee. I thank Professor Gary Eiceman for sharing knowledge regarding ion mobility spectrometry.

I would like to thank my Indonesian and Malaysian friends in Finland, Eka Kauppinen, Fitriyah, Tauran, Dr. Margaretta Christita, Fitri, Dr. Keni, Dr. Satia Zen, and Nurhazlina Hamzah, for the discussion, entertainment, and Indonesian foods. Dr. Sofna Banjarnahor and my niece Milva, thank you for always motivating me with a lot of positivity and being my health and wellness counselors. The National Research and Innovation Agency of Indonesia (BRIN) is thanked for its support. Dr. Wuri Wuryani, the late Dr. M. Sokolowski, and Mr. Setyabudhi Zuber are warmly acknowledged as my forever Indonesian supervisors who inspire and encourage me to create and pursue my dreams.

I would like to thank Professor Jyrki Mäkelä and Dr. Heidi Hellén for the time spent reading and improving this thesis as pre-examiners. Marina Kurtén is thanked for proofreading this thesis. I would also like to thank Associate Professor Marianne Glasius for being my thesis opponent.

My special thanks go to my family, especially my grandparents, for all the genuine support throughout my life that cannot be described in words.

Above all, my heartfelt and utmost appreciation is to my mother and brother Dani Pratama Putra to whom I wish to dedicate this doctoral dissertation. You always let me make my own choices and support me in whatever I want to attempt. Your endless support, unconditional love, and prayers during the day and night strengthen me to pursue all these dreams. These make impossible things possible.

Helsinki, June 2023

Eka Dian Pusfitasari

Table of Contents

List of original publications

This doctoral dissertation is based on the following publications referred to in this thesis by their Roman numerals [I-IV]:

I. **Pusfitasari, E.D.**, Ruiz-Jimenez, J., Heiskanen, I., Jussila, M., Hartonen, K., Riekkola, M.-L. (2022). Aerial drone furnished with miniaturized versatile air sampling systems for selective collection of nitrogen-containing compounds in boreal forest. **Science of the Total Environment**, 808 (11), 152011. https://doi.org/10.1016/j.scitotenv.2021.152011.

II. **Pusfitasari, E.D.**, Ruiz-Jimenez, J., Tiusanen, A., Suuronen M., Haataja, J., Wu, Y., Kangasluoma, J., Luoma, K., Petäjä, T., Jussila, M., Hartonen, K., Riekkola, M.-L. (2023). Vertical profiles of volatile organic compounds and fine particles in atmospheric air by using aerial drone with miniaturized samplers and portable devices. **Atmospheric Chemistry and Physics**, 23 (10), p. 5885-5904. https://doi.org/10.5194/acp-23-5885-2023.

III. **Pusfitasari, E.D.**, Youngren, C., Ruiz-Jimenez, J., Sirkiä, S., Smatt, J-H., Hartonen, K., Riekkola, M.-L. (2023). Selective and efficient sampling of nitrogen-containing compounds from air by in-tube extraction devices packed with zinc oxide-modified mesoporous silica microspheres. **Journal of Chromatography Open**, 3, 100081. https://doi.org/10.1016/j.jcoa.2023.100081.

IV. **Pusfitasari, E.D.**, Ruiz-Jimenez, J., Samuelsson, J., Besel, V., Fornstedt, T., Hartonen, K., Riekkola, M.-L. (2023). Assessment of physicochemical properties of sorbent materials in passive and active sampling systems towards gaseous nitrogen-containing compounds. **Journal of Chromatography A**, 1703, 464119. https://doi.org/10.1016/j.chroma.2023.464119.

The contribution of the author:

The author carried out experimental works related to the testing of microextraction devices, validation, sample collection, sample preparation, chromatography, mass spectrometry, and data collection **(*Papers I-IV*)**. The responsibility of data analysis included chromatography peaks deconvolution, alignments, and compound identification and integration to obtain analytical features **(*Paper I, II, IV*)**. The author also prepared the packing materials for ITEX and the coatings for SPME Arrow devices for microextraction devices testing, optimization, validation, and air sampling **(*Paper I-IV*)**. She had the main responsibility for writing the manuscripts **(*Papers I, II, IV*)**, and part of the manuscript in ***Paper III***.

List of abbreviations

AAS	Active air sampling
ACN	Acetonitrile
ADAP	Automated data analysis pipeline
BC	Black carbon
BrC	Brown carbon
CCS	Carbon capture and storage
CF-SPME	Cold fiber solid-phase microextraction
CO	Carbon monoxide
COSMO-RS	The COnductor-like Screening MOdel for Real Solvent
CO_2	Carbon dioxide
CPC	Condensation particle counter
CWR	Carbon wide range
DCM	Dichloromethane
DI	Direct immersion
DPA	Dipropylamine
DVB	Divinyl benzene
EDS	Energy dispersive spectra
EI	Electron ionization
ESI	Electrospray ionization
FA	Formic acid
GC	Gas chromatography
HA	Hexanamine or hexylamine
He	Helium
HPLC	High performance liquid chromatography
HILIC	Hydrophilic interaction liquid chromatography
HS	Headspace
IBA	Isobutylamine
i.d.	Internal diameter
ITEX	In-tube extraction
IT-SPME	In-tube solid-phase microextraction
LDA	Linear discriminant analysis
LLE	Liquid-liquid extraction
LPME	Liquid-phase microextraction
MAS	Miniaturized air sampling
MCM-41	Mobil Composition of Matter No. 41
MCM-41-TP	Titanium hydrogen phosphate-modified MCM-41
MSD	Mass spectrometry detector
MS/MS	Tandem mass spectrometry
NO	Nitrogen monoxide
NO_2	Nitrogen dioxide
NTD	Needle trap device

NTME	Needle trap microextraction
Pa	Pascal
PAN	Polyacrylonitrile
PDMS	Polydimethylsiloxane
PFO	Pseudo-first-order
PLSR	Partial least squares regression
PM	Particulate matter
PS	Passive sampling
PTFE	Polytetrafluoroethylene
SMEAR	Station for measuring ecosystem-atmosphere relations
SOA	Secondary organic aerosol
SPDE	Solid-phase dynamic extraction
SPE	Solid-phase extraction
SPME	Solid-phase microextraction
TEA	Triethylamine
TEM	Transmission electron microscopy
TF-SPME	Thin-film solid-phase microextraction
THF	Tetrahydrofuran
T.P.	Temperature program
US-EPA	United States Environmental Protection Agency
VOC	Volatile organic compounds
XRD	X-ray diffractometer
ZnO	Zinc Oxide

List of symbols

a	Initial adsorption rate (area·s^{-1})
C_o	Initial concentration of analytes in the sample (M)
C_e^{∞}	Equilibrium concentration of analytes in sorbent coating (M)
C_f^{∞}	Equilibrium concentration of analytes in the liquid polymer fiber coating (M)
C_{fA}^{∞}	Equilibrium concentration of analyte A (M)
C_{fB}^{∞}	Equilibrium concentration of analyte B (M)
$C_{f\,max}$	Maximum concentration of active sites on the coating (M)
C_h^{∞}	Equilibrium concentration of analytes in the headspace (M)
C_s^{∞}	Equilibrium concentration of analytes in the sample (M)
I_x	Retention index
K	Analyte's adsorption equilibrium (affinity) constant
K_A	Adsorption equilibrium constant of analyte A
K_B	Adsorption equilibrium constant of analyte B
k_d	Rate constant (s^{-1})
K_{es}	Distribution constant of the analytes between the SPME sorbent coating and the sample matrix
K_{fh}	Distribution constant of the analytes between the SPME fiber coating and the sample headspace
K_{fs}	Distribution constant of the analytes between the SPME fiber coating and the sample matrix
K_{hs}	Distribution constant of the analytes between the sample matrix and the sample headspace
n	Mass amount of analytes extracted by the SPME coating at equilibrium (ng)
p	Vapor pressure of analyte (mmHg)
p_0	Normal pressure (mmHg)
p_z	Vapor pressure of n-alkane eluting before the analyte (mmHg)
p_{z+1}	Vapor pressure of n-alkane eluting after the analyte (mmHg)
q	The amount of analytes adsorbed by the adsorbent
T	Temperature (^{0}C)
t	Adsorption /or desorption time (min)
V_e	Volumes of the sorbent coating (µL)
V_f	Volume of liquid polymer fiber coating (µL)
V_h	Volume of the headspace (mL)
V_s	Volumes of the sample (mL)

1. Introduction

Research on atmospheric organic compounds has grown in recent decades due to their impact on the environment and human health. These compounds can serve as a source of secondary organic aerosol that in turn, as an example, can contribute to the production of fine aerosol particulate matter, like PM 10 and PM 2.5, which pollutes the environment [1–5]. Nitrogen-containing compounds are important components of organic aerosols that can lead to the formation of air pollution. It is very challenging to determine them due to their high volatility, high polarity, and low concentrations in mixtures. Although many air sampling techniques have been recently developed [6], many nitrogen-containing compounds still need new, especially selective sampling techniques for their reliable analysis from complex sample mixtures to provide better understanding of their distribution in the environment, to clarify their effect on air quality and human health, and their specific role in the atmosphere.

Selecting appropriate sampling techniques with selective sorbent/coating materials is a crucial step before performing the analysis. They should be functional under different atmospheric conditions (humidity, temperature, wind speed, ozone) and for compounds with different physicochemical properties. The mass transfer of nitrogen-containing compounds from air to the sorbents of sampling devices, and then from these sorbents to analytical instruments, are important processes that can be evaluated by adsorption and desorption kinetics.

Miniaturized air sampling (MAS) techniques are ideal for on-site sampling due to their small size, flexibility for practical applications, low sampling time, low cost and environmental friendliness. Two different MAS techniques were selected for this study: passive solid-phase microextraction (SPME) Arrow and active in-tube extraction (ITEX). They combine the sampling and sample preparation steps without any need for organic solvent and they have been successfully used for the collection of volatile organic compounds (VOCs) from environment samples with straightforward analysis and quantification [6–8].

The main goal of this doctoral dissertation was to study the effect of different materials on the performance of microextraction techniques and thereby to develop

corresponding analytical methods for environmental, food, and biogenic chemistry studies. One objective was to compare commercially available and newly developed sorbent materials in terms of extraction affinity, extraction selectivity, and extraction kinetics. The potential applicability of an aerial drone as the carrier for new miniaturized passive and active samplers was demonstrated.

In this doctoral thesis, the applicability of different materials as ITEX sorbents for reliable selective collection of nitrogen-containing compounds in air samples was evaluated. To improve the selectivity further the ITEX sampling system was furnished with accessories that were assessed and a new sorbent material was synthesized. The physical properties of different materials for the adsorption and desorption kinetics of nitrogen-containing compounds were compared when the materials were packed into the ITEX and coated onto the SPME Arrow sampling systems. The mass transfer process of nitrogen-containing compounds from air to sorbents was examined through the adsorption kinetic models, to improve sampling selectivity and find optimum sampling conditions. The desorption kinetic model assisted in determining the typical adsorbent-adsorbate interactions, and to clarify optimal conditions for analyte desorption. Saturation vapor pressures were also determined. Accurate vapor pressure calculations are needed to investigate compounds partitioning into atmospheric organic aerosols since the gas/particle partitioning mechanism depends on these values.

The performance of the ITEX sampling system with selective sorbent materials, furnished with various accessories, was assessed by simultaneous collection of gas phase and aerosol particles in boreal forest SMEAR II Station, Finland. A drone was utilized to carry the miniaturized air sampling systems at high altitudes. The compositions of various aerosol and gas fractions collected by ITEX and SPME Arrow systems, as well as real-time measurement of black carbon (BC) and particle numbers using portable BC and condensation particle counter (CPC) devices, were evaluated with temporal variation and at different altitudes at SMEAR II Station, Finland.

1.1. Aims of the study

The main aim of the doctoral thesis was to develop miniaturized microextraction sampling techniques for selective collection of volatile nitrogen-containing compounds in air samples.

The specific aims of the thesis were:

1. To clarify the suitability of ITEX and SPME Arrow systems for air sampling **(*Papers I-III*)**.
2. To study the applicability of different materials as ITEX sorbents **(*Papers I-III*)**.
3. To study the adsorption and desorption kinetics of selective sorbent materials for the mass transfer process of gaseous nitrogen-containing compounds to ITEX and SPME Arrow sampling systems **(*Paper IV*)**.
4. To utilize a variety of ITEX accessories for air sampling **(*Papers I and II*)**.
5. To evaluate the applicability of aerial drones as the platform for simultaneous collection of atmospheric air and real-time particle measurement at high altitudes **(*Papers I and II*)**.

2. Background to the work

2.1. Volatile organic compounds

The role and importance of organic compounds in atmospheric chemistry are well known. A variety of compounds from numerous sources, including some volatile organic compounds (VOCs), contributes to the pollution of the atmosphere [9–11].

According to the European Union, VOCs are defined as organic compounds having an initial boiling point lower than or equal to 250 °C at 101.3 kPa, whereas organic compounds themselves are any compound containing at least the element carbon and one or more of hydrogen, oxygen, sulphur, phosphorus, silicon, nitrogen, or a halogen, except for carbon oxides and inorganic carbonates and bicarbonates [12]. Meanwhile the United States Environmental Protection Agency (US-EPA) specifies VOCs as any carbon compound that participates in the atmospheric photochemical

reaction, with the exception of carbon monoxide, carbon dioxide, carbonic acid, metallic carbides, or those designated by EPA to have negligible photochemical reactivity [13].

Due to their frequent occurrence in everyday routine such as at the workplace and consumer products, VOCs can be found anywhere both indoors and outdoors [14]. Their cycling across major environmental media such as in atmospheric air, somehow poses threats to all humans, the environment, and climate.

The ubiquitous VOCs that are present in the atmosphere are caused by human activities including industrial processes, vehicular emission, solvent usage, oil refining, food manufacture, agriculture, residential activities, and landfill wastes. In addition, biogenic sources like plants, trees, wild animals, volcanoes, and forest fires all emit VOCs [10,11]. Their emission to the atmosphere is due to their low boiling points and high vapor pressures. The higher the volatility, the easier the compound emitted from the surface into the air. VOCs are typically released into the environment through various pathways as mixtures with different concentrations rather than as a single compound. These compounds are a major concern due to many reasons, such as some of them are important precursors for ozone formation and secondary air pollutants [15–17]. These pollutants can accumulate and persist in the environment, enhance the global greenhouse effect, and pose unpredicted health risks ranging from various kinds of allergies to cancers due to their hazardous nature [9,12,16–18].

2.2. Nitrogen-Containing Compounds

Nitrogen is an important nutrient for organism growth [19]. This constituent exists in many chemical forms and undergoes various chemical transformations that are unique to this element [2,20,21]. Unique because for some gaseous nitrogen-containing compounds, such as amines, only few atmospheric models encompass them since little is known about their atmospheric chemistry behavior, particularly in terms of physicochemical properties such as gas/particle partitioning [2,22]. This is because of the fact that these compounds are very challenging to determine or analyze due to their high polarity, volatility, and their presence in mixtures with low concentrations [23–25].

Nitrogen-containing compounds are emitted by numerous anthropogenic (*e.g*. road vehicles and industrial) and biogenic sources (*e.g*. plants, trees, and soil). Like other VOCs, gaseous nitrogen-containing compounds also play a crucial role in the formation of atmospheric aerosols. For instance, Wedyan *et al.* [26] reported that up to 80 % of the atmospheric aerosols in the Coastal Gulf of Aqaba was caused by these compounds. Nakamura *et al.* [27] also observed that the primary source of atmospheric nitrogen in the Pacific Ocean's coastal regions is particle phase nitrogen-containing compounds from East Asia.

Nitrogen-containing compounds also have adverse effects on environment, climate, and human health. Their emission to the atmosphere involves the formation and growth of new aerosol particles [1,28]. The aerosol particles in the atmosphere have both direct and indirect effects on the climate system, for instance, they scatter sunlight, transmit and absorb radiation, and serve as nuclei for cloud formation [1,16,29–31]. The inhalable particle can transport toxic chemicals into lungs causing health problems.

In addition to their unfavorable effects, nitrogen-containing compounds have drawn a lot of attention due to their ability to complex with carbon dioxide resulting in carbon capture and storage (CCS) [28,32–35]. Because of the significant amount and environmental implications of CO_2 emission, CSS becomes one of key approaches to mitigate CO_2 negative effects, such as climate change.

Low vapor pressure nitrogen-containing compounds, such as alkanolamines, have been extensively used in commercial technologies as an adsorbent-based CO_2 capture unit [28,32]. The most common solvent alkanolamines employed in this process are those that generate the formation of ammonium carbamate species under anhydrous condition and transforms to ammonium bicarbonate and carbonate species in the presence of water [33,36]. The use of solvent poses many drawbacks, including high-energy consumption, equipment corrosion, solvent regeneration, and toxic emission [36,37]. Therefore, many studies have switched to the attachment of amine functional group onto high surface area sorbents based on polymers, zeolites, graphite, clay, *etc.* to overcome these drawbacks [36–39]. Despite the fact that the use of amines in CCS is desirable, it is still likely for amines to be released into the atmosphere during operation, either at the amine treatment

plant or during amine attachment to the solid sorbent material [40]. Moreover, amines are widely generated or emitted in a range of processes [2,41].

2.2.1. Some nitrogen-containing compounds and their possible reactions in the atmosphere

This section includes the instances of nitrogen-containing compounds that are known to make major contributions to atmospheric chemistry.

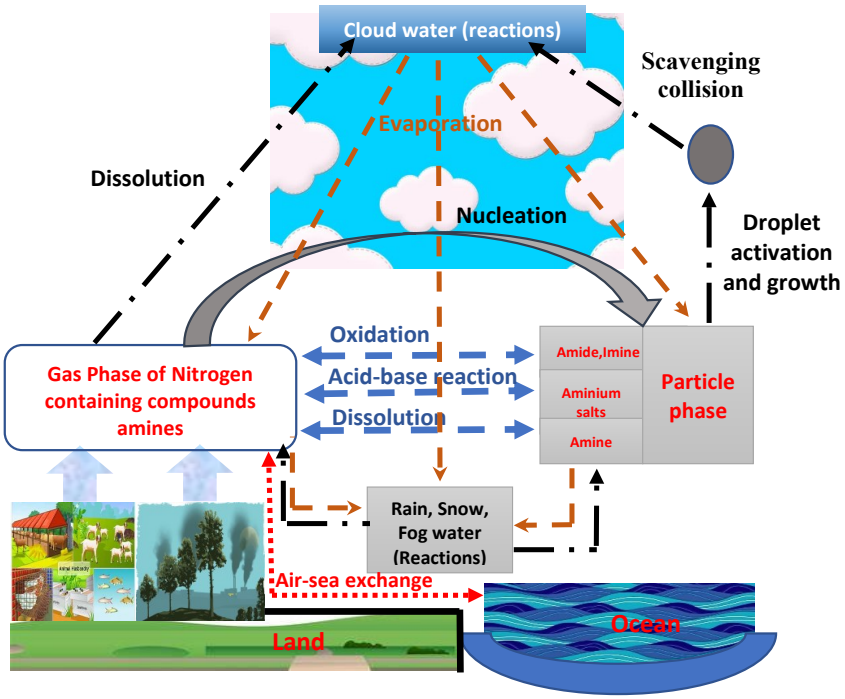

Figure 1. The schematic diagram describing the emission-to-deposition cycle of atmospheric amines. This figure is reproduced from Ref. [2].

Amines are an example of nitrogen-containing compounds that have gained huge attention in the past decades. Amines, which are basic compounds, are derivatives of ammonia in which one or more hydrogen atoms are replaced by an alkyl or aryl group.

Some reactions of amines in the atmosphere can be seen as below:

$NR_{3(g)} + HX_{(g)} \rightleftarrows HNR_3X_{(s)}$, where X refers to Cl or NO_3 (1)

$2NR_{3(g)} + H_2SO_{4(g)} \rightleftarrows (HNR_3)_2\,SO_{4(s)}$ (2)

Similar to ammonia, gaseous aliphatic amines may undergo quick acid-base reactions to form salt particles when exposed to atmospheric acids such as *HCl*, *HNO_3*, and *H_2SO_4* (Eqs (1) and (2)) [2,4]. Short aliphatic amines with high vapor pressures most likely occur in the form of alkyl ammonium salts when present in the particle phase [42]. These constituents continually form molecular clusters in the atmosphere, and can lead to the formation of growing nanoparticles in a process called nucleation [3–5,18,43].

Amines also react with organic acids to produce amides, and with atmospheric oxidants such as O_3^-, OH^-, and NO_3^- to form less volatile products and further subsequently partition into aerosol particles leading to the formation of the secondary organic aerosol (SOA) [3,5,18,43]. The SOAs are the major components of fine aerosol particulate matter (such as PM 10 and PM 2.5) that pollute the environment [2,5,44]. Gaseous amines are not only reacting with atmospheric acids or oxidants to form less volatile products to form SOA, but they can also be adsorbed or directly partitioned into aerosol particles (Fig. 1).

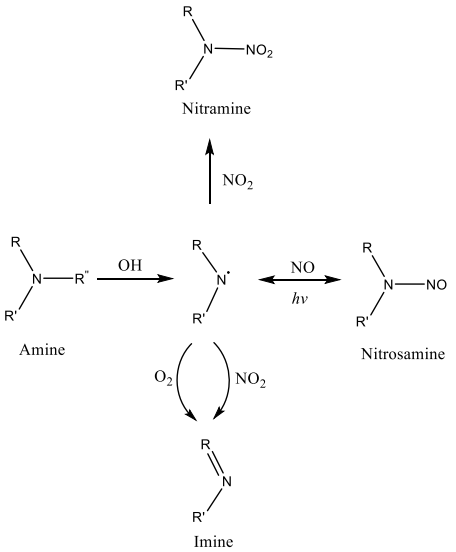

Figure 2. Example of routes of atmospheric photo-oxidation of tertiary amine. This figure is reproduced from Ref. [45].

In addition to particle formation, amines can lead to the formation of toxic compounds, such as nitrosamines and nitramines, through reactions between precursor amines and oxidants (Fig. 2).

Some other nitrogen-containing compounds that have attracted a lot of attention from atmospheric scientists are imidazoles and pyridines. Imidazoles are an important constituent in atmospheric N-heterocycle brown carbon (BrC) due to their unprecedented light absorption properties [46]. According to Kampf *et al.* [47], even trace levels of imidazoles can significantly increase an aerosol's capacity to absorb light. BrC aerosol scatters and absorbs solar radiation which affects the Earth's radiative budget. Imidazoles can be produced in the atmosphere in the presence of primary amines or ammonium salts by nucleophilic attack [46,48]. Some studies have proposed the reaction pathways of imidazole as the part to produce the N-heterocycles which have been suggested to be the cause of browning [47–50].

Pyridine is one of the nitrogen-containing compounds listed in EPA 8270 as volatile organic pollutants that need to be assessed from air samples [51]. In addition to pyridine, the oxidation of pyrrole will also generate NO that is known as a toxic pollutant to cause serious environmental problems such as acid rain [52–54].

Reactions (3) and (4) show how pyridine and pyrroles produce NO in the atmosphere, respectively.

$$C_5H_5N_{(g)} + \frac{27}{4} O_{2\,(g)} \rightarrow 5\, CO_{2\,(g)} + \frac{5}{2}\, H_2O_{(g)} + NO_{(g)} \quad (3)$$

$$C_4H_5N_{(g)} + \frac{23}{4} O_{2\,(g)} \rightarrow 4\, CO_{2\,(g)} + \frac{5}{2}\, H_2O_{(g)} + NO_{(g)} \quad (4)$$

2.3. Miniaturized sampling systems

Sample preparation has always been a crucial step in separation science to determine targeted compounds from a complex matrix. The analytes isolation from the sample matrix is a major task to ensure the success of the qualitative and quantitative analysis of the compounds. Liquid-liquid extraction (LLE) is a classical sample preparation technique that is time-consuming, labor-intensive, and consumes large volumes of organic solvents. This method is considerably expensive

and generates a large amount of waste that is harmful for human health and environment [55,56].

In the last three decades, significant progress has been made in the development of miniaturized sampling techniques based on microextraction that enable the efficient extraction and preconcentration of targeted analytes from a broad range of samples. Typically, this method uses an appropriate extraction phase, which can be a liquid or a solid material. Miniaturized sampling techniques based on sorbent microextraction and liquid-phase microextraction are extremely important since they are environmentally friendly and serve as an alternative to traditional extraction methods. Other benefits of these systems include their ability to extract samples quickly, concentrate samples simultaneously, possibly automate the process, and directly inject all analytes into the analytical instrument, enabling rapid qualitative and quantitative analysis of complex matrices [6–8].

Sorbent microextraction, such as solid-phase microextraction (SPME), is regarded as an advance miniaturized solid-phase extraction (SPE) technique [57,58], while liquid-phase microextraction (LPME) like single drop microextraction (SDME) is recognized as a miniaturized LLE procedure [59,60].

Particularly for air samples, SPME has been exploited as a successful miniaturized sampling technique in numerous studies [61–68]. Air sampling techniques can be classified into two categories, namely non-exhaustive (passive sampling) and exhaustive (active sampling), which will be discussed in more detail in sections 2.4 and 2.5. SPME belongs to a passive sampling technique, whereas an active sampling technique such as in-tube extraction (ITEX) [61,63,65,69] and needle trap microextraction (NTME) [7,70,71] have also been developed for air collection and employed with reliable results.

2.4. Passive sampling

Passive sampling (PS) has been developed for various gaseous pollutants including CO, NO_2, and VOCs. This technique was invented in 1927 [72] and used for the first time to quantify the atmospheric sulphur dioxide in 1973 [73,74]. A physical process, such as diffusion through a static air layer or permeation through a membrane, controls the sampling rate of a passive sampler [75]. Because of the

difference in chemical potential between the two media, the analytes in this process move from the sampling medium with higher concentration to the sorbent (collecting medium) until the equilibrium is reached. Therefore, in order to ensure reproducibility results and use this tool for quantitative analysis, control of the extraction time and other extraction parameters, such as humidity, temperature, ionic strength, and wind conditions is essential [57,67,75,76].

Most miniaturized passive samplers work based on the diffusion, which is known as diffusive sampling. Examples of these include the SPME, solid-phase dynamic extraction (SPDE), and diffusive needle trap device (NTD)[6].

2.4.1. Solid-phase microextraction

Early in the 1990s, SPME was licensed and commercialized following its late 1980s patenting [77]. To address the need for quick sample preparation both in the laboratory and on-site analysis, several different SPME formats including fiber (SPME-fiber), cold fiber (CF-SPME), arrow (SPME-Arrow), in-tube (IT-SPME) and thin-film (TF-SPME), have been extensively explored both theoretically and experimentally [6,57,78].

The first invented SPME is based on externally coated fibers mounted in a syringe-like needle for protection. In this case, the fiber can be either solid or hollow [57,79]. There are three basic modes of extraction in SPME, namely direct immersion (DI), headspace extraction (HS), and a membrane protection approach (Fig. 3). In the DI type, the coated sorbent is placed into the liquid sample medium, and the analytes are transferred directly from the sample to the collecting phase. This mode is designed primarily to extract less volatile or non-volatile compounds from liquid or solid samples.

In the HS mode, the analytes need to be transported through an intermediate substance, usually atmospheric air, before they can reach the coating. HS is widely used to extract semi-volatile and volatile compounds from the headspace of the samples. This mode is suitable to eliminate high-molecular weight or non-volatile interference, whereas the membrane protection mode is used to protect the sorbent (specific for SPME fiber) against damage when analyzing very dirty samples. The

latter is also utilized to determine analytes with too low volatilities for the headspace approach. The membrane is made of a material that can improve the extraction process's selectivity [57,80].

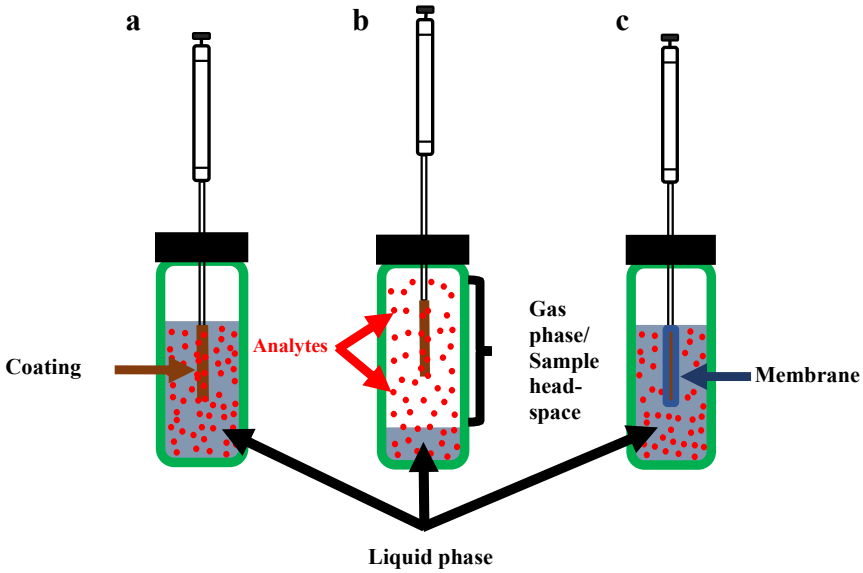

Figure 3. SPME Extraction modes: (a) direct immersion; (b) headspace mode; (c) membrane protection.

Quantification in SPME can be defined by two approaches. First, if an equilibrium between the sample matrix and sorbent phase is reached, the amount extracted will not be affected by the convection conditions. The second quantification approach uses short pre-equilibrium extraction times, where the amount of analyte extracted is proportional to time if convection is constant. In the latter situation, quantitation is performed based on analytes' time accumulation in the coating sorbent [57,81].

2.4.2. SPME Principle

As has been discussed in the previous section, the first approach of SPME quantification is when the analytes concentration reaches equilibrium in the sample medium and the sorbent coating.

In direct immersion (DI) mode, the phases that contribute significantly to the extraction process are sample and extraction phase (sorbent material), thus, the equilibrium condition can be described by equation (5):

$$C_0 V_s = C_s^{\infty} V_s + C_e^{\infty} V_e \quad (5)$$

where C_o is the initial concentration of analytes in the sample, while C_s^{∞} and C_e^{∞} are equilibrium concentration of analytes in the sample and sorbent coating, respectively. V_s and V_e are volumes of the sample and the sorbent coating, respectively.

When immobilized liquid fiber (liquid polymer coated SPME fiber) is used, we can consider $C_e^{\infty} V_e$ as $C_f^{\infty} V_f$, where C_f^{∞} and V_f are equilibrium concentration of analytes in the liquid polymer fiber coating and volume of liquid polymer fiber coating, respectively.

The distribution coefficient of the analytes (K_{fs}) between the fiber coating and the sample matrix is defined as:

$$K_{fs} = \frac{C_f^{\infty}}{C_s^{\infty}} \quad (6)$$

Equation (5) and (6) can be combined into equation (7) below:

$$C_f^{\infty} = C_0 \frac{K_{fs} V_s}{K_{fs} V_f + V_s} \quad (7)$$

The mass of analytes (n) extracted by the fiber coating can be calculated from equation (8). This equation shows the linear relation between the amount of analyte extracted onto the coating (n) and the analyte concentration in the sample (C_0).

$$n = C_f^{\infty} V_f = C_0 \frac{K_{fs} V_s V_f}{K_{fs} V_f + V_s} \quad (8)$$

In some determination, the sample volume V_s is much larger than the capacity of the sorbent coating V_f, resulting in a very simple relationship:

$$n = C_0 K_{fs} V_f \quad (9)$$

In contrast to the DI mode that only considers two media (*i.e.* sample and sorbent coating), the headspace method includes three phases, namely the original sample, the sample headspace, and the sorbent coating. Therefore, the equilibrium condition is achieved by equation (10):

$$C_0 V_s = C_s^{\infty} V_s + C_h^{\infty} V_h + C_f^{\infty} V_f \quad (10)$$

where C_h^{∞} and V_h are equilibrium concentration of analytes in the headspace and headspace volume, respectively.

If: $K_{hs} = \frac{C_h^{\infty}}{C_s^{\infty}}$; and $K_{fh} = \frac{C_f^{\infty}}{C_h^{\infty}}$, are the headspace/sample matrix and the sorbent coating/headspace distribution constants, respectively, thus, the amount of analyte (n) extracted by the sorbent coating can be calculated from equation (11):

$$n = C_f^{\infty} V_f = C_0 \frac{K_{fh} K_{hs} V_s V_f}{K_{fh} K_{hs} V_f + K_{hs} V_h + V_s} \quad (11)$$

If the effect of moisture in the gaseous headspace can be neglected, then we assume that:

$$K_{fs} = K_{fh} K_{hs} \quad (12)$$

Thus, equation (11) can be rewritten to equation (13):

$$n = C_0 \frac{K_{fs} V_s V_f}{K_{fs} V_f + K_{hs} V_h + V_s} \quad (13)$$

As long as the sample volume $V_s >> K_{fs} V_f$, it is not necessary to sample a well-defined volume since the amount of analyte extracted is independent of V_s. As a result, an SPME device can be immediately placed in the analytical instrument for quantification [82].

When solid sorbent coated SPME fiber is employed, analytes bind to surface active sites, so that the equilibrium amount of analytes is determined by:

$$n = C_0 \frac{K V_s V_f \, (C_{fmax} - C_f^{\infty})}{V_s + K V_f \, (C_{f\,max} - C_{fA}^{\infty})} \quad (14)$$

where K is the analyte's adsorption equilibrium (affinity) constant, while $C_{f\,max}$ is the maximum concentration of active sites on the coating.

The amount of analyte A extracted at equilibrium is also affected by the presence of other analytes, for instance analyte B. As a result, the following equation (15) determines the amount of analyte A that was extracted under this condition.

$$n = C_0 \frac{K_A V_s V_f \left(C_{fmax} - C_{fA}^{\infty}\right)}{K_A V_f \left(C_{f\,max} - C_{fA}^{\infty}\right) + V_S\left(1 + K_B C_{fB}^{\infty}\right)} \tag{15}$$

The second approach on SPME quantification is the use of a short pre-equilibrium extraction time, where the amount of analyte extracted is related to time if convection or agitation are kept constant. The entire kinetic process of SPME in this circumstance can be described by:

$$n = C_0 \frac{K_{fs} V_f V_s}{K_{fs} V_f + V_s} \left[1 - \exp\left(-a_R t\right)\right] \tag{16}$$

where n is the amount of extracted analyte at time "t", and a_R is a constant that depends on the volume extraction phase, headspace and sample volumes, mass transfer constant, distribution coefficients, and the surface of extraction phase [57,83].

In the SPME sampling system, the device affinity is proportional to the number of molecules extracted from the sample matrix. This indicates that the amount of analyte increases as the sample volume increases, until a point where the sample volume is significantly higher than the sorbent volume and the distribution coefficient. The analytes distribution is affected by temperature, humidity, agitation, ionic strength, pH, and the polarity of analytes and SPME sorbent phase. For instance, according to Alpendurada [84], a rise in temperature can cause an analyte's distribution constant to decrease. Addition of salt will change the ionic strength of the sample solution, salting-out polar analytes [57,85]. Adjusting the pH will improve the extraction efficiency of basic and acidic analytes [57]. Consequently, careful optimization and thorough calibration are required to develop a reliable and robust quantitative SPME method.

2.4.3. SPME Arrow

A variety of SPME sampling systems, including thin-film SPME, in-tube SPME, and SPME Arrow, have been developed as a result of the rapid growth of technology to overcome issues encountered during SPME implementation. In this thesis, only the most recent SPME Arrow system is discussed. The SPME Arrow that was introduced in 2015 by CTC Analytics AG, was designed to overcome the traditional SPME fiber drawbacks, such as small sorbent volume, fragility, limited mechanical robustness, and relatively poor reproducibility [8,77].

SPME Arrow has larger coating volume (3.8-11.8 µL) than SPME Fiber (0.03-0.61 µL), which enhances extraction efficiency, measurement sensitivity, and detection limit [8,64]. The SPME Arrow's body is made of stainless steel with a diameter approximately 2 – 3 times bigger than that of conventional SPME fibers (Fig. 4).

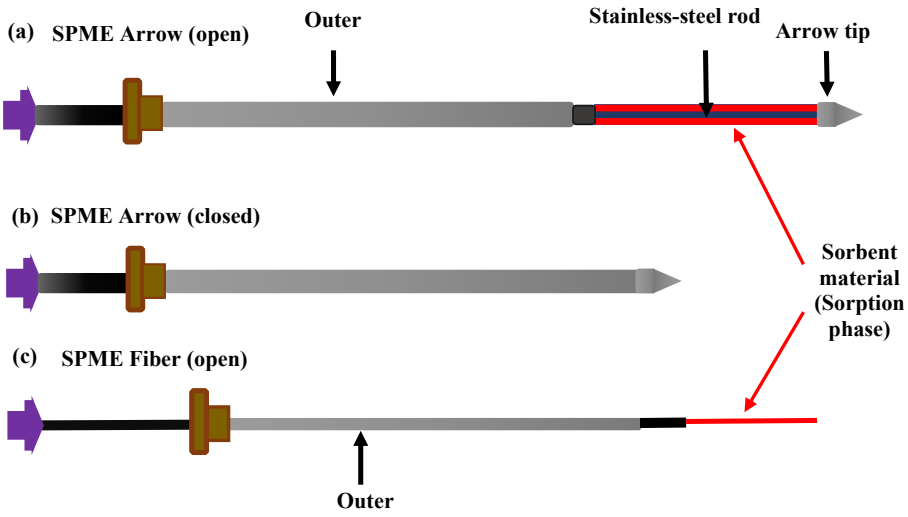

Figure 4. The SPME Arrow with sorbent exposed (a) and with sorbent covered by a stainless-steel rod (b). These Arrows are compared to SPME fiber (c) that has smaller surface area and thinner sorbent than that in SPME Arrow (a).

The stainless-steel rod also replaces the fragile fused silica fiber. The Arrow tip at the end of the rod allows the complete closure of SPME Arrow to prevent contamination of the sorbent during the transfer process (Fig. 4b). Due to its design,

the SPME Arrow tip also enables the SPME Arrow to directly inject the analytes into the GC injector without modifying the GC injection port, such as by installing a desorption unit. This approach thereby improves mechanical durability, versatility, and maintains the compatibility for direct thermal desorption for GC analysis [8,64,77]. SPME Arrow coated with various stationary phases such as commercial polydimethylsiloxane (PDMS), carbon wide range (CWR), and divinyl benzene (DVB)/PDMS have been utilized in many applications, such as for food and environmental analyses [6,24,61,62,64,65,77,86].

2.5. Active sampling

The active air sampling (AAS) technique has been regarded as the most accurate method to measure VOCs concentration in air as they collect both gas and particle phase [6,76]. Due to its independence from wind speed, temperature, and pressure, the AAS offers more accurate and reliable quantification when compared to the passive sampling technique [87]. Different to passive air sampler (Fig. 5a), AAS requires a pump as the driving force to collect air samples (Fig. 5b). The collection device can be a filter or a trap, such as an adsorbent packed tube [7,70,76,88].

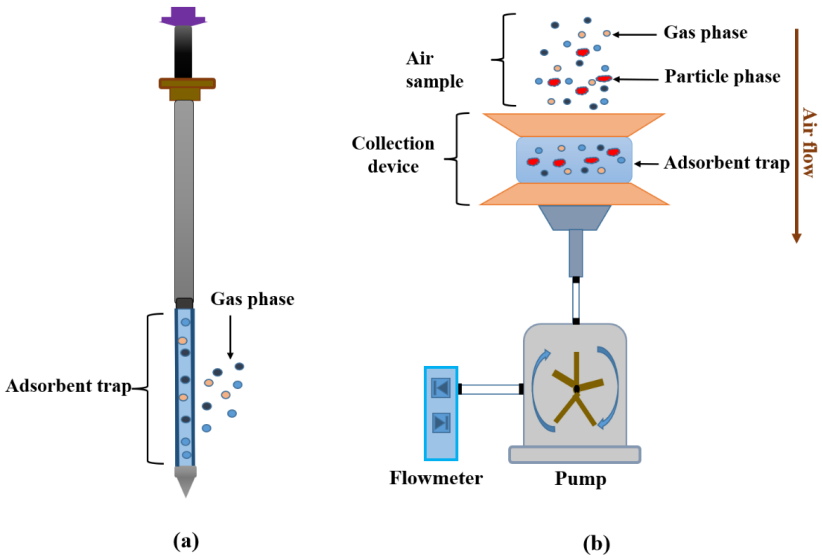

Figure 5. Schematic of (a) passive and (b) active air samplings. In active air sampling (b), the air sample is drawn through the adsorbent by the help of the pump.

AAS can be classified into high volume and low volume samplers based on their flow rates and sample collection times. High volume samplers typically have flow rates between 15 and 80 $m^3.h^{-1}$ and total sample volumes more than 400 m^3, while low volume samplers typically have flow rates of less than 3 $m^3.h^{-1}$. Depending on the sorbent capacity, low volume samplers can extend the sampling period for continuous sampling, for instance, up to 14 days [76,89]. The pump's variable speed allows the collection of samples over the desired sampling time. Compared to passive air sampling, AAS offers several advantages, including a shorter sampling time, higher sampling capacity and efficiency, simultaneous collection of gas and particle phase, and a lower detection limit.

In AAS, sampling efficiency is affected by the type of sampling device and sorbent, the artifact of collection device and sorbent, degradation of sorbent and analytes, and breakthrough (analytes loss from the adsorbent trap) [90,91]. In order to prevent low sampling efficiency, some configurations and parameters such as sampling device configuration, sampling flow rate, and sampling time should be assessed and optimized.

The innovative miniaturized active air samplers were developed in the 2000s, such as needle trap microextraction (NTME) and in-tube extraction (ITEX) [87,92]. These miniaturized samplers have several benefits including a short sampling system, simple operation and automation, and on-line coupling with analytical instruments like gas chromatography-mass spectrometry.

2.5.1. In-tube extraction

ITEX belongs to active samplers that was first made commercially available in 2006 and was upgraded in 2009 to be compatible with any PAL-type autosampler without modification [87]. Dynamic ITEX, which pumps the sample headspace using a gastight syringe through a connected tube filled with sorbent material, can be fully automated for CTC PAL series autosamplers. In this configuration, an electric heater is placed around the gastight syringe (that has a 1.3 mL volume size) and ITEX sorbent tube to prevent sample condensation and enable thermal desorption to the gas chromatograph's injector.

ITEX conditioning can be performed through a side-port hole in the glass body of the gastight syringe. Lifting the syringe plunger over the side-port hole allows the continuous inert gas (*e.g.* nitrogen) flushing of the syringe and the packed sorbent to prevent carryover between analyses. For headspace dynamic extraction, the syringe plunger is moved up and down (defined as a stroke) to collect the headspace sample and pass through the sorbent material. For desorption, a predetermined volume of helium is aspirated from the GC inlet into the syringe as a desorption volume. The heater is then heated to the desorption temperature, and the syringe plunger is then lowered to inject and desorb the analytes into the GC injector system at a fixed desorption flow rate. Following desorption, the inert gas is introduced through the syringe's side-port hole to flush the sorbent material at the optimized temperature for post-conditioning.

Figures 6 - 8 show the steps of the ITEX procedure including ITEX conditioning, sample extraction, and desorption, respectively.

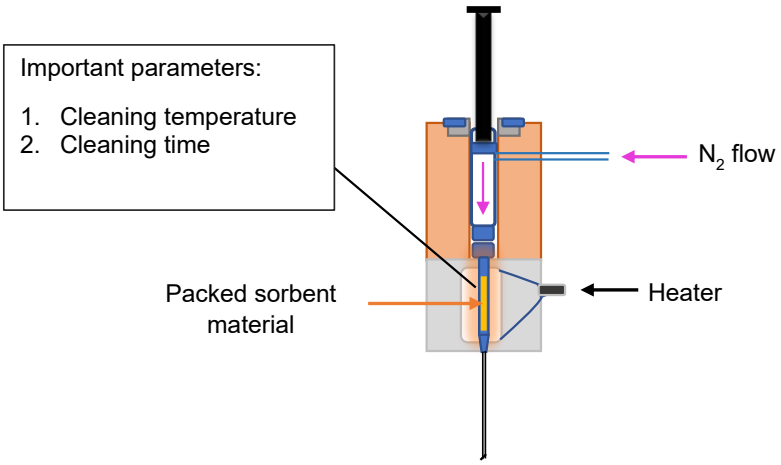

Figure 6. ITEX conditioning stage. This figure is reproduced from Ref [93]

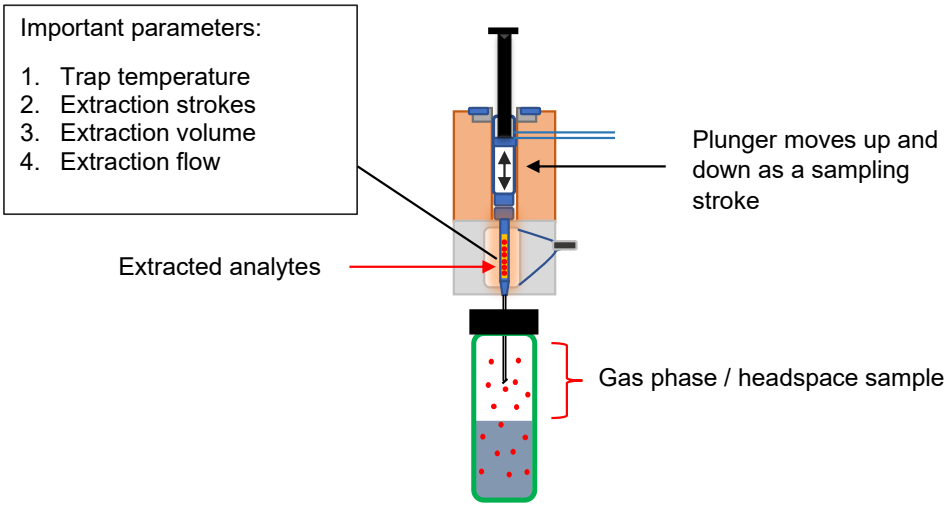

Figure 7. ITEX sampling stage. This figure is reproduced from Ref [93]

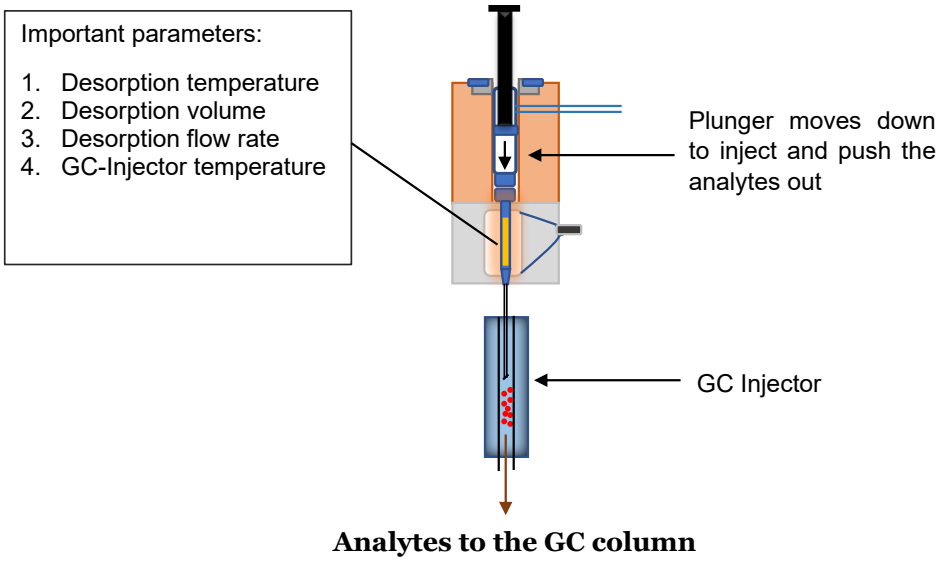

Figure 8. ITEX desorption stage. This figure is reproduced from Ref [93]

ITEX has been exploited for on-site determination of VOCs from air sample, beverage, and cigarette smoke [61–63,65,69,94]. Additionally, a fully automated

and integrated ITEX system for continued air sampling and online measurement has been successfully developed [62].

2.6. Air sampling methods

Owing to the challenge posed to air sampling at high altitude, very little is known about the abundance, diversity, and extent of nitrogen-containing compounds in the Earth-atmosphere system. Consequently, there is very little data available on the diversity and concentration of nitrogen-containing compounds in the high altitude resulting in difficulties of studying their roles in the atmosphere. To directly address this knowledge gap, some aerosol sampling platforms at high altitudes have been designed and constructed such as aircraft [95–97], helicopter [98], tower [99–101], balloons [102,103], zeppelin [104,105], and aerial drone [61,63,65,106,107]. Of these, the uncrewed vehicles (*e.g.* balloons and aerial drone) are a more cost-effective and feasible method than the piloted flights (*e.g.* zeppelin and helicopter) [108].

Instrumentations that are attached in the tall tower (Fig. 9a) can conduct continuous monitoring of VOCs and a broad range of aerosol characteristics. However, it can only be used to study the tower surrounding and at fixed altitude, since it cannot be flexibly moved vertically or horizontally.

A balloon-based sampler is inexpensive, has a long duration of sampling, and can reach altitudes of up to 40 km. Balloons can lift the payload at various weights and can be lifted to different altitudes depending on the balloon capacity. However, the drawback would be that it could only conduct sampling limited to the vertical range and at a certain altitude, or, it would be expensive to exploit a controlled balloon [103,109]. Another risk that may happen is sample contamination and being lost during payload retrieval or when the balloon landed by exhausting the balloon gas. For example, Bryan *et al.* [103] developed a bioaerosol sampling payload to collect microbial aerosols from air at different altitudes. The payload was transported using a latex sounding balloon and was released and descended by parachute. In this case, there is risk that there is no way to ascertain a safe landing site for the payload.

Piloted flight for air sampling covers a wider range of sampling area and is able to flexibly collect samples with both vertical and horizontal movements. In addition, it has higher reliability in terms of securing the samples from damage and loss. However, it would be costly to perform the sampling [108].

A Zeppelin, a semi-rigid airship, has a hull diameter of about 14 m and a length of 75 m. It can lift up to 1900 kg using He as the lifting gas. The high payload capacity enables scientists to carry state-of-the-art instrumentation designed to collect information on the process between chemical compounds and aerosol particles to better estimate their role in the atmospheric chemistry [104]. The Zeppelin NT has a maximum range of 900 km and a maximum flight altitude of 2600 m. The highest height that could be reached when carrying the heaviest instrument combination, for instance the aerosol mass spectrometer (AMS) and weighting more than 1000 kg, was between 400 and 750 m [105]. In Zeppelin, the instrumentation can be installed inside the gondola (highlighted in red in Fig. 9c).

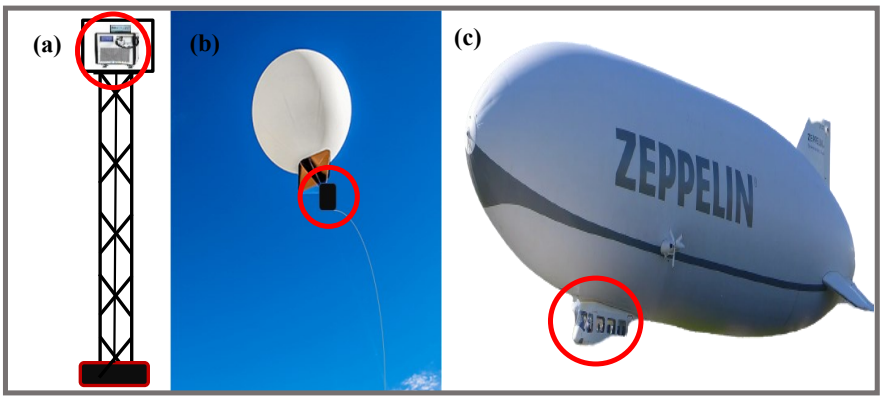

Figure 9. Various platforms for air sampling and measurement systems: (a) Towers, (b) Tethered balloon, and (c) Zeppelin. The instrumentation is located in the red circle.

The aerial drone, a remotely piloted aircraft system, has grown very popular for aerosol measurement over the last decades. Aerial drones as carriers of air sampling devices and aerosol measurement devices such as sensors and portable miniature-mass spectrometry allow samplings at high altitudes and in areas with poor accessibility and with low cost [110,111]. Aerial drones also use electrical power

engines that limit the potential contamination sources [65,112]. The versatility of air sampling with a drone system has become an advantage in comparison with conventional sampling platforms such as towers, balloons, or aircraft.

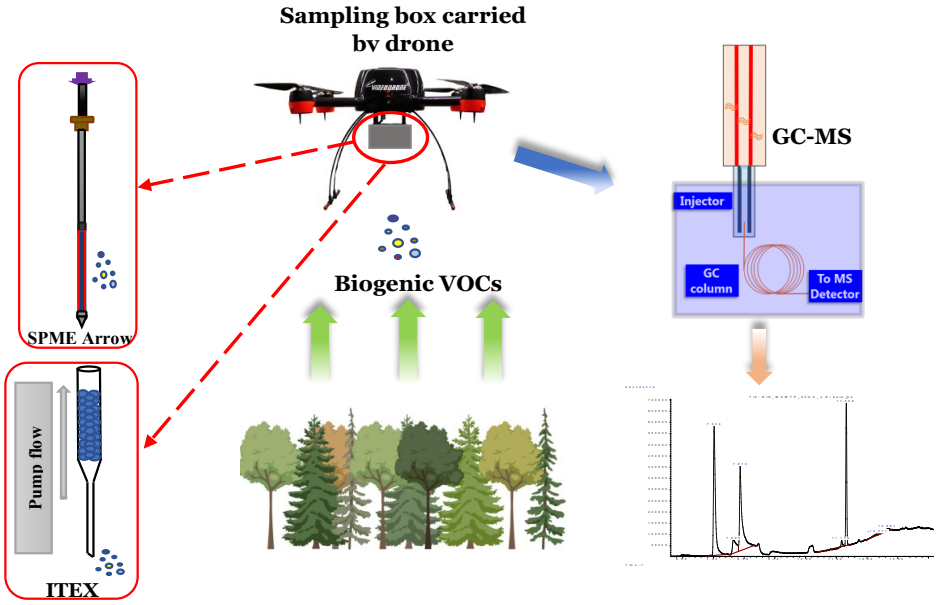

Figure 10. Schematic picture of the aerial drone as a carrier for a miniaturized air sampling system (SPME Arrow and ITEX). The collected samples are then analyzed using the gas chromatography-mass spectrometry (GC-MS).

The applicability of an aerial drone as a carrier for miniaturized air sampling devices such as SPME Arrow an ITEX has been studied in recent studies allowing the simultaneous collection of multiple air samples as well as both gas and particle phases [61,63,65,113]. Aerial drones have also been used as carriers of aerosol measurement devices such as sensors and miniature-mass spectrometry [110]. A wide variety of sensors have been attached to aerial drones for monitoring of different parameters such as temperature, humidity, black carbon, CO_2, NO_2, and VOCs concentration [110,112,114,115].

3. Experimental

The main aim of this doctoral thesis was to develop reliable microextraction techniques to selectively collect nitrogen-containing compounds from air samples. The applicability of various sorbents, including a new material that was developed in this thesis and some other commercial sorbents, were compared. The physicochemical properties of those materials were also studied when they were packed into the ITEX and coated onto the SPME Arrow sampling systems.

The lists of chemicals (Table 1), materials, instruments, and equipment (Table 2), methods and experimental conditions used in the studies are provided in this chapter. Detailed information is found in ***Papers I-IV***.

Table 1. List of chemicals.

Chemical	Purity	Supplier	Papers
1-Butanamine	99%	Sigma Aldrich (St. Louis, MO, USA)	II
1-Butanenitrile	99%	Merck KGaA (Darmstadt, Germany)	II
1-Butanol	99.8%	Sigma Aldrich (Steinheim, Germany)	III
1-Methylimidazole	99%	Alfa Aesar GmbH (Karlsruhe, Germany)	I
1-Methylimidazole	99%	Sigma Aldrich (St. Louis, MO, USA)	IV
1-Nitropropane		Sigma Aldrich (Steinheim, Germany)	I
1-Propanol	HPLC grade	Rathburn Chemicals (Walkerburn, Scotland)	III
1,3-Diaminopropane	98%	TCI (Tokyo, Japan)	I
2-Butanol	99.5%	E Merck (Darmstadt, Germany)	I, II
2-Butanone	≥99.5%	Sigma Aldrich (St. Louis, MO, USA)	I
2-Methylimidazole	99%	Alfa Aesar GmbH (Karlsruhe, Germany)	I
2-Propen-1-amine	98%	Sigma Aldrich (St. Louis, MO, USA)	II
2,3-Butanedione	97%	Sigma Aldrich (Steinheim, Germany)	II
3-Amino-1-propanol	98%	Sigma Aldrich (Steinheim, Germany)	I
4-Ketopimelic acid	98%	Sigma Aldrich (St. Louis, MO, USA)	II
4-Methyl benzylamine	≥97%	Fluka (Steinheim, Germany)	I
(+) Camphene	≥90%	Sigma Aldrich (St. Louis, MO, USA)	III
Acetonitrile	≥99,9%	Honeywell GmbH (Seelze, Germany)	II, III
Acetophenone	95%	The British Drug Houses Ltd. (Poole, England)	II, III
Acetic acid	≥99,8%	Merck KGaA (Darmstadt, Germany)	II
Adipic acid	≥99,9%	The British Drug Houses Ltd. (Poole, England)	II
Azelaic acid	≥99%	Fluka (Buchs, Switzerland)	II
Ammonium acetate	99.9 %	Fisher Scientific (USA)	II

Table 1 (cont.). List of chemicals.

Chemical	Purity	Supplier	Papers
Ammonium carbonate	chem. Pure	Riedel de Häen (Seelze, Germany)	II
Benzaldehyde	≥99%	Fluka (Buchs, Switzerland)	II
Cis-pinonic acid	98%	Sigma Aldrich (St. Louis, MO, USA)	II
Citric acid	≥99,5%	Sigma Aldrich (St. Louis, MO, USA)	II
Crotonic acid	98%	Sigma Aldrich (St. Louis, MO, USA)	II
Decafluorobiphenyl	99%	Sigma Aldrich (St. Louis, MO, USA)	I, II, III
Decane	98%	E Merck (Darmstadt, Germany)	IV
Dichloromethane	HPLC grade	Sigma Aldrich (St. Louis, MO, USA)	III, IV
Diethylamine	≥99.5%	Fluka (Steinheim, Germany)	I, II
Dimethylamine·HCl	99.5%	Fluka (Steinheim, Germany)	I
Dimethylformamide	99.9%	Sigma Aldrich (St. Louis, MO, USA)	I, II, IV
Dipropylamine	99%	Fluka (Buchs, Switzerland)	I, III, IV
Ethanolamine	>95.5%	Sigma Aldrich (Steinheim, Germany)	I
Ethyl acetate	≥99.7%	Sigma Aldrich (Steinheim, Germany)	II, III
Ethylbenzene	99%	Sigma Aldrich (St. Louis, MO, USA)	II
Ethylenediamine	for synthesis	Sigma Aldrich (St. Louis, MO, USA)	I
Formic acid	99-100%	VWR Chemicals (Fontenay-sous-Bois, France)	II
Fumaric acid	≥98%	Fluka (Buchs, Switzerland)	II
Glutaric acid	≥99%	E Merck (Darmstadt, Germany)	II
Glycolic acid	≥99%	Fluka (Buchs, Switzerland)	II
Hexadecyltrimethylammonium bromide	~99%	Sigma Aldrich (St. Louis, MO, USA)	III
Helium	99.996 %	AGA, Espoo, Finland	I – IV
Heptane	p.a	E Merck (Darmstadt, Germany)	IV
Hexane	≥97%	Honeywell (Seelze, Germany)	III, IV
Hexanal	98%	Sigma Aldrich (St. Louis, MO, USA)	II, III
Hexylamine	99%	Sigma Aldrich (St. Louis, MO, USA)	I – IV
Isobutanol	≥98.5%	E Merck (Darmstadt, Germany)	II
Isobutylamine	99%	Sigma Aldrich (St. Louis, MO, USA)	I – IV
L-Tartaric acid	99%	Sigma Aldrich (St. Louis, MO, USA)	II
Maleic acid	≥99%	Fluka (Buchs, Switzerland)	II
Malonic acid	≥98%	Fluka (Buchs, Switzerland)	II
Mandelic acid	≥99,5%	The British Drug Houses Ltd. (Poole, England)	II
Methanol	≥99.9%	Honeywell GmbH (Seelze, Germany)	I, II
Methyl isobutyl ketone	98.5%	Sigma Aldrich (St. Louis, MO, USA)	II, III
Nonane	99%	E Merck (Darmstadt, Germany)	IV

Table 1 (cont.). List of chemicals.

Chemical	Purity	Supplier	Papers
N,N-Dimethylformamide	≥99.99 %	Sigma Aldrich (St. Louis, MO, USA)	I, II
Octanal	≥95%	Sigma Aldrich (St. Louis, MO, USA)	III
Octane	95%	JT Baker (Deventer, Holland)	IV
o-Toluidine	≥99.5%	Fluka (Buchs, Switzerlands)	III, IV
Pentane	95%	Lab Scan Analytical Science (Sowinskiego, Poland)	IV
p-Cymene	99%	Sigma Aldrich (St. Louis, MO, USA)	I, II, III
Phthalic acid	≥99.5%	E Merck (Darmstadt, Germany)	II
Polyacrylonitrile (Mw = 150000)		Sigma Aldrich (St. Louis, MO, USA)	I, II, IV
Pyridine	~100%	VWR Chemicals (Fontenay-sous-Bois, France)	I – IV
Sodium hydroxide	99%	E Merck (Darmstadt, Germany)	III
Spherical silica microparticles (M.S.GEL. EP-DF-5-120A)		AGC Si-Tech Co., Ltd. (Fukuoka, Japan)	III
Suberic acid	98%	Sigma Aldrich (St. Louis, MO, USA)	II
Succinic acid	99%	E Merck (Darmstadt, Germany)	II
Tenax-GR		Alltech (Deerfield, IL, USA)	I
Tenax-TA		Alltech (Deerfield, IL, USA)	I
Tetrahydrofuran	≥99.9%	Honeywell GmbH (Seelze, Germany)	I, III
Toluene	≥99.8	Fischer Scientific (Loughborough, UK)	III
Triethylamine	≥99%	Merck KGaA (Darmstadt, Germany)	I, III, IV
Trimestic acid	95%	Sigma-Aldrich (St. Louis, MO, USA)	II
Trimethylamine		VICI Metronics Inc., (Poulsbo, USA)	I, II
Triphenyl phosphate	≥99%	Sigma-Aldrich (St. Louis, MO, USA)	II
Ultrapure water		Millipore DirectQ-UV, Billerica, MA, USA	I, II, IV
Undecane	99%	Fluka (Buchs, Switzerlands)	IV
Vanillic acid	≥97%	Fluka AG (Buchs, Switzerland)	II
Zinc nitrate hexahydrate	>99%	Sigma-Aldrich (St. Louis, MO, USA)	III

Table 2. Materials, instruments, and equipment

Material/Instruments/Equipment	Model and manufacture	Papers
Autosampler	PAL RTC, CTC Analytics, Zwingen, Switzerland	I – IV
Aerial Drone	Geodrone X4L, Videodrone Finland Oy, Muurame, Finland	I, II

Table 2 (cont.). Materials, instruments, and equipment

Material/Instruments/Equipment	Model and manufacture	Papers
Heating block	Pierce Reacti-Therm Heating Module, Rukford, Illinois, USA	I
Bare ITEX	BGB Analytik AG, Zurich, Switzerland	I – IV
Bare SPME Arrow	BGB Analytik AG, Zurich, Switzerland	I, II, IV
Black Carbon (BC) portable	AethLabs AE51-S6-1408, application version of 2.2.4.0, San Francisco, CA, USA	II
Energy dispersive spectra (EDS)	Zeiss GeminiSEM 450 instrument, Oberkochen, Germany	III
Flow meter and controller	Alicat Scientific, Arizona, USA.	I – IV
Gas Chromatograph	6890 N, Agilent Technologies, Palo Alto, USA	I – IV
GC capillary column	HP-1 (30 m length x 0.25 mm i.d. x 0.1 μm phase thickness), Agilent Technologies, Palo Alto, USA	IV
GC capillary column	InertCap™ for amines (30 m length x 0.25 mm i.d.), GL Sciences, Tokyo, Japan	I – IV
GC retention gap	Deactivated fused silica (2.5 m x 0.25 mm id.) Agilent Technologies, Palo Alto, USA	I – IV
Glass press-fit connector	BGB Analytik, Switzerland	I – IV
Headspace vial	20 mL, Phenomenex, Torrance, California, USA	III
Heating oven	Heraeus, Hanau, Germany	I
High performance liquid chromatography (HPLC) system	Agilent 1260 Infinity HPLC system, Agilent Technologies, Palo Alto, CA, USA	II
HILIC column	SeQuant ®ZIC®-cHILIC (2.1x150 mm, 3 μm particle size), MerckKGaA, Darmstadt, Germany	II
Lab-made permeation system	Laboratory made, Analytical Chemistry Lab, University of Helsinki, Finland	I – IV
Lab-made condensation particle counter (CPC)	University of Helsinki, Finland	II

Table 2 (cont.). Materials, instruments, and equipment

Material/Instruments/Equipment	Model and manufacture	Papers
Shaker	IKA VIBRAX-VXR, Breslau, Germany	I, II, IV
Mass Spectrometer	5973C, Agilent Technologies, Palo Alto, USA	I, II
Mass Spectrometer	5975C, Agilent Technologies, Palo Alto, USA	I – IV
Mass Spectrometer	Agilent 6420 triple-quadrupole mass spectrometer, Agilent Technologies, Palo Alto, CA, USA	II
Membran filter	0.45 mm pore size, Millipore, Ireland	II
Particle cutter	Ultramicrotome, Leica EM UC7	III
Polytetrafluoroethylene (PTFE) filter	Phenomenex, Torrance, California, USA	I, II
Scanning electron microscope	Zeiss GeminiSEM 450 instrument, Oberkochen, Germany	III
SPME Arrow	Carbon WR (Arrow diameter 1.1 mm, sorbent film thickness 120 µm, sorbent length 20 mm), CTC Analytics AG, Zwingen, Switzerland	II
SPME Arrow	DVB/PDMS (Arrow diameter 1.1 mm, sorbent film thickness 120 µm, sorbent length 20 mm), CTC Analytics AG, Zwingen, Switzerland	II, IV
Surface area and porosity analyzer	ASAP-2010, Micromeritics Co., Norcross, GA, USA	III
Transmission electron microscopy	JEOL JEM-1400 Plus transmission electron microscope, Tokyo, Japan	III
ULTRA HPLC in-line filter	0.5 µm, Phenomenex Inc, Torrance, CA, USA	II
Water purification system	Millipore DirectQ-UV, Billerica, MA, USA	I, II, IV
X-ray diffractometer	Bruker D8 Discover instrument, Bruker AXS GmbH, Karlsruhe, Germany	III

3.1. Synthesis of materials

The mesoporous silica-based materials, Mobil Composition of Matter No. 41 (MCM-41) and titanium hydrogen phosphate-modified MCM-41 (MCM-41-TP), were synthesized via sol-gel template routes as described in literatures [86,116]. These materials were used in ***Paper I-IV***.

ZnO incorporated into mesoporous silica materials were prepared via pseudomorphic transformation **(*Paper III*)**. The pseudomorphic transformation of commercially available spherical silica microparticles was carried out to produce a pseudomorphic silica material called PM-SiO_2 [117]. The PM-SiO_2 material was then infiltrated with 1-3 cycles of ZnO using a double solvent approach to obtain a nanocomposite sample called the PM-SiO_2/ZnO-1, PM-SiO_2/ZnO-2, and PM-SiO_2/ZnO-3 materials, respectively [118].

The infiltration cycle was done as following: 250.0 mg of the silica particles were dispersed in 4.0 mL of hexane. 190.0 µL of a 2 M aqueous $Zn(NO_3)_2{\cdot}6H_2O$ solution was added to this dispersion, and stirred for 1 h. The hexane phase was then removed carefully, and the particles were dried at room temperature for 4 h. Finally, the particles were calcined at 300 °C for 2 h with a 1 °C/min heating ramp **(*Paper III*)**.

As a reference, smaller ZnO-modified silica nanoparticles (~0.5 µm) were synthesized. The MCM-41-type spherical silica particles were synthesized according to the Lind *et al.* protocol [119]. The ZnO loading of the pore structure followed the same two infiltration/heating cycles protocol as described above **(*Paper III*)**.

3.2. Material characterization

Zeiss GeminiSEM 450 Scanning electron microscopy was used to observe the surface morphology of the synthesized materials. A few nanometers Pt layer was sputtered onto the materials prior to analysis. For the transmission electron microscopy (TEM) measurements, particles were embedded in resin and ultrathin sections were cut using an ultramicrotome Leica EM UC7 to a thickness of 70 nm. JEOL JEM-1400 Plus TEM was then employed at 80 kV acceleration voltage to examine the sections. ASAP-2010 instrument was used to investigate the materials'

porosity with nitrogen physisorption. Bruker D8 Discover instrument was employed to examine the X-ray diffraction spectra of the synthesized material in the 2θ range 1-10° (step size: 0.01°) as well as in the 2θ range 10-70° (step size: 0.04°).

3.3. In-tube extraction packing and SPME Arrow coating procedures

The ITEX packing instruction were similar to those in the literature [69]. The MCM-41-TP and PM-SiO_2/ZnO-2 sorbent materials, were packed separately onto the ITEX tube as follows: 10 mg of deactivated silica wool, 30 mg of adsorbent, 10 mg of deactivated silica wool, and a stainless-steel spring, respectively **(*Papers I-IV*)**, while TENAX-GR sorbent was packed with 60 mg rather than 30 mg **(*Paper II*)**. Each ITEX was then preconditioned with nitrogen flow at 250 ^{0}C for 12 h before first time sampling.

The procedure for SPME Arrow coating was done according to Lan *et al.* [86]. In order to clean the bare SPME Arrow, methanol/water (50/50, v/v) and MilliQ water were used consecutively. After cleaning, the Arrow was sonicated and dried with nitrogen flow. A total of 12 cycles of gentle dipping into adsorbent /PAN mixture were performed on the cleaned SPME Arrow, followed by drying with nitrogen flow between each cycle. The SPME Arrow was then preconditioned at 250 ^{0}C for 12 h before first-time sampling.

3.4. Permeation system

The laboratory-made permeation system was employed to create the gas phase of standards for on-line ITEX and SPME Arrow samplings **(*Papers I-IV*)** [69]. Figure 11 shows how the permeation system produces the gas flow. Briefly, the permeation system consisted of a metal cylinder used to put vials containing pure nitrogen-containing compounds. The metal cylinder was kept in the oven at 30°C, and a constant nitrogen flow (*i.e.* 50 mL min^{-1}) was introduced to flush the permeated model compounds out. Additional nitrogen flows were used for the dilution, with the total dilution of up to 1:10492. The determination of dilution

factors is described in ***Paper IV***. The diluted gas-phase compounds were then directed to the auto sampler's extraction port for sample collections. The compounds' vapors in the permeation system were stabilized overnight before doing the first sampling. In this thesis, a PAL Cycle Composer and PAL RTC autosampler were employed to collect gas samples from the permeation system **(*Papers I-IV*)**.

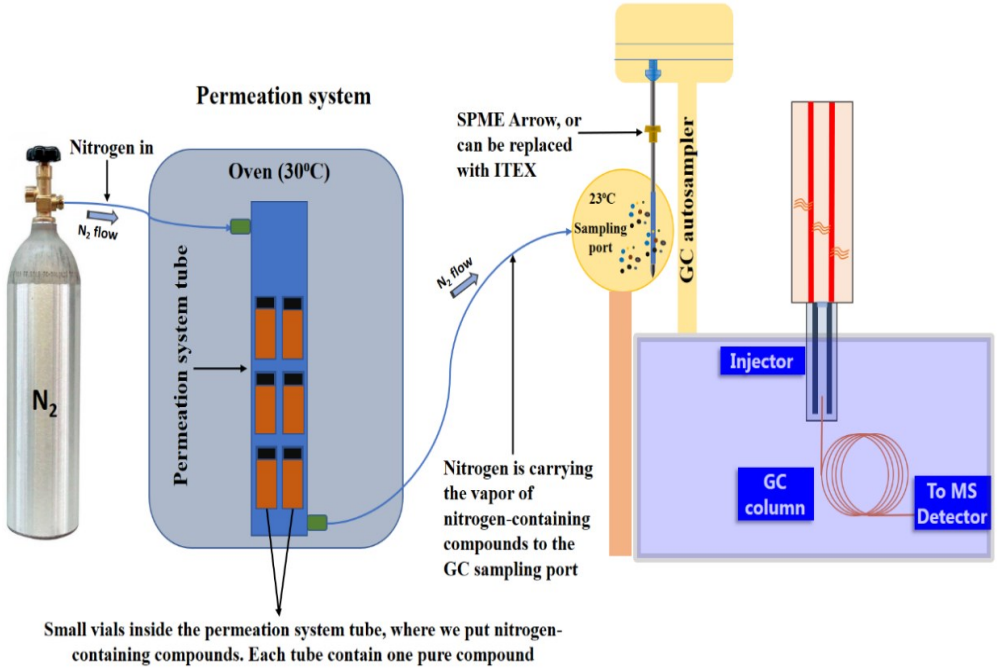

Figure 11. Simple laboratory-made permeation system.

The permeation system was also employed to develop standard calibration curves for quantitative analysis. The compounds used are listed in ***Papers I-IV***. However, for those detected compounds that we did not have the standards, were semi-quantified using the partial least squares regression (PLSR) method. In this case, the data collected from the standard calibration curves were used to estimate the concentration of the identified compounds based on PLSR of the ion intensities **(*Papers I-III*)**.

3.5. Adsorption selectivity study

3.5.1. Selection of in-tube extraction sorbent materials

Several different ITEX sorbent materials were evaluated for the selective extraction of gaseous nitrogen compounds using model VOCs (Table 3). Two different approaches were used to produce headspace samples. The first approach involved the introduction of 1.0 µL of standard solution (5.0 µg mL^{-1} in DCM) into the 20.0 mL headspace vials. The vial was then incubated at 40°C for 15 min **(*Paper III*)**. While the second approach was based on the use of the permeation system **(*Papers I and III*)**.

The selection of sorbent material was done after comparing their affinity towards nitrogen-containing compounds. The chromatogram peak area of the individual compounds was used as response factor.

Table 3. Compounds used for selectivity study

Model compounds used for selectivity study	Paper
Dimethylamine, diethylamine, dipropylamine, dimethyl benzylamine, isobutylamine, pyridine, trimethylamine, triethylamine, 2-butanone, 2-butanol, and p-cymene	**I**
Dipropylamine, hexylamine, isobutylamine, *o*-toluidine, pyridine, triethylamine, acetonitrile, butanol, camphene, cyclohexane, ethyl acetate, hexane, hexanal, methyl isobutyl ketone, octanal, propanol, tetrahydrofuran, toluene	**III**

3.6. ITEX accessories

ITEX's trap accessory was prepared to remove undesired VOCs (*i.e.* other than nitrogen-containing compounds) from air samples. In this study, three different sorbents namely polyacrylonitrile (PAN) 10%, Tenax-TA, and Tenax-GR were evaluated for ITEX's trap accessory. Tetrahydrofuran (THF) was added to materials, separately, to produce material slurry and then coated into the Pasteur pipet's walls and then dried in the oven at 90 ˚C. The coating procedure was

repeated five times to obtain proper coating thickness. The coating material was then conditioned at 250 ˚C for 30 minutes to remove the THF and other impurities **(*Paper I*)**.

As an active sampler, ITEX system allows the simultaneous collection of gas and particle phase compounds. In order to collect gas phase only using ITEX, a polytetrafluoroethylene (PTFE) filter with the pore size of 0.2 µm was used as ITEX filter accessory to remove aerosol particles from air samples [120]. Figure 12 describes the schematic of the ITEX sampling system furnished with trap and filter accessories **(*Paper I*)**.

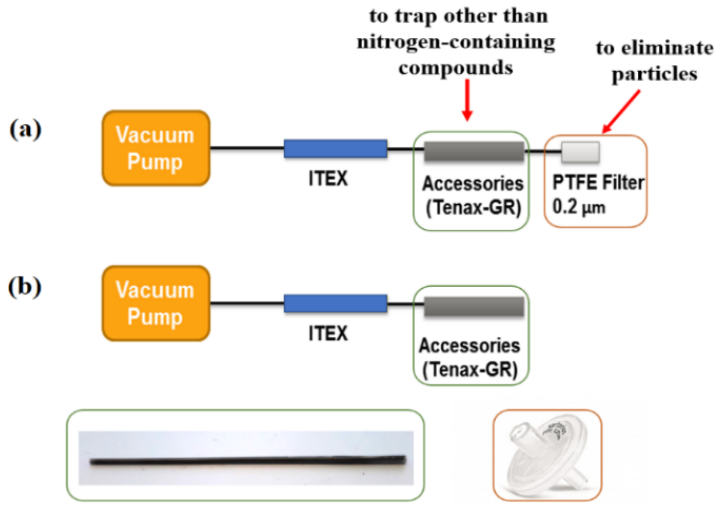

Figure 12. Schematic of ITEX sampling system to selectively collect the nitrogen-containing compounds from (a) gas phase and (b) aerosols (gas and particle phases). This figure is adopted from ***Paper I***.

3.7. Sampling and desorption conditions of ITEX and SPME Arrow

Before sampling, ITEX and SPME Arrow were pre-conditioned at 250°C for 10 min under inert gas N_2, followed by internal standard addition (*i.e.* decafluorobiphenyl vapor) and subsequent sample collections. For desorption, ITEX was heated at a temperature of up to 250 °C for one minute, and the analytes were injected at a

speed of up to 200 µl s^{-1} with an injection volume of 800 µl **(*Papers I-III*)**, whereas SPME Arrow was directly desorbed in the GC inlet for one minute at 250 °C **(*Papers I-III*)**. In the case of on-site analysis, the preconditioning and desorption conditions were similar as in the laboratory as described above, except the ITEX pre-heating time was 2 min **(*Paper I-II*)**.

3.7.1. Sampling and desorption condition of ITEX and SPME Arrow for kinetic studies

For the kinetics study **(*Paper IV*)**, two different adsorbents (MCM-41-TP and TENAX-GR) for ITEX systems and three different coating materials (MCM-41, MCM-41-TP, and DVB/PDMS) for SPME Arrow systems, were compared.

The sampling times for the adsorption kinetics study ranged between 2 and 30 min for both ITEX and SPME Arrow systems (Fig. 13). The gaseous nitrogen-containing compounds were collected from the permeation system at a constant temperature of 23°C **(*Paper IV*)**. Both ITEX and SPME Arrow systems then desorbed the analytes at the temperature of 250°C with desorption volumes and rates of 800 µL and 50 µL·s^{-1} for ITEX system, and a 1-min desorption for SPME Arrow, respectively.

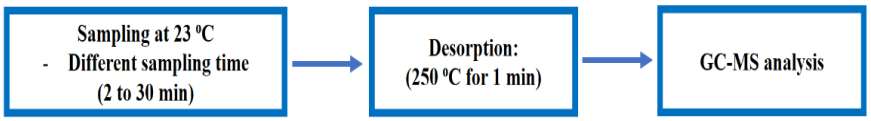

Figure 13. Diagram for adsorption kinetic study

In order to study desorption kinetics, Origin 2022b was employed to design the experiment using a central composite design 2^2 + star, involving 11 experiments (3 center points) per adsorbent material. All experiments used the same sampling time, which was 15 min for ITEX system, and 20 min for SPME Arrow system. The sample collection temperature for both ITEX and SPME Arrow systems was 23°C, while the desorption temperatures ranged from 180 to 280°C. The desorption time in SPME Arrow was varied from 20 to 100 s for each desorption temperature, whereas the length of desorption time in ITEX system was calculated by the ITEX desorption flow rate which was from 20 to 80 µL·s^{-1} (Fig. 14). Three replicates of

each experiment were made, and average retention times and peak areas were used in the calculations.

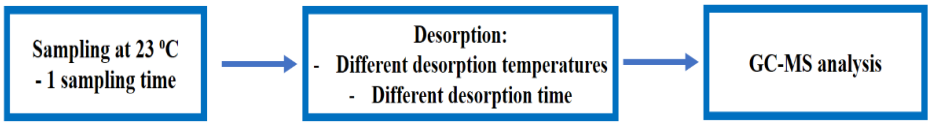

Figure 14. Diagram for desorption kinetic study

3.7.2. SPME Arrow conditions for vapor pressure study

The DVB/PDMS-SPME Arrow sampler was used to study vapor pressures of selected nitrogen-containing compounds **(*Paper IV*)**. The SPME Arrow was conditioned for 10 min at 250°C, followed by 10 min sampling from the permeation system. Desorption was done in the GC inlet for one min at various injector temperatures, *i.e.* 100, 150, 200, and 250°C. This study was done in a constant pressure of 70.0 kPa. The GC oven was maintained at six to eight isothermal temperatures that differed by five degrees during each run in order to build an $I_x(T)/T$ plot for each different desorption temperature (Table 4 and ***Paper IV***). The temperature range for the measurement was between 35 and 80°C (Table 4 and ***Paper IV***).

3.8. Drone platform construction

A remote-controlled Geodrone X4L was employed to carry out miniaturized air sampling and analysis systems. With the dimension of 58x58x37 cm (width x depth x height), it was furnished with a modified sampling box that contained up to four SPME Arrow units, up to four ITEXs, and a sampling pump for ITEX system (Fig. 15). Some portable devices were also attached to the drone, namely a portable BC monitor (AethLabs AE51-S6-1408) and a lab-made CPC. BC device was operated at 880 nm wavelength with the air flowrate of 99 mL min^{-1}. The portable lab-made CPC measured total aerosol particle number concentration for sizes from 20 nm to 5 μm.

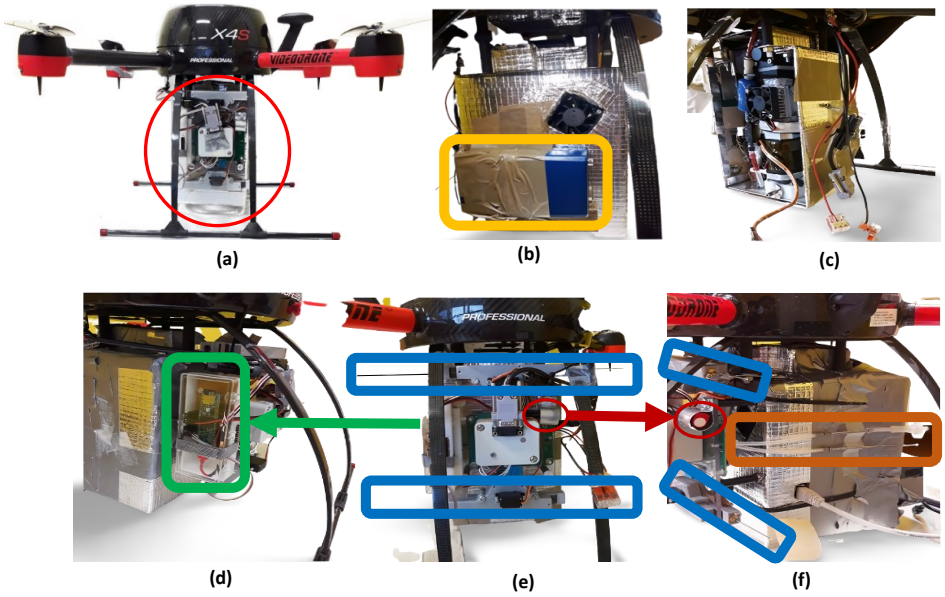

Figure 15. Construction of the air sampling unit and measurement devices for the drone: (a) Air sampling box. (b) BC placed behind the box. (c) CPC placed inside the sampling box. (d) Sensor that measures temperature and relative humidity. (e) Front position of the sampling box consisted of SPME Arrow units (blue) and a VOC sensor (red circle). (f) The sampling box's sides featured ITEX units and filter accessory (brown). This figure is adopted from ***Paper II***.

3.9. Measurement sites and sample collections in the field

3.9.1. VOCs collections from outdoor samples

The samplings were carried out at the SMEAR II station (Station for Measuring Ecosystem–Atmosphere Relations, with the coordinate of 61.846350˚N - 24.295333˚E), Hyytiälä, from 6 to 16 July 2020 and from 4 to 14 October 2021. SPME Arrow units with different coating materials: DVB/PDMS, MCM-41, Carbon WR, were used to collect gas phase samples. While MCM-41-TP-ITEX and TENAX-GR-ITEX sampling systems were used to simultaneously collect gas and particle phases. Both diurnal and vertical profiles of nitrogen-containing compounds were

observed by collecting samples in different time series and heights (height from 0.25 m to 400 m) **(*Papers I and II*)**.

For the time series study, all the air samples were collected at the altitudes of 50 m **(*Paper I*)**. ITEX furnished with trap accessory was exploited to simultaneously collect gas phase and particles, while ITEX furnished with trap accessory + filter accessory was employed to collect the gas phase only **(*Paper I*)**. The concentrations of aerosol particles were then calculated as the subtraction between those two techniques.

The evaluation of ITEX's filter accessory was also studied in ***Paper II***. ITEX furnished with filter accessory was employed to collect the gas phase only. The results obtained were directly compared with those achieved by Carbon WR-SPME Arrow sampling system. In this case, the recovery was calculated from the difference between concentrations obtained by ITEX furnished with filter accessory and by SPME Arrow.

For the vertical profiles observation, the ITEX was used to collect aerosol, while SMPE Arrow was used to collect gas-phase samples. The altitudes of sampling collection were between 0.25 and 150 m in ***Paper I***, and between 50 and 400 m in ***Paper II***. The concentrations of aerosol particles were obtained from the subtraction of aerosol and gas-phase samples. A total sampling time was up to 20 min for each sample. The ITEX airflow ranged from 40 to 78 mL min^{-1}, and it was carefully measured before the sampling and after analyte desorption. The ITEX airflow rates were multiplied with the total sampling time to obtain the ITEX sampling volumes used for quantification.

The VOC composition at the altitudes of 50 m and 400 m was also determined **(*Paper II*)**. A detailed schematic picture on our sampling system can be seen in Fig. 16 (sampling at 50 m for 10 min), Fig. 17 (sampling at 400 m for 10 min), and Fig. 18 (mixed altitudes from 50 m to 400 m).

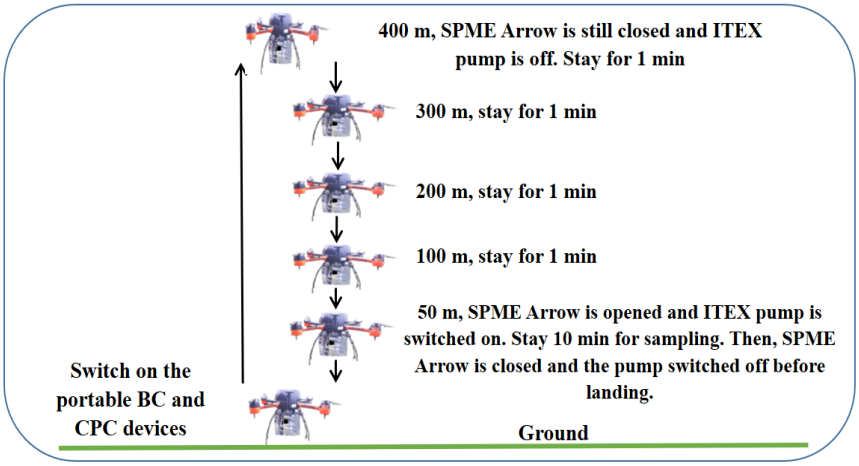

Figure 16. The schematic of sample collection using ITEX and SPME Arrow sampling systems at the altitude of 50 m. This figure is adopted from ***Paper II***.

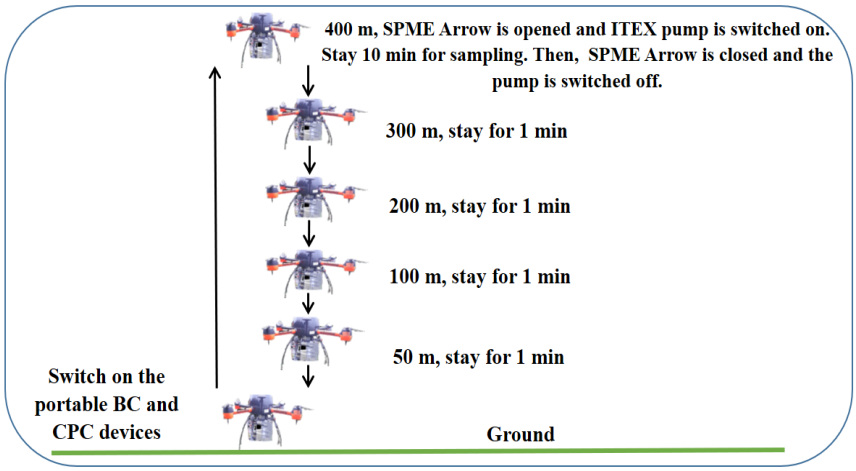

Figure 17. The schematic of sample collection using ITEX and SPME Arrow sampling systems at the altitude of 400 m. This figure is adopted from ***Paper II***.

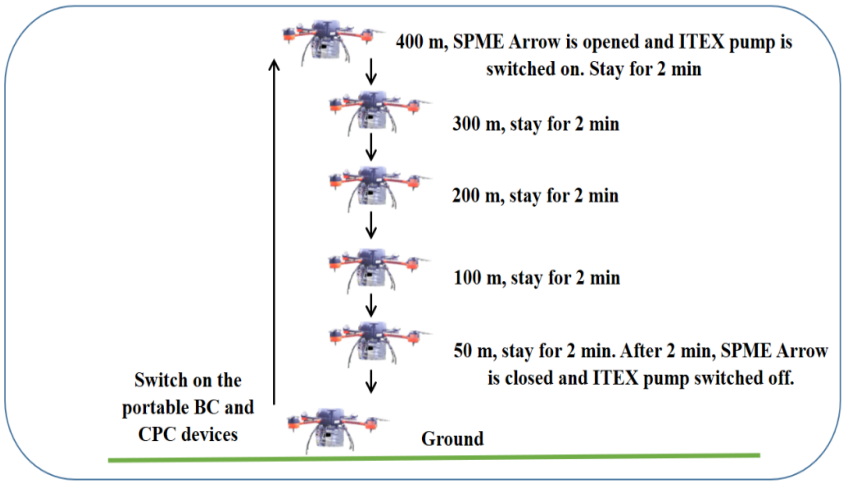

Figure 18. The schematic of sample collection using ITEX and SPME Arrow sampling systems from mixed altitudes, from 50 to 400 m. This figure is adopted from ***Paper II***.

The potential influence of meteorological variables, *i.e.* air temperature, wind speed, wind direction, rainfall, and humidity, on the sample composition, were evaluated using a linear discriminant analysis (LDA) model (***Paper I***).

In addition to sampling in the forest, consecutive outdoor air samples were also collected near the highway located close to Kumpula Campus in Helsinki, Finland. The samples were collected in triplicate in autumn 2022 **(*Paper III*)**.

3.9.2. VOCs collection from Indoor air samples

Indoor air samples were collected from the chemistry laboratory close to the cabinet containing the nitrogen-containing compounds in autumn 2022. The samples were collected for 15 min with the ITEX using a flowrate of 50 mL min^{-1}, and in triplicate (3 consecutive samples). The collected samples were then directly analyzed with the GC-MS system **(*Paper III*)**.

3.9.3. Organic acid collection from outdoor samples

ITEX's filter accessory that was used to collect particles was subsequently analyzed for the determination of the organic acids **(*Paper II*)**. Aerosol particles were

collected onto the filter attached to the ITEX unit in the drone. Aluminum foil was used to wrap all the collected filter samples and placed into separate Minigrip bags which were stored in freezer (-20 °C) prior to analysis.

3.9.4. On-site measurement of black carbon and total particle number

Portable BC and CPC devices as mentioned in section 3.8 were always active on measuring BC and total particle numbers during the flight of the drone (Figs. 16 to 18). The detected BC and total particle numbers obtained with the portable devices were compared with those obtained with reference devices at the SMEAR II Station **(*Paper II*)**.

3.9.5. Cigarette smoke samples

Figure 19 shows the experimental setup used to collect cigarette smoke samples. This setup was designed to simulate the human puffs during the smoking. The total sampling times were 5 min, with ITEX flowrate of 50 mL min^{-1}. The samplings were done in triplicate and then directly analyzed using the GC-MS system **(*Paper III*)**.

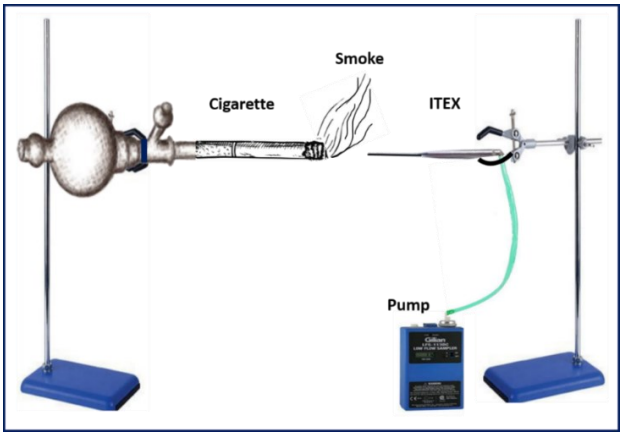

Figure 19. Experimental setup used to simulate human puff during smoking. This figure is adopted from ***Paper III***.

3.10. Gas chromatography-mass spectrometry conditions

The chromatographic separation and identification were achieved with gas chromatography-mass spectrometry (GC-MS). The experimental parameters including types of GC-MS and GC capillary column and their conditions are under Tables 4 and 5.

Table 4. Analytical conditions used during laboratory measurement.

Instrument	GC column	GC conditions	MS conditions	Papers
• GC 6890 N, Agilent • MSD 5975 C, Agilent	InertCap for amines (30 m x 0.25 mm)	• Injector, 250°C • Splitless • Oven T.P, 40 °C (2 min), 20 °C min^{-1} to 250 °C (10 min) • Helium, constant flow rate, 1.2 mL min^{-1}.	• Transferline, 250°C • Ion source, 230°C • Quadrupole, 150°C • EI mode (70 eV) • Scanning range, m/z of 15 to 350	**I-III**
• GC 6890 N, Agilent • MSD 5975 C, Agilent	InertCap for amines (30 m x 0.25 mm)	• Injector, 250°C • Splitless • Oven T.P, 40 °C (3 min), 25 °C min^{-1} to 250 °C (5 min) • Helium, constant flow rate, 1.2 mL min^{-1}.	• Transferline, 250°C • Ion source, 230°C • Quadrupole, 150°C • EI mode (70 eV) • Scanning range, m/z of 15 to 350	**IV**
• GC 6890 N, Agilent • MSD 5975 C, Agilent	HP-1 (30 m x 0.25 mm x 0.1 μm)	• Injector: 100, 150, 200, and 250°C • Splitless • Isothermal, 35, 40, 45, 50, 55, 60, 65, 70, 75, and 80°C. • Helium, constant pressure, 70.0 kPa	• Transferline, between 35 and 80°C • Ion source, 230°C • Quadrupole, 150°C • EI mode (70 eV) • Scanning range, m/z of 29 to 350	**IV**

T.P = Temperature program

Table 5. Analytical conditions used during field measurement.

Instrument	GC column	GC conditions	MS conditions	Paper
• GC 6890 N, Agilent • MSD 5973 C, Agilent	InertCap for amines (30 m x 0.25 mm)	• Injector, 250°C • Splitless • Oven T.P, 40 °C (2 min), 20 °C min^{-1} to 250 °C (10 min) • Helium, constant flow rate, 1.2 mL min^{-1}.	• Transferline, 250°C • Ion source, 230°C • Quadrupole, 150°C • EI mode (70 eV) • Scanning range, m/z of 15 to 350	**I-II**

3.11. Hydrophilic Interaction liquid chromatography-tandem mass spectrometry conditions

Hydrophilic interaction liquid chromatography tandem mass spectrometry (HILIC-MS/MS) was employed for organic acid determination (***Paper II***). Specifically, an Agilent 1260 Infinity high performance liquid chromatography (HPLC) system was coupled to an Agilent 6420 triple-quadrupole mass spectrometer equipped with electrospray ion source (ESI). Chromatographic separations were performed with a 2.1x150 mm SeQuant ZIC-cHILIC HILIC column, with 3 µm particle size, while a KrudKatcher ULTRA HPLC in-line filter (0.5 µm) protected the column from particulate impurities. The ESI was operated in both positive and negative modes.

3.12. Data Processing and statistical analysis

Agilent ChemStation and Agilent MassHunter softwares were used for peak identification and integration **(*Papers I – IV*)**. An Mzmine2 (version 2.53) software consisting of an algorithm Automated Data Analysis Pipeline (ADAP-GC) was exploited to pre-process the untargeted mass spectrometric data for deconvolution and alignment of the chromatographic peaks in the collected samples **(*Papers I-III*)** [61,63,65]. NIST2017 and NIST2020 (NIST MS Search v.2.3) mass spectral databases were used to compare the mass spectra of the aligned peaks and their retention indices. The criterion for the spectral match was >800,

while the maximum allowable difference between experimental and library Kováts retention indices was ± 45 unit.

Origin 2022b and R 3.5.1 software were used for the development and evaluation of the experimental design, including for desorption and conditioning method optimization, while PLSR equations were used for the quantification/semiquantification of the detected nitrogen-containing compounds from air samples **(*Papers I-III*)** [121]. Python 3.9.15 was used to model the adsorption and desorption kinetics with support libraries Matplotlib, Spicy, Numpy and lmfit **(*Paper IV*)**.

The COnductor-like Screening MOdel for Real Solvent (COSMO-RS) model was exploited to calculate saturation vapor pressures of selected nitrogen-containing compounds that involved three-step modeling approaches **(*Paper IV*)**. First, the COSMOconf program that utilized the COSMO-RS model executes a conformer sampling routine where the final conformer structures are calculated on a density functional theory level of theory [122]. The next step is to calculate the conformers in the gas phase on the same level of theory. The last step is by exploiting the COSMOtherm program to calculate a saturation vapor pressure at 25.0°C, where it weights multiple conformers according to Boltzmann distribution of states with different free energies.

Vapor pressures of selected nitrogen-containing compounds were also defined using retention indices (I_x) approach as described in Hartonen *et al.* [123]. The laboratory experiments are described in section 3.7.2. Retention time data that were collected from these experiments were used to calculate the analytes' retention indices with the help of the n-alkane series, and the data points were plotted to draw an $I_x(T)/T$ plot for each different desorption temperature to obtain analytes' retention indices at 298 K. The vapor pressures of analytes then were calculated using Equations (17) and (18) below **(*Paper IV*)**.

$$ln\left(\frac{p}{p_0}\right) = \left(1 - \frac{T_0}{T}\right) e^{(A_0 + A_1 T + A_2 T^2)} \quad (17)$$

$$lnP = lnP_z + \frac{(100z - I_x) ln\left(\frac{P_z}{P_{z+1}}\right)}{100} \quad (18)$$

where p is the n-alkane vapor pressure, p_0 is a normal atmospheric pressure, p_z and $p_{(z+1)}$ are the vapor pressures of the n-alkanes eluting before and after the analyte, respectively. T_0 is the temperature at which the constants were determined, T is the temperature where the experiment was conducted, whereas A_0, A_1, and A_2 are constants of n-alkanes in which the values were taken from literature [124].

4. Results and discussion

The main objective of this thesis was to develop microextraction techniques to selectively collect nitrogen-containing compounds from air samples. In order to achieve this aim, the applicability of different materials as ITEX sorbents was evaluated. Some of the selected materials were also employed as SPME-Arrow sorbents. The physicochemical properties of different materials in the collection of nitrogen-containing compounds, were compared when they were packed into the ITEX and coated onto the SPME Arrow sampling systems. The vapor pressures of the selected nitrogen-containing compounds were also studied to identify their behaviors that would be useful for analysis. In order to improve the selectivity and sensitivity of the ITEX sampling system, accessories were added, and a new sorbent material was synthesized. The applicability of ITEX and SPME Arrow sampling systems were also compared for the collection of nitrogen-containing compounds in air. This section summarizes the main findings obtained from both laboratory studies and on-site measurement in the boreal forest. More detailed information is presented in the original articles.

4.1. Saturation vapor pressure of nitrogen-containing compounds

Two methods were used to determine the saturation vapor pressures of the selected nitrogen-containing compounds, experimentally using a retention index (I_x) approach after GC-MS analysis [123], and from computational modelling utilizing the COSMO-RS model [125,126].

An SPME Arrow sampling system coated with DVB/PDMS material was exploited for vapor pressure determination in the laboratory using the I_x approach.

DVB/PDMS presents a medium polarity sorbent that is critical for sampling collection in order to reduce the discrimination towards very non-polar and polar volatile nitrogen-containing compounds [127]. A non-polar column, HP-1 MS was used as the stationary phase to prevent some polar interactions, such as weak hydrogen bonding, which lengthen the retention times of model compounds relative to those of the n-alkane reference compounds, resulting in the lower vapor pressure values [123]. The analytes' retention indices from each experiment were plotted to draw an $I_x(T)/T$ plot to obtain analytes' retention indices at 25 °C.

The study was conducted at four injector temperatures. The accuracy of the measured vapor pressure values was accessed by comparison to those found in the literature. The vapor pressures of analytes were calculated using Equations (17) and (18), and the results are presented in Table 6 **(*Paper IV*)**.

Table 6. Vapor pressures (p) at 25 °C measured experimentally by GC-MS (retention indices I_x approach), and theoretically calculated using CosmoTherm Program. Samples collected by SPME Arrow coated by DVB/PDMS.

Compound	Formula	p (mmHg)					
		Literature	Theoretical (modelling)	Experimental using I_x with injector T of (°C):			
				100	150	200	250
Triethylamine	$C_6H_{15}N$	57.1 [128]	69.0	55.4	52.7	78.0	133.3
Dipropylamine	$C_6H_{15}N$	20.1 [129]	29.6	11.1	14.7	15.8	13.5
Hexylamine	$C_6H_{15}N$	8.0 [129]	9.8	5.1	6.0	6.7	6.9
1-Me Imidazole	$C_4H_6N_2$	0.5 [130]	0.4	0.2	0.2	0.4	0.45
Pyridine	C_5H_5N	20.7 [131]	13.2	12.8	19.0	17.8	14.6
o-Toluidine	C_7H_9N	0.3 [132]	0.34	0.9	0.9	0.9	0.9

Table 6 shows that when the experiments were conducted at lower injector temperatures, the results of compounds with higher vapor pressure were closer to those found in literature. Triethylamine has the highest vapor pressure at 25 °C, suggesting that it is easier to measure experimentally by using GC-MS technique due to its high gas-phase concentrations, whereas less volatile compounds, such as hexylamine and 1-methylimidazole, needed higher injector temperatures for more accurate results. The order of the vapor pressure values of triethylamine, dipropylamine, and hexylamine, which have the same molecular formula ($C_6H_{15}N$),

demonstrates that branched compounds tend to exhibit higher vapor pressures than corresponding linear isomers.

The laboratory results were also compared to the results modelled by the COSMOconf and COSMOtherm programs that utilize the COSMO-RS model. The computed saturation vapor pressures showed good agreement with experimental and literature values (Table 6), demonstrating that the modeling works well for molecules with just one functional group **(*Paper IV*)**.

4.2. Physicochemical properties of ITEX and SPME Arrow in collection of nitrogen-containing compounds

Understanding the physicochemical properties that control a compound's partitioning between gas and particle phases in the environment is necessary for accurate sampling and measurement. These properties can be used to collect substances by adsorption onto sorbent material of the sampling device, and to release the analytes in a desorption process, *e.g.* in gas chromatography-mass spectrometry (GC-MS). In this thesis work, the adsorption and desorption kinetics of model compounds with different sampling techniques (ITEX and SPME Arrow) and adsorbents (DVB/PDMS, MCM-41, MCM-41-TP, and TENAX-GR) were observed **(*Paper IV*).** The model compounds used in this study were isobutylamine, triethylamine, pyridine, dipropylamine, hexylamine, and *o*-toluidine.

4.2.1. Adsorption kinetics

The adsorption rates of 2-30 min were performed to investigate the rate-limiting step in the mass transfer of analytes through the adsorbent of SPME Arrow and ITEX **(*Paper IV*)**. Among various models tested, only the Elovich model worked in this study.

$$q(t) = \frac{1}{b}\left(\ln\left(t + \frac{1}{ab}\right) + \ln ab\right) \quad (19)$$

The initial adsorption parameter a was calculated by fitting the adsorption data using nonlinear regression to Eq. (19). The peak areas were used as the measured amount of analytes adsorbed by the adsorbent (q), during time t [133–136].

A moderately high R^2 value ($R^2 > 0.800$) indicates that the Elovich model could describe the adsorption kinetics of model compounds to the selected sorbent materials. The adsorbent-adsorbate kinetics will be discussed in more detail in section 4.4.1.

Table 7. Initial adsorption rates (a) and quality of model fit (R^2) of selected compounds with several SPME Arrow and ITEX sorbent materials using Elovich Eq. (19)

Compounds	DVB/PDMS-SPME Arrow		MCM-41-SPME Arrow		MCM-41-TP-SPME Arrow		MCM-41-TP-ITEX		TENAX-GR-ITEX	
	a (area·s^{-1})	R^2	a (area·s^{-1})	R^2	a (area·s^{-1})	R^2	a (area·s^{-1})	R^2	a (area·s^{-1})	R^2
Isobutylamine	50.6	0.959	$3.2{\cdot}10^2$	0.913	14.2	0.844	$1.8{\cdot}10^2$	0.941	$2.1{\cdot}10^2$	0.922
Triethylamine	$2.6{\cdot}10^3$	1.000	$2.2{\cdot}10^3$	0.949	$2.3{\cdot}10^2$	0.971	$2.3{\cdot}10^3$	0.994	$2.2{\cdot}10^3$	0.985
Pyridine	$4.9{\cdot}10^2$	0.997	$2.7{\cdot}10^2$	0.950	38.9	0.969	$3.1{\cdot}10^2$	0.989	$4.4{\cdot}10^2$	0.953
Dipropylamine	$3.8{\cdot}10^3$	0.992	$6.5{\cdot}10^2$	0.913	$1.3{\cdot}10^2$	0.954	$1.6{\cdot}10^3$	0.984	$1.8{\cdot}10^3$	0.954
Hexylamine	94.2	0.856	80.4	0.796	26.3	0.927	$5.0{\cdot}10^2$	0.949	$3.0{\cdot}10^2$	0.915
o-Toluidine	$1.9{\cdot}10^2$	0.950	27.2	0.889	8.0	0.908	72.2	0.947	53.8	0.904

As can be seen in Table 7, in general active ITEX sampling methods showed higher adsorption rates than the passive SPME Arrow, most probably due to the aid of the pump that speeded up the sample enrichment. While in passive SPME Arrow sampling, the adsorption rates were mostly affected by the adsorbent's surface functional group and pore size **(*Paper IV*)**.

4.2.2. Desorption kinetics

The Pseudo-first-order (PFO) model was used to study the desorption of targeted analytes from the adsorbent materials of two different techniques, passive SPME Arrow and active ITEX sampling systems, with good model fitting (*i.e.* $R^2 > 0.9$ for 72% of total experiments). Desorption parameters used in SPME Arrow were desorption temperature and time, while in the active ITEX sampling, in addition to heat, gas flow pushing the analytes out from the adsorbent was exploited **(*Paper IV*)**.

The active ITEX sampling demonstrated faster desorption rates than the passive SPME Arrow, which is similar to that in the adsorption kinetics study **(*Paper IV*)**. This is most probably due to the extra pressure used in the ITEX as a driving force to push the analytes out for desorption. An efficient heater that is placed directly around the ITEX tube (Fig. 8) also aids in quick desorption. Therefore, with the combination of higher adsorption rates, bigger adsorption volume, and faster desorption rates, ITEX is considered better for the analysis, especially when gas chromatography is used with need for quick injection.

4.3. Sorbent selectivity for ITEX

Four sorbent materials, namely MCM-41, MCM-41-TP, porous ZnO, and PAN 10%, were evaluated for ITEX sorbent selectivity **(*Paper I*)**. The comparison of the selected ITEX sorbents in extracting the model compounds with different functional groups are shown in Fig. 20.

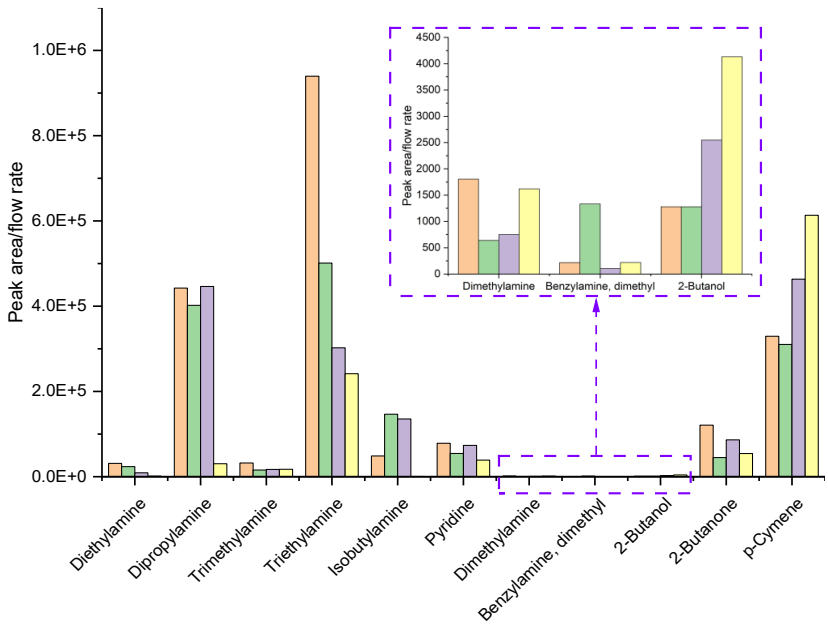

Figure 20. Comparison of ZnO, MCM-41-TP, MCM-41, and PAN 10% as ITEX sorbents in trapping compounds in terms of GC-MS normalized peak area (peak area/ITEX flow rate). This figure is adopted from ***Paper I***.

Overall, ZnO as an ITEX sorbent showed the highest extraction efficiency towards nitrogen containing compounds among other sorbents, except for isobutylamine and dimethyl benzylamine. However, the ZnO-ITEX encountered a mechanical issue where it was quickly getting blocked only after a few extraction cycles.

MCM-41 and MCM-41-TP exhibited slightly lower extraction affinity than ZnO but better than PAN 10%, particularly for all aliphatic and aromatic amines **(*Paper I*)**. Although MCM-41 demonstrated better extraction efficiency than MCM-41-TP when they were used as coating materials of SPME Arrow (Table 7), MCM-41-TP showed better selectivity towards a wider range of nitrogen-containing compounds such as for diethylamine, dimethylbenzylamine, isobutylamine, and triethylamine, due to the presence of the titaniumphosphate (-TP) enhancing its surface acidity (Fig. 20). In addition to amines, MCM-41 also extracted ketones, alcohols, and hydrocarbons which we tried to eliminate. Hence, the MCM-41-TP was regarded as the best selective material for extraction of amines without any ITEX mechanical problems **(*Paper I*)**.

4.4. Sorbent selectivity study based on their physicochemical properties.

The sorbent selectivity was also investigated further by using passive SPME Arrow sampling in terms of their physicochemical phenomena, specifically their adsorption and desorption kinetics **(*Paper IV*)**. In the passive sampling approach, both adsorbent pore size and surface functional groups play significant roles in the adsorption and desorption processes **(*Paper IV*)**. In this section, the selective mesoporous silica-based sorbents (described in section 4.3), namely MCM-41 and MCM-41-TP, were compared with DVB/PDMS, which is a universal type of sorbent for VOCs collection.

4.4.1. Adsorbent-adsorbate adsorption kinetics.

The curve shapes (*i.e.* concave upward) shown in Fig. 21, explained that the dominant mechanism of the intraparticle mass transfer of all sorbents is a surface diffusion model, that belongs to physical adsorption [137,138]. Since there is limited

information in the literature about the adsorption kinetics of nitrogen-containing compounds in mesoporous materials, the transport mechanism could be simplified by assuming that the intraparticle transport is controlled by pore or surface diffusion. However, there have been some publications that revealed the possibility of poor adsorbent-adsorbate interactions on mesoporous adsorbents [139,140]. In this study, the curve did not achieve the plateau shape, indicating there was no pore condensation on the mesoporous silica **(*Paper IV*)**.

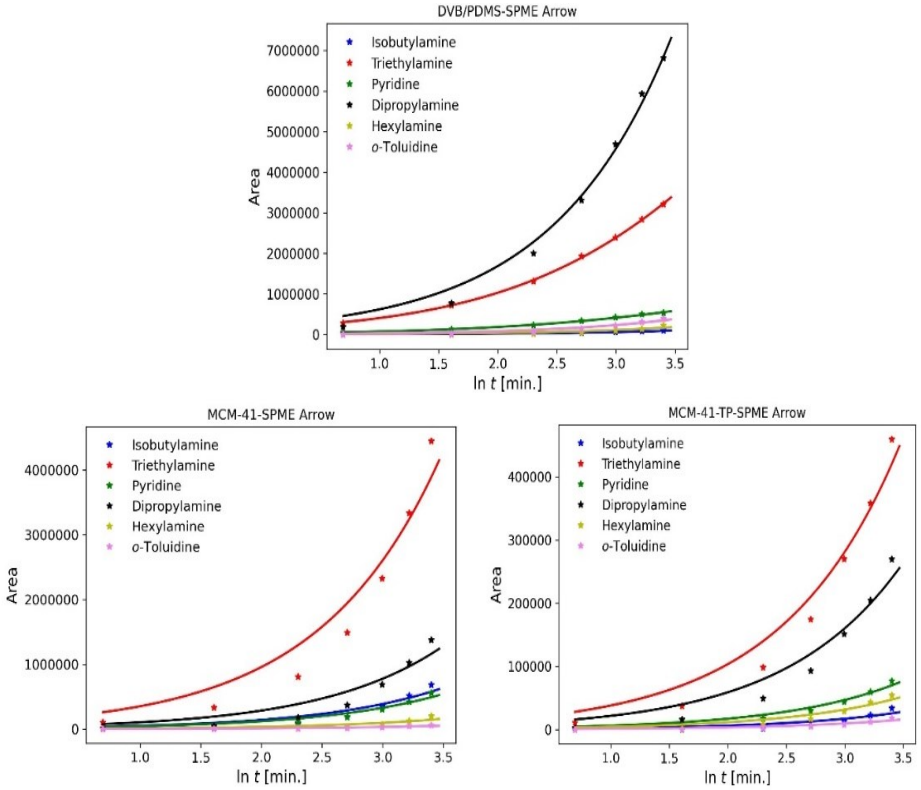

Figure 21. Adsorption kinetic plots that were fitted with the Elovich model for DVB/PDMS-SPME Arrow, MCM-41-SPME Arrow and MCM-41-TP-SPME Arrow systems. This figure is adopted from ***Paper IV***.

In passive SPME Arrow sampling, the material's pore size played an important role due to the random diffusion of molecules onto the pore channels. DVB/PDMS with pore sizes of 40 nm gave comparable initial kinetic rates (see Table 7, parameter *a*) to an MCM-41 (pore size 3.8 nm). This can be explained by the fact that even though

the DVB/PDMS sorbent had larger pore size, its neutral and hydrophobic surface afforded limited interactions with the highly polar nitrogen-containing compounds. Whereas the silanol group on the surface of the silica-based MCM-41 coating material allowed it to interact with basic analytes, like the nitrogen-containing compounds. The addition of –TP group to the MCM-41 unfortunately decreased the material's volume, resulting in a slower adsorption rate than the original MCM-41 (Table 7, parameter *a*). However, both MCM-41 and MCM-41-TP showed the same order in adsorbing nitrogen-containing compounds based on compounds' basicity, where the most basic amines posed the fastest adsorption rates. The basicity order for the alkyl group of gaseous nitrogen-containing compounds is as follows: tertiary (most basic) > secondary > primary (least basic). In the case of aromatic compound (pyridine), the aromatic ring decreases its basicity due to the nitrogen atom directly linked to an aromatic ring, which affects its electron withdrawing properties.

4.4.2. Adsorbent-adsorbate desorption kinetics.

The desorption rates were calculated using the PFO model, and it was found that for all analytes desorbed from the adsorbents under study, the rate increased as the temperature increased **(*Paper IV*)**.

The DVB/PDMS material demonstrated faster desorption rates than MCM-41 and MCM-41-TP as sorbents in releasing nitrogen-containing compounds **(*Paper IV*)**. The low affinity sorption sites of the DVB/PDMS sorbents, where the analytes are attached via physisorption, can be the cause of the analytes' rapid release. The weak van der Waals forces contribute to the physisorption when the molecules are sufficiently close, thus resulting in easy desorption especially with the passive SPME Arrow sampling technique.

The slower increase in k_d rates in desorption experiments using sorbents MCM-41 and MCM-41-TP indicated the desorption process from higher affinity sorption sites [141], supporting that in addition to physisorption, chemical adsorption may be involved. This explains why the desorption did not easily occur as chemical adsorption is stable [142]. The silanol groups on the mesoporous silica surface might interact with the nitrogen atom in the amine groups that were responsible for the hydrogen bonding [143–145]. The hydrogen bonds are weaker than ionic or

covalent bonds but stronger than van der Waals forces [146,147]. Owing to the energies of 1-40 kJ mol^{-1}, the intermolecular hydrogen bonding can be disrupted at high temperature [146], as they were in this work where the desorption temperatures ranged from 180 to 280°C. Raised temperature increases the kinetic energy of the molecules, which decreases the amount of hydrogen bonding.

The silanol group on mesoporous silica surface and the titanium phosphate (–TP) grafted on mesoporous silica (MCM-41-TP) could also interact with gaseous amines via Lewis and Brønsted mechanisms [145,148–150]. In this case, amines act as a Brønsted-Lowry base since they have a lone electron pair that is used to accept protons [151].

It can be concluded that MCM-41 is regarded as the best option for SPME Arrow's adsorbent for the collection of volatile nitrogen-containing compounds due to its adsorption kinetics rates compared to other adsorbents under study. A thermal desorption approach can be used to address the MCM-41-SPME Arrow's slower desorption rates because of the chemical interaction that might be present. Further studies, including longer sampling time, are required to prove this chemisorption theory. However, since the MCM-41-TP is proved to be more selective than the MCM-41 material, then the use of ITEX packed with MCM-41-TP, as described also in sections 4.2 and 4.3, is recommended for the most selective sampling method to collect nitrogen-containing compounds and best for GC-MS analysis.

4.5. Sampling accessories for ITEX

Two different accessories were investigated in this study, namely a trap accessory made from the material coated in the Pasteur glass pipet and a filter accessory (PTFE filter) **(*Paper I*)**.

4.5.1. The evaluation of ITEX trap and filter accessories

Tenax-GR was chosen among three different sorbents as the best material for the ITEX trap accessory, since it captured more alcohols and ketones (Fig. 22). In comparison to TENAX-GR, TENAX-TA as a trap accessory provided slightly better recovery for several model compounds such as dipropylamine, isobutylamine, and

triethylamine, but this material did not effectively trap 2-butanol, 2-butanone, and p-cymene.

According to Fig.22, further studies exploiting other types of materials as sorbent trap accessory, which more selectively retain non-polar compounds and without losing much of the targeted nitrogen-containing compounds, is needed.

In the case of filter accessory, PTFE as hydrophobic material was selected due to its low background, interference-free determination, and low affinity for water [152,153]. Since the ITEX can simultaneously collect both gas phase and aerosol particles, the PTFE filter accessory can prevent the particles from entering the ITEX if one wants to collect only gas phase compounds (Schematic is shown in Fig. 12) **(*Papers I and II*)**.

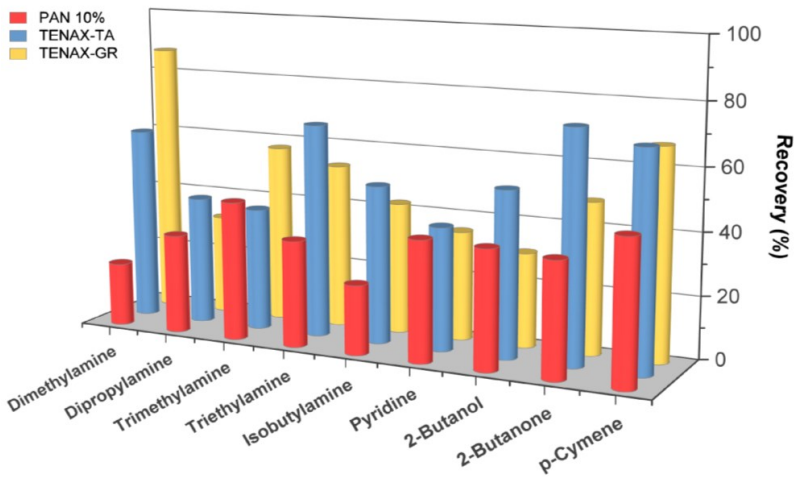

Figure 22. Compounds recovery after the use of PAN 10%, TENAX-TA, and TENAX-GR as materials for trap accessory. The trap accessory was placed in front of the ITEX (Fig. 12b). The sorbent material packed in the ITEX tube was MCM-41-TP. This figure is adopted from ***Paper I***.

The applicability of ITEX equipped with the trap and filter accessories, and SPME Arrow for the collection of gaseous amines was compared. As described in sections

4.3 and 4.4, MCM-41 was selected as the best sorbent material for SPME Arrow, whereas the material used for the ITEX was MCM-41-TP.

As can be seen in Fig. 23, MCM-41-TP-ITEX, furnished with trap-and-filter accessories, collected the gas-phase higher chain amines (≥C3) better, whereas the MCM-41-SPME Arrow was better for collection of lower chain amines such as dimethylamine and trimethylamine **(*Paper I*)**. This study demonstrates good agreement with the desorption kinetics study as described in section 4.4.2. The consistent results are shown in Table 7 (section 4.2.1), where MCM-41-TP-ITEX exhibits faster initial adsorption rates (a) for higher chain amines than MCM-41-SPME Arrow **(*Paper IV*)**. Only gas-phase samples were used for the kinetics research.

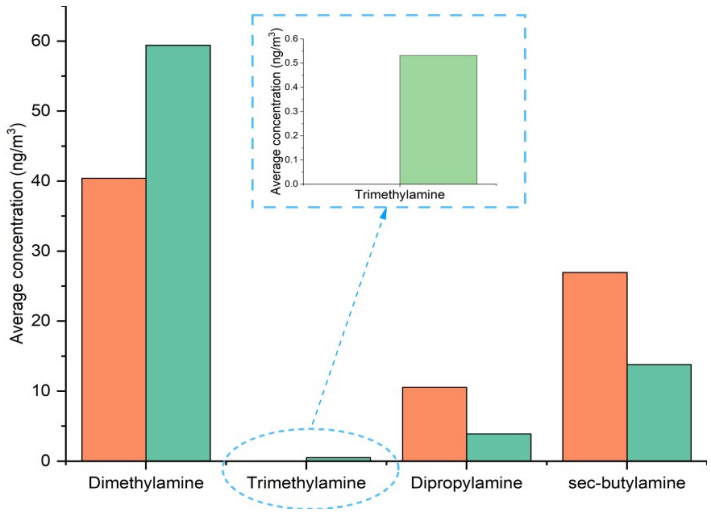

Figure 23. Comparison of MCM-41-TP-ITEX (ITEX furnished with trap-and-filter accessories) and MCM-41-SMPE Arrow for collection of gas-phase amines. This figure is adopted from ***Paper I***.

The evaluation of the ITEX filter accessory was also conducted in a different study targeting VOCs **(*Paper II*)**. In this study, a filter accessory was attached to the ITEX packed with TENAX-GR, which was used as a sorbent material, instead of a trap accessory. TENAX-GR was selected as ITEX sorbent due to its good capability

to collect different VOCs present in the air [61,69]. Similarly, the SPME Arrow coated with carbon wide range (Carbon WR) was selected for comparison.

The concentrations of the VOCs collected from atmospheric outdoor air by TENAX-GR-ITEX furnished with a filter were comparable with those obtained by the Carbon-WR-SPME Arrow, even though they are not exactly the same (Fig. 24). Slightly higher concentrations obtained by the ITEX system could be caused by higher collected amount compared to that collected by the passive SPME Arrow sampler.

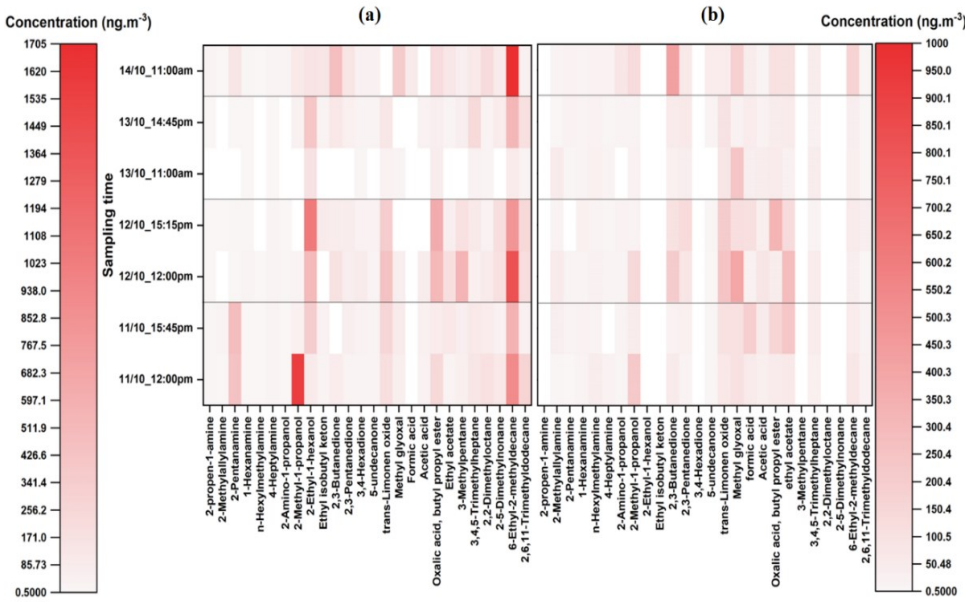

Figure 24. Evaluation of ITEX filter accessories in collecting gas phase. The gaseous samples were collected using (a) TENAX-GR-ITEX system with filter accessories and (b) Carbon WR-SPME-Arrow system. White color represents that a compound was not detected. This figure is adopted from ***Paper II***.

Table 8. Recoveries obtained for compounds collected by ITEX sampling system furnished with filter accessory.

Compounds	Recovery (%)	Compounds	Recovery (%)
2-Methyl-1-propanol	81.4	3,4,5-Trimethylheptane	26.8
2,3-Butanedione	58.3	6-Ethyl-2-methyldecane	37.5
2,3-Pentanedione	84.9	2,6,11-Trimethyldodecane	13.2

Compounds	Recovery (%)	Compounds	Recovery (%)
5-Undecanone	9.2	2-methyl-2-propen-1-amine	99.2
Trans-limonen oxide	94.4	2-Pentanamine	87.2
Methyl glyoxal	98.8	1-Hexanamine	96.8
Acetic acid	79.7	n-Hexylmethylamine	15.3
Oxalic acid, butyl propyl ester	5.8	4-Heptylamine	64.9
Ethyl acetate	95.1	2-Amino-1-propanol	41.4

Alkanes, which are non-polar compounds, only show recoveries of about <50 % (Table 8), while the more polar compounds, such as alcohols and nitrogen-containing compounds, were mainly found at higher recoveries from 50 % to 99 %. PTFE that has a non-polar structure most likely adsorbed the non-polar compounds due to the *like dissolve like* principle [154,155]. This study demonstrated that ITEX furnished with PTFE filter does not only allow ITEX to remove particles, but is also excellent for the collection of polar compounds, such as gaseous nitrogen-containing compounds **(*Paper II*)**.

4.6. Synthesis of new sorbent material

As has been described in section 4.3, porous ZnO as an ITEX sorbent demonstrated a strong affinity towards amines [61,69]. However, these materials had poor mechanical stability, getting blocked after a very small number of analyses. Another study found that functionalized mesoporous silica material has excellent mechanical stability for ITEX packing in addition to good selectivity for the collection of nitrogen-containing compounds. Unfortunately, the selectivity of mesoporous silica materials towards nitrogen-containing compounds was not as good as porous ZnO [61]. In order to acquire both good selectivity and mechanical stability, ZnO-modified mesoporous silica materials were evaluated in terms of selectivity and mechanical stability for the collection of nitrogen-containing compounds from air **(*Paper III*)**.

In this study, commercial silica microspheres with a particle diameter of ~5.0 μm were modified using the pseudomorphic transformation approach to produce a material with narrow mesopores (2.75 nm), while the particles' spherical morphology was retained (sample PM-SiO_2 in Figs. 25 and 26a) [117,156]. The

original pore structure in the silica material is rearranged during pseudomorphic transformation process to an ordered MCM-41-like pore structure.

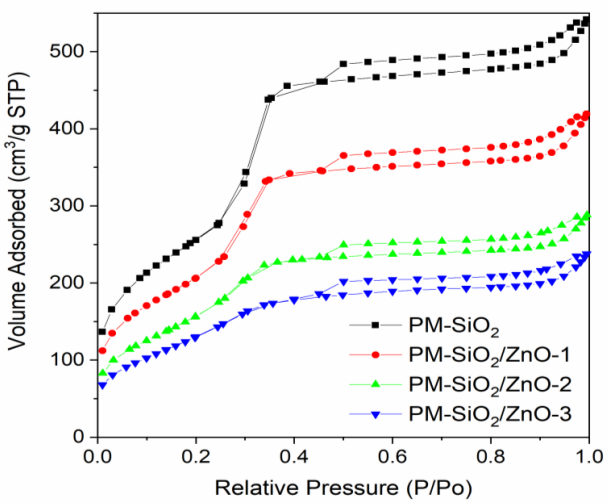

Figure 25. Nitrogen physisorption isotherms of (a) the PM-SiO_2/ZnO nanocomposite materials with different ZnO loadings. This figure is adopted from ***Paper III***.

After the transformation process, the PM-SiO_2 sample showed a typical MCM-41-type material, which is a type IVa nitrogen physisorption isotherm (see Fig 25). The surface area, pore size, and pore volume were 936.0 $m^2 g^{-1}$, ~2.75 nm, and 0.80 $cm^3 g^{-1}$, respectively (Table 9).

Table 9. Textural properties (derived from the nitrogen physisorption data) of the PM-SiO_2 sample with different ZnO loadings.

	Number of ZnO infiltration cycles	BET surface area ($m^2 g^{-1}$)	Pore volume ($cm^{-3} g^{-1}$)	Pore size (nm)
EP-DF-5-120A	0	317	1.03	13
PM-SiO_2	0	936	0.80	2.75
PM-SiO_2/ZnO-1	1	754	0.61	2.75
PM-SiO_2/ZnO-2	2	580	0.42	2.75
PM-SiO_2/ZnO-3	3	485	0.34	2.75

The pores of PM-SiO_2 sample were infiltrated with zinc nitrate salt, which underwent mild thermal processing at 300 °C to produce amorphous ZnO. The infiltration was done in 1-3 cycles to produce PM-SiO_2/ZnO-1, PM-SiO_2/ZnO-2, and PM-SiO_2/ZnO-3, respectively. The morphology of the particles was unaffected by the ZnO infiltration process, but the available surface area and pore volume decreased steadily with each infiltration cycle, suggesting that additional ZnO was introduced into the pore in each step (Table 9).

Figure 26 shows the SEM images of the starting PM-SiO_2 sample and after 3 infiltration cycles that are identical. While Fig. 27 demonstrates the sharp reflections from the zincite phase in the samples loaded with 3 cycles of ZnO (PM-SiO_2/ZnO-3). It indicates that the location of the additional ZnO should be outside of the pore system. Suggesting that when three cycles are used, the pores will be overfilled, and will lead to the formation of large ZnO structures on the exterior of the silica pores.

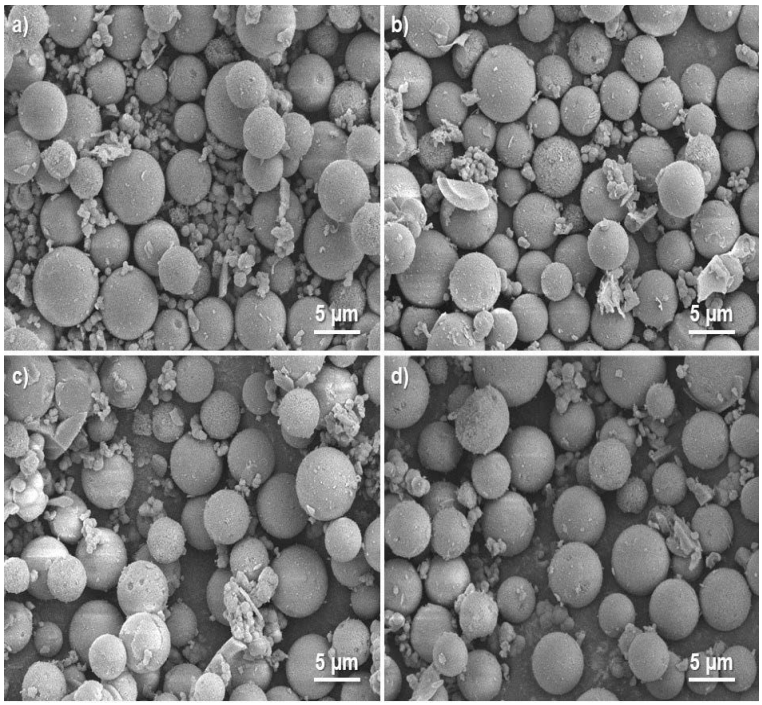

Figure 26. SEM images of the a) PM-SiO_2, b) PM-SiO_2/ZnO-1, c) PM-SiO_2/ZnO-2, and d) PM-SiO_2/ZnO-3 materials. This figure is adopted from ***Paper III***.

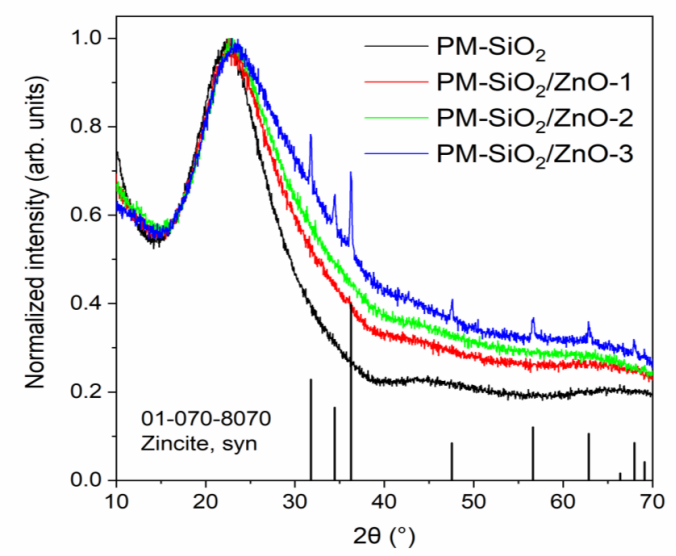

Figure 27. High-angle XRD results of the pseudomorphic silica material as well as of PM-SiO_2 / ZnO composites made with 1-3 infiltration cycles. This figure is adopted from ***Paper III***.

4.7. Selectivity test of PM-SiO_2/ZnO materials towards nitrogen-containing compounds

Figures 28 and 29 show that the sample with three infiltration cycles (PM-SiO_2/ZnO-3) gave the best results in collecting nitrogen-containing compounds. Ballerini *et al* [157] suggested that ZnO surfaces can interact with gaseous amines, by both Lewis and Brønsted mechanisms (with Zn^{2+} and hydroxyl groups on the surface of ZnO, respectively), where the reversible Brønsted interaction would be the dominant one.

The materials' affinity towards the nitrogen-containing compounds increased with the number of ZnO infiltration cycles. However, problems with the mechanical stability of the packed ITEX or backpressure were observed when the number of cycles was higher than 2. To eliminate this problem, PM-SiO_2 material infiltrated with only two ZnO cycles (PM-SiO_2/ZnO-2) was chosen as the best material for further experiments.

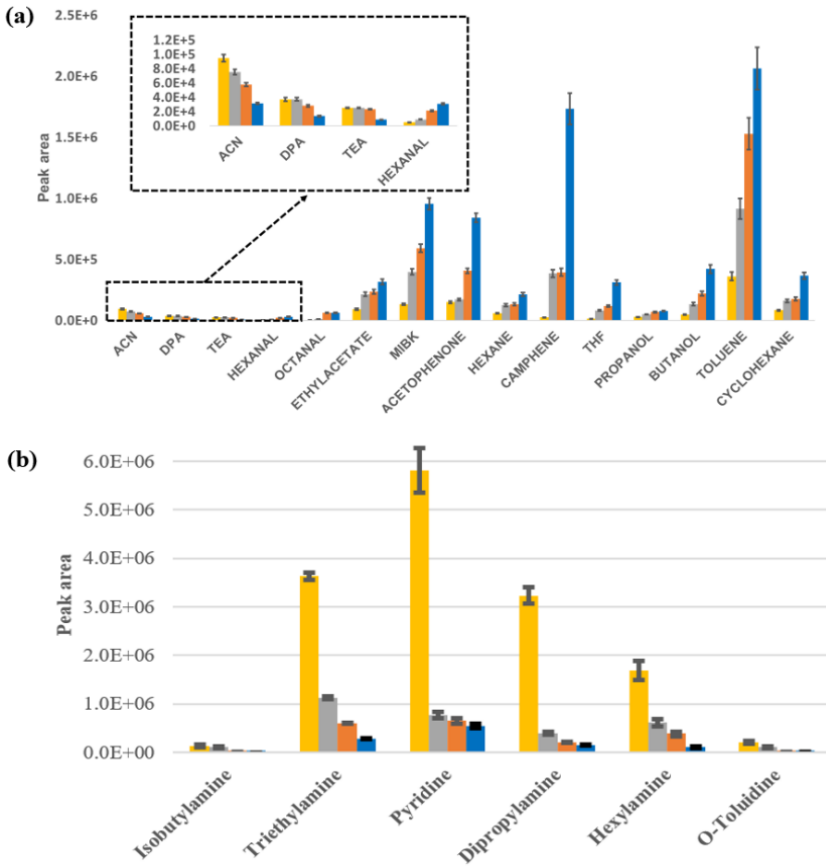

Figure 28. Evaluation of MCM-41-ZnO material selectivity using ITEX from a) headspace vials spiked with model compounds and from b) permeation system (nitrogen-containing compounds). PM-SiO2 (■), PM-SiO2/ZnO-1 (■), PM-SiO2/ZnO-2 (■), PM-SiO2/ZnO-3 (■). Error bars calculated for n= 3. This figure is adopted from ***Paper III***.

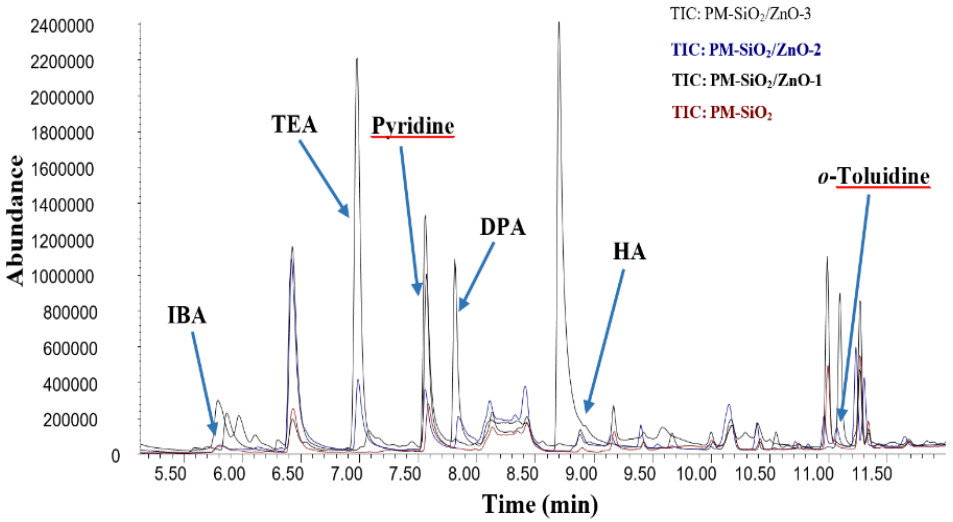

Figure 29. Total ion chromatograms (TIC) obtained for the evaluation of MCM-41-ZnO material selectivity from permeation system. This figure is related to Fig. 28 (b). IBA = isobutylamine; TEA = triethylamine; DPA=dipropylamine; HA=hexylamine.

4.8. Optimization of the desorption and conditioning procedures

4.8.1. Optimization of MCM-41-TP-ITEX for air sampling

Three parameters were optimized in this study: ITEX pre-cleaning, desorption condition, and ITEX breakthrough volume ***(Paper I)***. As a result, a temperature of 250˚C for 300 s was chosen as the optimal setting for conditioning. While for desorption, 800 µl injection volume, 200 µl s^{-1} injection speed, and 240˚C desorption temperature was the optimal method for complete and fast desorption.

In the case of breakthrough evaluation, three different flow rates representing low (33 mL min^{-1}), moderate (70 mL min^{-1}), and high flow (105 mL min^{-1}) were evaluated (Fig. 30). Dipropylamine and trimethylamine showed breakthrough after 15 min using low and mid flow rates, while diethylamine was still quantitatively extracted without breakthrough even up to 30 min. After 20 min of low flow-rate

sampling, breakthroughs were occurring for triethylamine, isobutylamine, and pyridine. Triethylamine with mid flow showed breakthrough after 15 min, while isobutylamine and pyridine only after 20 min of sampling. In the case of high flow, only isobutylamine and pyridine exhibited good extraction affinity for up to 20 min, whereas the others had breakthrough after 10-15 min of sampling. Hence, the ITEX flowrate of 40 to 50 mL min^{-1} and 20 min sampling time were selected as optimal to minimize breakthrough and to provide the best sampling efficiency for quantitative analysis.

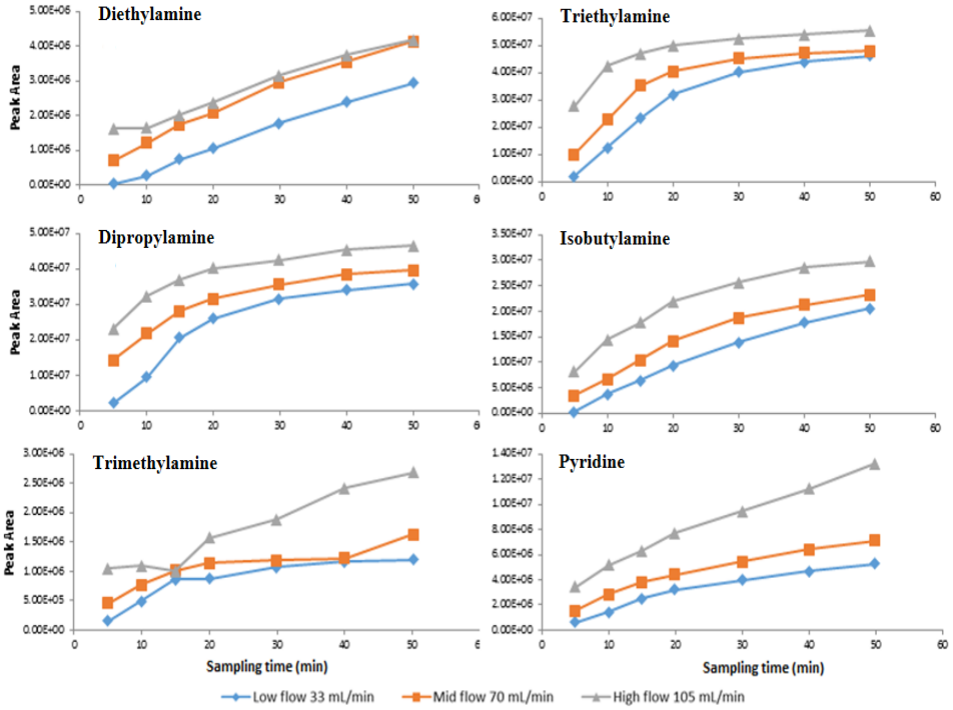

Figure 30. GC-MS response as a function of the sampling time for model compounds for MCM-41-TP-ITEX. The breakthrough was evaluated from the bending of the curve. This figure is adopted from ***Paper I***.

4.8.2. Optimization of PM-SiO_2/ZnO-2 for air sampling

The conditioning, desorption, and breakthrough volume were also optimized for PM-SiO_2/ZnO-2 as an ITEX sorbent. The optimal circumstance for conditioning was at the temperature of 250˚C for 600 s. While for the desorption, 800 µl

injection volume, 50 μl s^{-1} injection speed, and 200 °C desorption temperature was selected as optimal desorption's method **(*Paper III*)**.

Only two low flowrates were used to evaluate the breakthrough, *i.e.* 55.0 and 25.6 mL min^{-1}, since high flow rates (over 100 mL min^{-1}) caused too high ITEX backpressure (Table 10).

Table 10. Evaluation of the ITEX breakthrough volume. Breakthrough expressed as time (min).

Amount of sorbent	**30.0 mg**	
Flow-rate (mL min^{-1})	**55.0**	**25.6**
Isobutylamine	10	10
Triethylamine	20	30
Pyridine	20	20
Dipropylamine	20	20
Hexylamine	10	20
O-Toluidine	10	30

As can be seen in Table 10, the ITEX flowrates of between 25.6 and 55.0 mL min^{-1} and 20 min sampling can be selected to provide the best sampling conditions for all analytes (with the exception of small isobutylamine, which is only 10 min sampling) without breakthrough. The repeatability and reproducibility of ITEX packed with PM-SiO_2/ZnO-2 sorbent were also evaluated, with deviations of under 16.8% and 19.4%, respectively.

4.9. Application of ITEX sampling systems for outdoor air, indoor air, and cigarette samples (*Paper III*).

All the nitrogen-containing compounds under study (*i.e.* dipropylamine, hexylamine, isobutylamine, pyridine, *o*-toluidine, triethylamine) were detected in the indoor air samples. This is due to the selection of the sampling place close to the storage cabinet of the nitrogen-containing compounds in the laboratory.

Acetonitrile was the main compound detected and semi-quantified in cigarette smoke samples. This is not surprising since acetonitrile is a well-known constituent of the cigarette smoke [158]. A relatively high number of amines and nitroso amines were also detected. However, nicotine was found in small concentrations, which is probably due to the design of the experimental setup to reproduce the natural

exhalation process after smoke intake. Compounds with low polarity and volatility might be adsorbed on the walls of the device used to mimic the smoking process.

The results achieved for untargeted analysis of outdoor air samples, collected near Kumpula Campus in Helsinki, showed that the highest concentrations of nitrogen-containing compounds were achieved for secondary and tertiary amines. Other nitrogen-containing compounds such as nitro-, azo-compounds and pyridine were also detected and semi-quantified with lower concentration compared to the previous ones.

4.10. Application in field measurement using drone as a carrier for miniaturized air sampling system

An aerial drone was employed as the carrier of a miniaturized air sampling system, featuring ITEX and SPME Arrow with selective sorbent materials for the reliable collection of nitrogen-containing compounds in both gas phase and aerosol particles. The applicability of this sampling system with the drone was successfully evaluated for the observation of diurnal patterns and spatial distribution of nitrogen-containing compounds in boreal forests in 2020 and 2021 **(*Papers I and II*)**.

Up to 17 nitrogen-containing compounds were detected at the altitudes of 50 m and 150 m with the concentration of up to 2927 ± 15 ng m^{-3} and 5480 ± 27 ng m^{-3} in gas phase and particle phase, respectively **(*Paper I*)**. These results were comparable to another study conducted a year after at higher altitudes (up to 400 m), where up to 18 nitrogen-containing compounds were detected with concentrations of up to 2005 ± 7 ng m^{-3} and 6122 ± 20 ng m^{-3} in gas phase and particle phase, respectively **(*Paper II*)**.

Most amines showed a diurnal variation with a daytime maximum due to their dependency on temperature for their emission, indicating the contribution from biogenic sources, according to both studies **(*Papers I and II*)**. In contrast, the morning and evening hours revealed the peak concentration of amines in the particle phase (Fig. 31). These findings were similar to those studied by You *et al.* (2014) and Hemmilä *et al.* (2018), which found that temperature dependencies

were affecting amine deposition at night, and as temperature rose in the morning, they partitioned back to the atmosphere. [159,160]

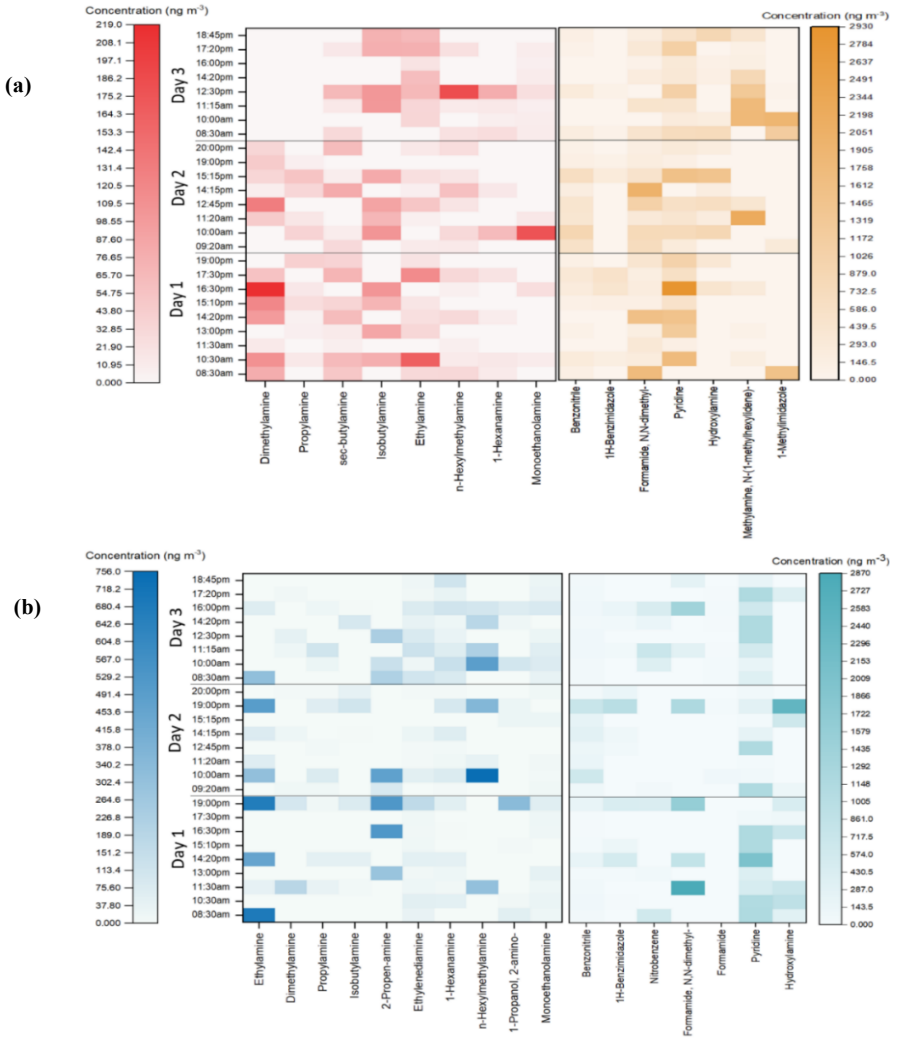

Figure 31. Concentrations of detected nitrogen-containing compounds in the gas-phase (a) and in particle-phase (b) at altitude of 50 m. This figure is adopted from ***Paper I***.

For the vertical profiles (Figs. 32 and 33), the concentration of amines that are emitted mainly from biogenic sources decreased at higher altitudes. This could be due to the turbulent transport and reaction with hydroxyl radical [161]. The soil in boreal forest, that is both a source and a sink of atmospheric alkylamines, might

also contribute to high amine concentration at lower altitudes. The concentrations of nitrogen-containing compounds that are mostly produced by anthropogenic sources, on the other hand, increased at the higher altitudes, suggesting that the wind direction transporting the compounds from other areas is also affecting these results.

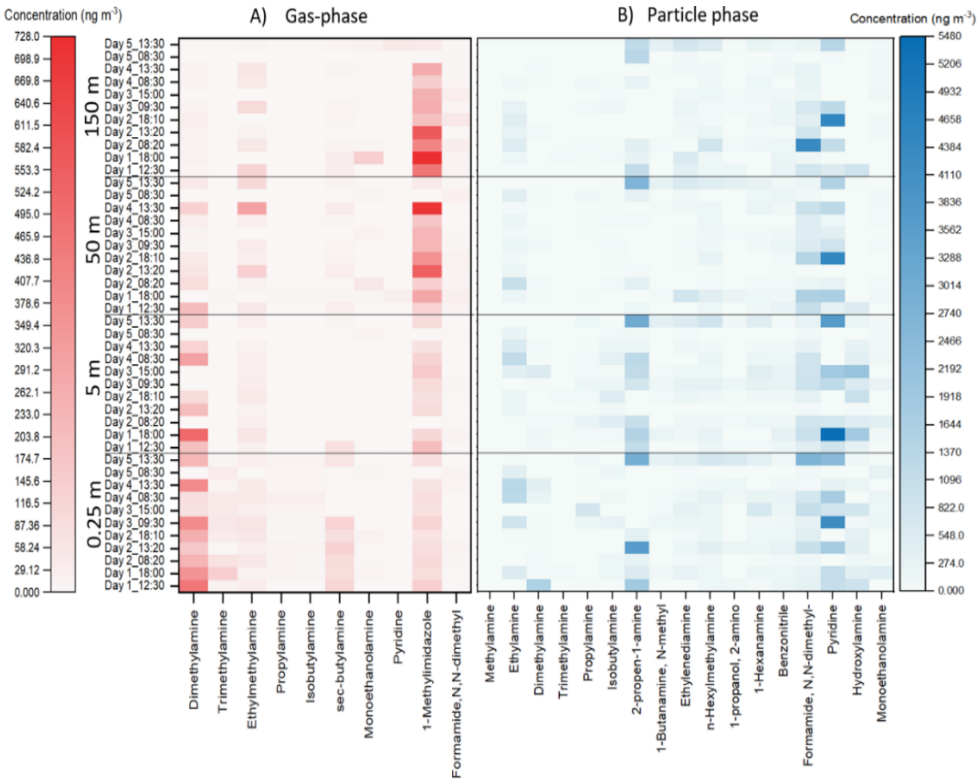

Figure 32. Concentrations of detected nitrogen-containing compounds at different altitudes in A) gas-phase and B) aerosol particles in July 2020. This figure is adopted from ***Paper I***.

Pyridine, which can be emitted from biomass such as peat burning [162,163], was detected in high concentrations only in 2020 (Figs. 32 and 33). Most of the peatlands are located in boreal and subarctic zones, including in Finland. However, some peatlands restorations that have been made to mitigate climate change, most likely affected the significantly lower amount of pyridine in 2021 (Fig. 33).

1-Methyl imidazole and 1H-imidazole were two different imidazoles found in 2020 and 2021, respectively. This could depend on the various sources that produce these compounds. Imidazoles can be formed via reaction between glyoxals (*e.g.* glyoxal or methylglyoxal) and amines, ammonia, or amino acids [164,165]. Glyoxal and methylglyoxal are dicarbonyls that are produced in the atmosphere through the oxidation of various VOCs [47,165,166].

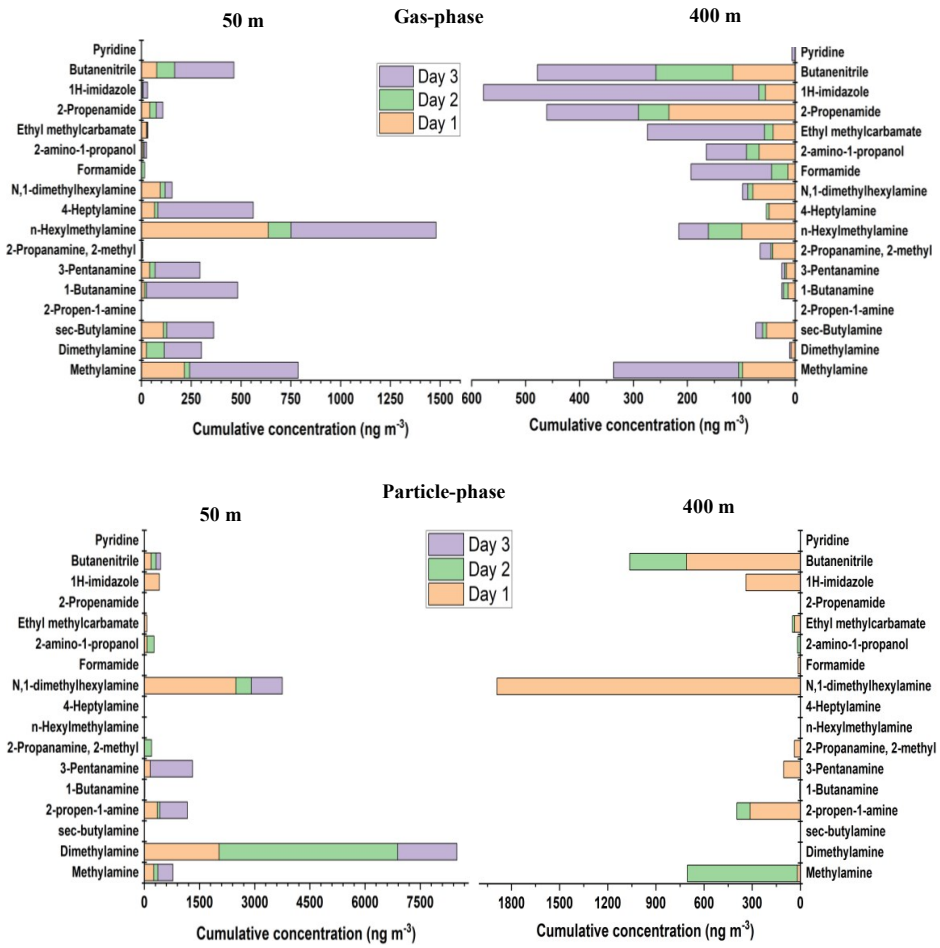

Figure 33. Concentrations of detected nitrogen-containing compounds at altitudes 50 and 400 m in the gas-phase and in particle-phase collected on 8 to 10 October 2021. This figure is adopted from ***Paper II***.

Methylglyoxal was detected by our system both in gas and particle phases, in which the concentration was higher at the altitude of 400 m **(*Paper II, Fig. 5*)**. Similar vertical trends with methylglyoxal and nitrogen-containing compounds were also seen for other identified VOCs. Those that were emitted from anthropogenic sources, such as ketones and alcohols, were found in high concentrations at higher altitudes. Whereas those produced by biogenic sources, like monoterpene p-cymene, were detected in higher concentrations at lower altitudes **(*Paper II, Fig. 5*)**. Universal sorbent materials Carbon-WR in SPME Arrow and TENAX-GR in ITEX sampling systems were successfully used to collect the non-nitrogenated VOCs.

The anthropogenic sources were most likely from the south and southwest - the direction of 174° to 250° (Fig. 34), which are the directions of harbors and industrial areas (***Paper I***). The evaluation of meteorological variables by using LDA showed that wind direction affected the sampling (***Paper I***).

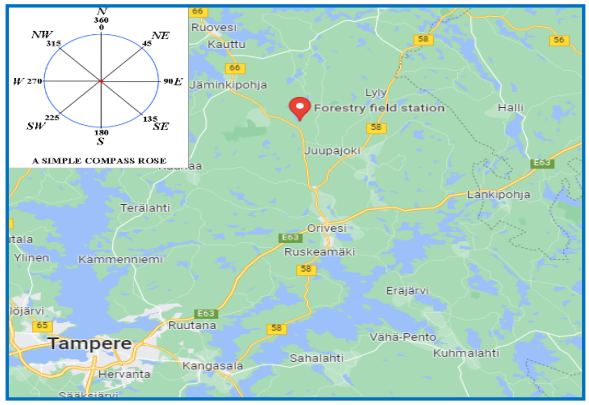

Figure 34. Map of the SMEAR II boreal forest site in Hyytiälä and its surrounding.

4.11. Analysis of aerosol particles collected by ITEX filter accessory using liquid chromatography tandem mass spectrometry

Aerosol particles collected by ITEX filter accessory were extracted and analyzed to quantify carboxylic and dicarboxylic acids **(*Paper II*)**. These organic acids are also

important constituents since they can increase the hygroscopicity of aerosol particles and contribute to the acidity of precipitation and cloud water. Five of the 18 identified acids were quantified, as can be seen in Table 11.

Table 11. Total concentrations of acids (ng m^{-3}) collected from the ITEX filters at the altitudes of 50-400 m.

Sampling time	Succinic acid	Benzoic acid	Phthalic acid	Glutaric acid	Adipic acid
11.10.2021	1416	1416	657	1619	10926
12.10.2021	435-789	1416	769	n.d.	n.d.
13.10.2021	496-4654	n.d.	n.d.	n.d.	n.d.
14.10.2021	n.d.	n.d.	n.d.	1720	6374

n.d. = not detected

4.12. On-site measurement of BC and total particle number at high altitude

The total particle number and BC concentrations were measured at high altitudes (100, 200, 300 and 400 m) by using portable CPC and BC monitors carried by the drone **(*Paper II*)**. Both total particle numbers and BC showed similar trends at all altitudes. Total particle numbers at all altitudes and BC at the altitude of 400 m revealed a diurnal cycle, with peak numbers observed in the morning of the working day. The highest concentration could be due to morning traffic or wind-driven pollution transport as suggested by other studies [167,168]. Long-range transport could be the main cause for the high BC concentration at high altitude, particularly at 400 m, while both BC and other particles contributed to overall particle number concentrations.

The drone stability was assessed while moving vertically and horizontally. Figure 35 demonstrates how the drone motions, particularly rapid ascending (area number I), had an impact on the readings of BC concentration and total particle numbers. When the drone began to warm up, take off, and then quickly moved vertically with the speed of 2.5 ms^{-1}, BC measurements revealed negative values. This could be because the BC sensor was very sensitive to the movement and temperature changes during these times [169]. The portable CPC device also showed a high amount of particle number concentrations, which could be due to the propellers that were

causing dust from the ground to rise into the air and then detected by the CPC. When the drone approached the altitude of 365 m, both BC device and CPC started to stabilize. In comparison to the portable BC device, the portable CPC was significantly less affected by the horizontal movements (area numbers III and IV).

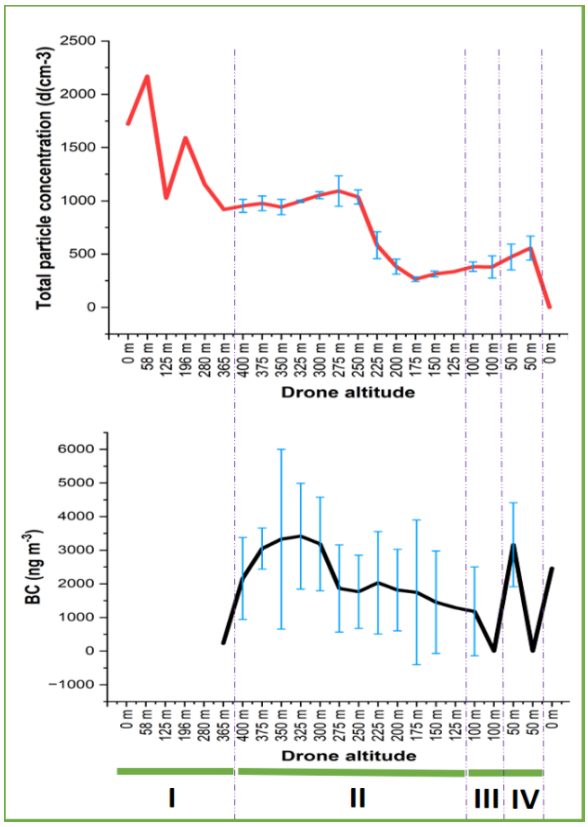

Figure 35. Evaluation of drone's vertical and horizontal movements. I = Drone is moving up (speed: 2.5 ms^{-1}); II= Drone is descending to each altitude (speed: 1.25 ms^{-1}) before staying for 30 s; III and IV = Horizontal movement (100 m far, speed: 5 ms^{-1}). This figure is adopted from ***Paper II***.

5. Conclusions

The main objective of this doctoral thesis was to develop reliable miniaturized microextraction techniques for selective collection of volatile nitrogen-containing compounds in air samples. The applicability of different materials as ITEX sorbent

played an important role in the studies. The suitability of ITEX and SPME sampling systems, packed or coated with selective sorbent materials for air sampling was also clarified in terms of the adsorption and desorption kinetics. The applicability of the aerial drone as the platform for remote passive and active air sampling and for the real-time particle measurement was demonstrated.

The selectivity of two mesoporous silica-based materials, MCM-41 and MCM-41-TP, was tested for miniaturized passive SPME Arrow and active ITEX air sampling systems. Due to the selectivity and pore structures (pore volume and size) of MCM-41 it was chosen as the best option for SPME Arrow adsorbent. MCM-41-TP was the best ITEX material for gas chromatography-mass spectrometry analysis and for selective collection of nitrogen-containing compounds without any mechanical problems. In addition, ITEX trap accessory containing TENAX-GR material for the elimination of other substances than nitrogen-containing compounds improved the selectivity of the sampling system still further.

MCM-41 and MCM-41-TP materials followed the same adsorption order of nitrogen-containing compounds under study in terms of basicity with the exception of isobutylamine and pyridine, giving the fastest adsorption rates for the most basic amines. The adsorption kinetics were well described by an Elovich model, while a pseudo-first-order kinetic model was utilized to describe the desorption kinetics. The desorption kinetics study proved the MCM-41 and MCM-41-TP sorbent materials to exhibit chemical adsorption in addition to physisorption, but additional studies with longer sampling times are needed to confirm this preliminary result.

The saturation vapor pressures, which are important for the prediction of the adsorption of nitrogen-containing compounds to airborne particulate matter, were also determined. The results achieved by laboratory experiments using a retention index approach agreed with only small deviations with those obtained by the COSMO-RS model.

A new material, PM-SiO_2/ZnO-2, synthesized from ZnO incorporated into mesoporous silica materials and prepared via pseudomorphic transformation, was evaluated as an ITEX sampling sorbent for the collection of nitrogen-containing compounds. Its selectivity and affinity was better than the silica material alone. The

mechanical problem of pure ZnO was avoided by the ZnO infiltration with less than three cycles into mesoporous silica. The ITEX system, packed with PM-SiO_2/ZnO-2 was successfully applied for the selective and efficient collection of nitrogen-containing compounds in cigarette smoke, indoor air, and outdoor air. The sorbent developed in this study can be used also as sorbent materials in other traditional sampler tubes such as in Carbograph tube.

An aerial drone carried reliably at high altitudes the versatile miniaturized air sampling systems SPME Arrow and ITEX, a portable black carbon monitor, and a condensation particle counter device, the latter used for particle real-time measurements. This combined system was also successfully employed for the evaluation of diurnal patterns and spatial distribution of the nitrogen-containing compounds and other VOCs in the boreal forest SMEAR II station, Finland.

In the gas phase, nitrogen-containing compounds had generally the largest concentrations in the warmer afternoons, whereas, in the particle phase, concentration peaks were seen in the mornings and evenings. The diverse sources of their emission, both biogenic and anthropogenic, affected the variations of their compositions at different altitudes. A similar trend was also observed for other VOCs.

The capability of the active ITEX sampling systems, furnished with a filter accessory for the collection of gas phase samples, was evaluated by comparing it with the passive SPME Arrow sampler. The results were in agreement, especially for polar compounds with recoveries up to 99 %. While non-polar compounds, such as alkanes, yielded low recoveries due to the *like dissolve like* rule meaning that they might be adsorbed to the non-polar PTFE filter of the ITEX sampling system.

The total particle number and black carbon gave similar diurnal trends, where the highest concentrations correlated with human activities. Black carbon concentrations were enhanced at higher altitudes due to long-range transport and the atmospheric boundary layer. The total particle numbers varied more depending on the sources.

Altogether, these findings provide an excellent platform for future research to evaluate the impact of nitrogen-containing compounds on human health and the

environment. Careful choice of the sorbent material, especially for the ITEX sampling systems, is crucial, not only to increase sampling selectivity but also to prevent ITEX from mechanical problems. The miniaturized active sampler ITEX packed with selective material proposed in this thesis has a number of advantages including better selectivity, a smaller sampling volume, a shorter sampling time, simple operation, and can be automated with online coupling with an analytical instrument. In addition, the established sampling system can be applied to other environmental studies, such as indoor air quality analysis, and to collect the volatile nitrogen-containing compounds from soil, water, and food samples. The calculations of kinetics and vapor pressures of the compounds were accurate and are useful in atmospheric chemistry applications. An aerial drone also proved to be an ideal carrier for miniaturized air sampling systems and portable instrumentations.

However, although several advances were achieved in this work, further studies are still needed. For instance, new materials to enhance selectivity towards small nitrogen-containing compounds, particularly for amines with $C \leq 2$ are required. Higher selectivity will provide a higher sensitivity method for ambient air measurement. Further studies for the ITEX trap-accessory materials would be beneficial, particularly those that aim for more selective retaining or trapping of the non-polar compounds, allowing only polar compounds to pass through the ITEX sampler. In addition to ITEX trap accessory, the compounds lost in the ITEX filter accessory must be studied further, even though the filter has lower polarity than the target analytes. The online dynamic ITEX system coupled to gas chromatography with high-resolution mass spectrometry would also be useful to provide better mass accuracy and higher sensitivity, especially for untargeted analysis. Moreover, the development of new models and equations to study kinetics for small gaseous nitrogen-containing compounds with better fits would be very important to model their physicochemical properties. Further experiments with longer sampling times are also needed to prove the chemical interactions between silica-based materials and the nitrogen-containing compounds during the adsorption processes. The portable gas chromatography-mass spectrometry would also accelerate on-site reliable measurements. The PLSR method for quantitative and semi-quantitative analyses needs to be evaluated especially for aerosol particle measurements. Last

but not least, a portable black carbon monitor with an improved electronic model and optimized position in the drone would be essential to increase the reliability of the black carbon results.

References

[1] M. Hemmilä, Chemical Characterisation of Boreal Forest Air with Chromatographic Techniques, University of Helsinki, 2020. http://hdl.handle.net/10138/313207.

[2] X. Ge, A.S. Wexler, S.L. Clegg, Atmospheric amines - Part I. A review, Atmos. Environ. 45 (2011) 524–546. https://doi.org/10.1016/j.atmosenv.2010.10.012.

[3] J. Zahardis, S. Geddes, G.A. Petrucci, The ozonolysis of primary aliphatic amines in fine particles, Atmos. Chem. Phys. 8 (2008) 1181–1194. https://doi.org/10.5194/acp-8-1181-2008.

[4] S.M. Murphy, A. Sorooshian, J.H. Kroll, N.L. Ng, P. Chhabra, C. Tong, J.D. Surratt, E. Knipping, R.C. Flagan, J.H. Seinfeld, Secondary aerosol formation from atmospheric reactions of aliphatic amines, Atmos. Chem. Phys. 7 (2007) 2313–2337. https://doi.org/10.5194/acp-7-2313-2007.

[5] M. Kulmala, T. Petäjä, M. Ehn, J. Thornton, M. Sipilä, D.R. Worsnop, V.M. Kerminen, Chemistry of atmospheric nucleation: On the recent advances on precursor characterization and atmospheric cluster composition in connection with atmospheric new particle formation, Annu. Rev. Phys. Chem. 65 (2014) 21–37. https://doi.org/10.1146/annurev-physchem-040412-110014.

[6] H. Lan, K. Hartonen, M.L. Riekkola, Miniaturised air sampling techniques for analysis of volatile organic compounds in air, TrAC - Trends Anal. Chem. 126 (2020) 115873. https://doi.org/10.1016/j.trac.2020.115873.

[7] H.L. Lord, W. Zhan, J. Pawliszyn, Fundamentals and applications of needle trap devices. A critical review, Anal. Chim. Acta. 677 (2010) 3–18. https://doi.org/10.1016/j.aca.2010.06.020.

[8] N. Lorenzo-Parodi, W. Kaziur, N. Stojanović, M.A. Jochmann, T.C. Schmidt, Solventless microextraction techniques for water analysis, TrAC - Trends Anal. Chem. 113 (2019) 321–331. https://doi.org/10.1016/j.trac.2018.11.013.

[9] R.E. Hester, R.M. Harrison, Volatile organic compounds in the atmosphere, Royal Society of Chemistry, Cambridge, 1995.

[10] J.C. Hanks, S.O. Louglin, Volatile organic compounds, Nova Science Publishers, New York, 2011.

[11] J.P. Moore, Volatile organic compounds : occurrence, behavior and ecological implications, Nova Science Publishers, Hauppauge, New York, 2016. https://www.ebsco.com/terms-of-use.

[12] The European Parliament and the Council of the European Union, Directive 2004/42/CE of the European Parliament and of the Council of 21 April 2004 on the limitation of emissions of volatile organic compounds due to the use of organic solvents in certain paints and varnishes and vehicle refinishing products and amendi, Off. J. Eur. Unio. (2004) 87–96. http://eur-

lex.europa.eu/LexUriServ/LexUriServ.do?uri=CELEX:32004L0042:EN:NOT.

[13] United States Environmental Protection Agency, Technical Overview of Volatile Organic Compounds, 2023. https://www.ecfr.gov/current/title-40/chapter-I/subchapter-C.

[14] R. Heinrich-Ramm, New International Union of Pure and Applied Chemistry recommendation 2000 on biomonitoring for exposure to volatile organic compounds, Int. Arch. Occup. Environ. Health. 74 (2001) 229–230. https://doi.org/10.1007/s004200000223.

[15] E. Oikonomakis, S. Aksoyoglu, G. Ciarelli, U. Baltensperger, A.S.H. Prévôt, Low modeled ozone production suggests underestimation of precursor emissions (especially NOx) in Europe, Atmos. Chem. Phys. 18 (2018) 2175–2198. https://doi.org/10.5194/acp-18-2175-2018.

[16] E. Ahlberg, J. Falk, A. Eriksson, T. Holst, W.H. Brune, A. Kristensson, P. Roldin, B. Svenningsson, Secondary organic aerosol from VOC mixtures in an oxidation flow reactor, Atmos. Environ. 161 (2017) 210–220. https://doi.org/10.1016/j.atmosenv.2017.05.005.

[17] V.A. Isidorov, E. Pirożnikow, V.L. Spirina, A.N. Vasyanin, S.A. Kulakova, I.F. Abdulmanova, A.A. Zaitsev, Emission of volatile organic compounds by plants on the floor of boreal and mid-latitude forests, J. Atmos. Chem. 79 (2022) 153–166. https://doi.org/10.1007/s10874-022-09434-3.

[18] P.J. Ziemann, R. Atkinson, Kinetics, products, and mechanisms of secondary organic aerosol formation, Chem. Soc. Rev. 41 (2012) 6582–6605. https://doi.org/10.1039/c2cs35122f.

[19] A. Laskin, J.S. Smith, J. Laskin, Molecular characterization of nitrogen-containing organic compounds in biomass burning aerosols using high-resolution mass spectrometry, Environ. Sci. Technol. 43 (2009) 3764–3771. https://doi.org/10.1021/es803456n.

[20] D.G. Capone, Nitrogen in the marine environment, 2nd ed., Elsevier, Boston, 2008.

[21] M.J. Alhnidi, P. Körner, D. Wüst, J. Pfersich, A. Kruse, Nitrogen-Containing Hydrochar: The Influence of Nitrogen-Containing Compounds on the Hydrochar Formation, ChemistryOpen. 9 (2020) 864–873. https://doi.org/10.1002/open.202000148.

[22] X. Ge, A.S. Wexler, S.L. Clegg, Atmospheric amines - Part II. Thermodynamic properties and gas/particle partitioning, Atmos. Environ. 45 (2011) 561–577. https://doi.org/10.1016/j.atmosenv.2010.10.013.

[23] N.R. Choi, J.Y. Lee, Y.G. Ahn, Y.P. Kim, Determination of atmospheric amines at Seoul, South Korea via gas chromatography/tandem mass spectrometry, Chemosphere. 258 (2020) 127367. https://doi.org/10.1016/j.chemosphere.2020.127367.

[24] H. Lan, T. Rönkkö, J. Parshintsev, K. Hartonen, N. Gan, M. Sakeye, J. Sarfraz, M.L. Riekkola, Modified zeolitic imidazolate framework-8 as solid-phase microextraction Arrow coating for sampling of amines in wastewater and food samples followed by gas chromatography-mass spectrometry, J. Chromatogr. A. 1486 (2017) 76–85. https://doi.org/10.1016/j.chroma.2016.10.081.

[25] A.P. Sullivan, K.B. Benedict, C.M. Carrico, M.K. Dubey, B.A. Schichtel, J.L. Collett, A quantitative method to measure and speciate amines in ambient

aerosol samples, Atmosphere (Basel). 11 (2020). https://doi.org/10.3390/ATMOS11080808.

[26] M. Wedyan, K. Fandi, S. Al-Rousan, Bioavailability of Atmospheric Dissolved Organic Nitrogen in The Marine Aerosol over the Gulf of Aqaba, 2007.

[27] T. Nakamura, H. Ogawa, D.K. Maripi, M. Uematsu, Contribution of water soluble organic nitrogen to total nitrogen in marine aerosols over the East China Sea and western North Pacific, Atmos. Environ. 40 (2006) 7259–7264. https://doi.org/10.1016/j.atmosenv.2006.06.026.

[28] T.H. Speak, D.J. Medeiros, M.A. Blitz, P.W. Seakins, OH Kinetics with a Range of Nitrogen-Containing Compounds:N-Methylformamide,t-Butylamine, andN-Methyl-propane Diamine, J. Phys. Chem. A. 125 (2021) 10439–10450. https://doi.org/10.1021/acs.jpca.1c08104.

[29] S.H. Kim, A. Kirakosyan, J. Choi, J.H. Kim, Detection of volatile organic compounds (VOCs), aliphatic amines, using highly fluorescent organic-inorganic hybrid perovskite nanoparticles, Dye. Pigment. 147 (2017) 1–5. https://doi.org/10.1016/j.dyepig.2017.07.066.

[30] Y.L. Zhao, S.L. Garrison, C. Gonzalez, W.D. Thweatt, M. Marquez, N-nitrosation of amines by NO2 and NO: A theoretical study, J. Phys. Chem. A. 111 (2007) 2200–2205. https://doi.org/10.1021/jp0677703.

[31] J.-S. Youn, E.. Crosbie, L.C. Maudlin, Z. Wang, A. Sorooshian, Dimethylamine as a major alkyl amine species in particles and cloud water: Observations in semi-arid and coastal regions, Atmos. Environ. 122 (2015) 250–258. https://doi.org/doi:10.1016/j.atmosenv.2015.09.061.

[32] C.J. Nielsen, H. Herrmann, C. Weller, Atmospheric chemistry and environmental impact of the use of amines in carbon capture and storage (CCS), Chem. Soc. Rev. 41 (2012) 6684–6704. https://doi.org/10.1039/c2cs35059a.

[33] B. Thitakamol, A. Veawab, A. Aroonwilas, Environmental impacts of absorption-based CO2 capture unit for post-combustion treatment of flue gas from coal-fired power plant, Int. J. Greenh. Gas Control. 1 (2007) 318–342. https://doi.org/10.1016/S1750-5836(07)00042-4.

[34] L. Zhu, G.W. Schade, C.J. Nielsen, Real-time monitoring of emissions from monoethanolamine-based industrial scale carbon capture facilities, Environ. Sci. Technol. 47 (2013) 14306–14314. https://doi.org/10.1021/es4035045.

[35] K. Yu, W.A. Mitch, N. Dai, Nitrosamines and Nitramines in Amine-Based Carbon Dioxide Capture Systems: Fundamentals, Engineering Implications, and Knowledge Gaps, Environ. Sci. Technol. 51 (2017) 11522–11536. https://doi.org/10.1021/acs.est.7b02597.

[36] V. Zelenak, D. Halamova, L. Gaberova, E. Bloch, P. Llewellyn, Amine-modified SBA-12 mesoporous silica for carbon dioxide capture: Effect of amine basicity on sorption properties, Microporous Mesoporous Mater. 116 (2008) 358–364. https://doi.org/10.1016/j.micromeso.2008.04.023.

[37] I. Sreedhar, R. Aniruddha, S. Malik, Carbon capture using amine modified porous carbons derived from starch (Starbons®), SN Appl. Sci. 1 (2019) 1–11. https://doi.org/10.1007/s42452-019-0482-8.

[38] L.J. Wang, H.L. Fan, J. Shangguan, E. Croiset, Z. Chen, H. Wang, J. Mi, Design of a sorbent to enhance reactive adsorption of hydrogen sulfide, ACS Appl. Mater. Interfaces. 6 (2014) 21167–21177. https://doi.org/10.1021/am506077j.

[39] J. Wang, L. Huang, R. Yang, Z. Zhang, J. Wu, Y. Gao, Q. Wang, D. O'Hare, Z. Zhong, Recent advances in solid sorbents for CO2 capture and new development trends, Energy Environ. Sci. 7 (2014) 3478–3518. https://doi.org/10.1039/c4ee01647e.

[40] B. Fostås, A. Gangstad, B. Nenseter, S. Pedersen, M. Sjøvoll, A.L. Sørensen, Effects of NOx in the flue gas degradation of MEA, Energy Procedia. 4 (2011) 1566–1573. https://doi.org/10.1016/j.egypro.2011.02.026.

[41] J.N. Cape, S.E. Cornell, T.D. Jickells, E. Nemitz, Organic nitrogen in the atmosphere - Where does it come from? A review of sources and methods, Atmos. Res. 102 (2011) 30–48. https://doi.org/10.1016/j.atmosres.2011.07.009.

[42] S. Angeling, D.T. Suess, K.A. Prather, Formation of aerosol particles from reactions of secondary and tertiary alkylamines: Characterization by aerosol time-of-flight mass spectrometry, Environ. Sci. Technol. 35 (2001) 3130–3138. https://doi.org/10.1021/es0015444.

[43] J. Almeida, S. Schobesberger, A. Kürten, I.K. Ortega, O. Kupiainen-Määttä, A.P. Praplan, A. Adamov, A. Amorim, F. Bianchi, M. Breitenlechner, A. David, J. Dommen, N.M. Donahue, A. Downard, E. Dunne, J. Duplissy, S. Ehrhart, R.C. Flagan, A. Franchin, R. Guida, J. Hakala, A. Hansel, M. Heinritzi, H. Henschel, T. Jokinen, H. Junninen, M. Kajos, J. Kangasluoma, H. Keskinen, A. Kupc, T. Kurtén, A.N. Kvashin, A. Laaksonen, K. Lehtipalo, M. Leiminger, J. Leppä, V. Loukonen, V. Makhmutov, S. Mathot, M.J. McGrath, T. Nieminen, T. Olenius, A. Onnela, T. Petäjä, F. Riccobono, I. Riipinen, M. Rissanen, L. Rondo, T. Ruuskanen, F.D. Santos, N. Sarnela, S. Schallhart, R. Schnitzhofer, J.H. Seinfeld, M. Simon, M. Sipilä, Y. Stozhkov, F. Stratmann, A. Tomé, J. Tröstl, G. Tsagkogeorgas, P. Vaattovaara, Y. Viisanen, A. Virtanen, A. Vrtala, P.E. Wagner, E. Weingartner, H. Wex, C. Williamson, D. Wimmer, P. Ye, T. Yli-Juuti, K.S. Carslaw, M. Kulmala, J. Curtius, U. Baltensperger, D.R. Worsnop, H. Vehkamäki, J. Kirkby, Molecular understanding of sulphuric acid-amine particle nucleation in the atmosphere, Nature. 502 (2013) 359–363. https://doi.org/10.1038/nature12663.

[44] P. Fermo, B. Artíñano, G. De Gennaro, A.M. Pantaleo, A. Parente, F. Battaglia, E. Colicino, G. Di Tanna, A. Goncalves da Silva Junior, I.G. Pereira, G.S. Garcia, L.M. Garcia Goncalves, V. Comite, A. Miani, Improving indoor air quality through an air purifier able to reduce aerosol particulate matter (PM) and volatile organic compounds (VOCs): Experimental results, Environ. Res. 197 (2021) 1–8. https://doi.org/10.1016/j.envres.2021.111131.

[45] P. Luis, Use of monoethanolamine (MEA) for CO2 capture in a global scenario: Consequences and alternatives, Desalination. 380 (2016) 93–99. https://doi.org/10.1016/j.desal.2015.08.004.

[46] C. He, H. Wang, D. Gong, S. Lv, G. Wu, R. Wang, Y. Chen, Y. Ding, Y. Li, B. Wang, Insights into high concentrations of particle-bound imidazoles in the background atmosphere of southern China: Potential sources and influencing factors, Sci. Total Environ. 806 (2022). https://doi.org/10.1016/j.scitotenv.2021.150804.

[47] C.J. Kampf, R. Jakob, T. Hoffmann, Identification and characterization of aging products in the glyoxal/ammonium sulfate system – Implications for light-absorbing material in atmospheric aerosols, Atmos. Chem. Phys. 12 (2012) 6323–6333. https://doi.org/10.5194/acp-12-6323-2012.

[48] W. Marrero-Ortiz, M. Hu, Z. Du, Y. Ji, Y. Wang, S. Guo, Y. Lin, M. Gomez-

Hermandez, J. Peng, Y. Li, J. Secrest, M.L. Zamora, Y. Wang, T. An, R. Zhang, Formation and Optical Properties of Brown Carbon from Small α-Dicarbonyls and Amines, Environ. Sci. Technol. 53 (2019) 117–126. https://doi.org/10.1021/acs.est.8b03995.

[49] M.M. Galloway, P.S. Chhabra, A.W.H. Chan, J.D. Surratt, R.C. Flagan, J.H. Seinfeld, F.N. Keutsch, Atmospheric Chemistry and Physics Glyoxal uptake on ammonium sulphate seed aerosol: reaction products and reversibility of uptake under dark and irradiated conditions, 2009. www.atmos-chem-phys.net/9/3331/2009/.

[50] G. Yu, A.R. Bayer, M.M. Galloway, K.J. Korshavn, C.G. Fry, F.N. Keutsch, Glyoxal in aqueous ammonium sulfate solutions: Products, kinetics and hydration effects, Environ. Sci. Technol. 45 (2011) 6336–6342. https://doi.org/10.1021/es200989n.

[51] US Environmental Protection Agency, US EPA 8270, SEMIVOLATILE ORGANIC COMPOUNDS BY GAS CHROMATOGRAPHY/MASS SPECTROMETRY (GC/MS), 2007.

[52] J. Luo, C. Zou, Y. He, H. Jing, S. Cheng, The characteristics and mechanism of NO formation during pyridine oxidation in O2/N2 and O2/CO2 atmospheres, Energy. 187 (2019). https://doi.org/10.1016/j.energy.2019.115954.

[53] A. Oita, A. Malik, K. Kanemoto, A. Geschke, S. Nishijima, M. Lenzen, Substantial nitrogen pollution embedded in international trade, Nat. Geosci. 9 (2016) 111–115. https://doi.org/10.1038/ngeo2635.

[54] Q. Ren, H. Chi, J. Gao, C. Zhang, S. Su, H. Leong, K. Xu, S. Hu, Y. Wang, J. Xiang, Experimental study and mechanism analysis of NO formation during volatile-N model compounds combustion in H2O/CO2 atmosphere, Fuel. 273 (2020). https://doi.org/10.1016/j.fuel.2020.117722.

[55] O. Filippou, D. Bitas, V. Samanidou, Green approaches in sample preparation of bioanalytical samples prior to chromatographic analysis, J. Chromatogr. B Anal. Technol. Biomed. Life Sci. 1043 (2017) 44–62. https://doi.org/10.1016/j.jchromb.2016.08.040.

[56] J. Stocka, M. Tankiewicz, M. Biziuk, J. Namieśnik, Green aspects of techniques for the determination of currently used pesticides in environmental samples, Int. J. Mol. Sci. 12 (2011) 7785–7805. https://doi.org/10.3390/ijms12117785.

[57] J. Pawliszyn, Theory of Solid-Phase Microextraction, Elsevier Inc., Ontario, Canada, 2012. https://doi.org/10.1016/B978-0-12-416017-0.00002-4.

[58] C.L. Arthur, J. Pawliszyn, Solid phase microextraction with thermal desorption using fused silica optical fibers, Anal. Chem. 62 (1990) 2145–2148. https://doi.org/10.1021/ac00218a019.

[59] M.A. Jeannot, A. Przyjazny, J.M. Kokosa, Single drop microextraction-Development, applications and future trends, J. Chromatogr. A. 1217 (2010) 2326–2336. https://doi.org/10.1016/j.chroma.2009.10.089.

[60] J. López-Darias, M. Germán-Hernández, V. Pino, A.M. Afonso, Dispersive liquid-liquid microextraction versus single-drop microextraction for the determination of several endocrine-disrupting phenols from seawaters, Talanta. 80 (2010) 1611–1618. https://doi.org/10.1016/j.talanta.2009.09.057.

[61] E.D. Pusfitasari, J. Ruiz-Jimenez, I. Heiskanen, M. Jussila, K. Hartonen, M.-L. Riekkola, Aerial drone furnished with miniaturized versatile air sampling

systems for selective collection of nitrogen containing compounds in boreal forest, Sci. Total Environ. 808 (2022) 152011. https://doi.org/10.1016/J.SCITOTENV.2021.152011.

[62] J. Ruiz-Jimenez, H. Lan, Y. Leleev, K. Hartonen, M.L. Riekkola, Comparison of multiple calibration approaches for the determination of volatile organic compounds in air samples by solid phase microextraction Arrow and in-tube extraction, J. Chromatogr. A. 1616 (2020) 460825. https://doi.org/10.1016/j.chroma.2019.460825.

[63] J. Ruiz-Jimenez, N. Zanca, H. Lan, M. Jussila, K. Hartonen, M.L. Riekkola, Aerial drone as a carrier for miniaturized air sampling systems, J. Chromatogr. A. 1597 (2019) 202–208. https://doi.org/10.1016/j.chroma.2019.04.009.

[64] A. Helin, T. Rönkkö, J. Parshintsev, K. Hartonen, B. Schilling, T. Läubli, M.L. Riekkola, Solid phase microextraction Arrow for the sampling of volatile amines in wastewater and atmosphere, J. Chromatogr. A. 1426 (2015) 56–63. https://doi.org/10.1016/j.chroma.2015.11.061.

[65] H. Lan, J. Ruiz-Jimenez, Y. Leleev, G. Demaria, M. Jussila, K. Hartonen, M.-L. Riekkola, Quantitative analysis and spatial and temporal distribution of volatile organic compounds in atmospheric air by utilizing drone with miniaturized samplers, Chemosphere. 282 (2021) 131024. https://doi.org/10.1016/j.chemosphere.2021.131024.

[66] J. Parshintsev, T. Rönkkö, A. Helin, K. Hartonen, M.L. Riekkola, Determination of atmospheric amines by on-fiber derivatization solid-phase microextraction with 2,3,4,5,6-pentafluorobenzyl chloroformate and 9-fluorenylmethoxycarbonyl chloride, J. Chromatogr. A. 1376 (2015) 46–52. https://doi.org/10.1016/j.chroma.2014.12.040.

[67] L. Tuduri, V. Desauziers, J.L. Fanlo, Potential of solid-phase microextraction fibers for the analysis of volatile organic compounds in air, J. Chromatogr. Sci. 39 (2001) 521–529. https://doi.org/10.1093/chromsci/39.12.521.

[68] P.Y. Schüpfer, C.K. Huynh, Solid phase microextraction as a short-term sampling technique for BTEX occupational exposure, J. Occup. Environ. Hyg. 5 (2008) 490–500. https://doi.org/10.1080/15459620802177484.

[69] H. Lan, J. Holopainen, K. Hartonen, M. Jussila, M. Ritala, M.L. Riekkola, Fully Automated Online Dynamic In-Tube Extraction for Continuous Sampling of Volatile Organic Compounds in Air, Anal. Chem. 91 (2019) 8507–8515. https://doi.org/10.1021/acs.analchem.9b01668.

[70] Y. Gong, I.Y. Eom, D.W. Lou, D. Hein, J. Pawliszyn, Development and application of a needle trap device for time-weighted average diffusive sampling, Anal. Chem. 80 (2008) 7275–7282. https://doi.org/10.1021/ac800884f.

[71] W.-H. Cheng, W. Zhan, J. Pawliszyn, Gaseous and Particle-bound VOC Products of Combustion Extracted by Needle Trap Samplers, J. Chinese Chem. Soc. 60 (2013) 1027–1032. https://doi.org/10.1002/jccs.201200654.

[72] C.S. Gordon, J.T. Lowe, US1644014 Carbon-monoxide detector, 1927.

[73] K.D. Reiszner, P.W. West, Collection and determination of sulfur dioxide incorporating permeation and West-Gaeke procedure, Environ. Sci. Technol. 7 (1973) 526–532. https://doi.org/10.1021/es60078a001.

[74] E.D. Palmes, A.F. Gunnison, Personal Monitoring Device for Gaseous Contaminants, Am. Ind. Hyg. Assoc. J. 34 (1973) 78–81.

https://doi.org/10.1080/0002889738506810.

[75] T. Górecki, J. Namienik, Passive sampling, TrAC - Trends Anal. Chem. 21 (2002) 276–291. https://doi.org/10.1016/S0165-9936(02)00407-7.

[76] L. Melymuk, P. Bohlin, O. Sáňka, K. Pozo, J. Klánová, Current challenges in air sampling of semivolatile organic contaminants: Sampling artifacts and their influence on data comparability, Environ. Sci. Technol. 48 (2014) 14077–14091. https://doi.org/10.1021/es502164r.

[77] J.S. Herrington, G.A. Gómez-Ríos, C. Myers, G. Stidsen, D.S. Bell, Hunting molecules in complex matrices with spme arrows: A review, Separations. 7 (2020). https://doi.org/10.3390/separations7010012.

[78] H.F. Garces, A.E. Espinal, S.L. Suib, Tunable shape microwave synthesis of zinc oxide nanospheres and their desulfurization performance compared with nanorods and platelet-like morphologies for the removal of hydrogen sulfide, J. Phys. Chem. C. 116 (2012) 8465–8474. https://doi.org/10.1021/jp210755t.

[79] J.B. Pawliszyn, US5691206 Method and Device for Solid Phase Microextraction and Desorption, 1997.

[80] L.M. Rosendo, A.T. Brinca, B. Pires, G. Catarro, T. Rosado, R.P.F. Guiné, A.R.T.S. Araújo, O. Anjos, E. Gallardo, Miniaturized Solid Phase Extraction Techniques Applied to Natural Products, Processes. 11 (2023) 243. https://doi.org/10.3390/pr11010243.

[81] R. V. Emmons, R. Tajali, E. Gionfriddo, Development, Optimization and Applications of Thin Film Solid Phase Microextraction (TF-SPME) Devices for Thermal Desorption: A Comprehensive Review, Separations. 6 (2019) 39. https://doi.org/10.3390/separations6030039.

[82] X. Liu, J. Pawliszyn, Determination of membrane permeability without calibration using solid-phase microextraction (SPME), J. Memb. Sci. 268 (2006) 65–73. https://doi.org/10.1016/j.memsci.2005.06.047.

[83] J. Ai, Headspace Solid Phase Microextraction. Dynamics and Quantitative Analysis Before Reaching a Partition Equilibrium, Anal. Chem. 69 (1997) 3260–3266. https://pubs.acs.org/sharingguidelines.

[84] F. Alpendurada, Solid-phase microextraction: a promising technique for sample preparation in environmental analysis´Maria analysis´ analysis´Maria de, 2000. www.elsevier.com/locate/chroma.

[85] N. Reyes-Garcés, E. Gionfriddo, G.A. Gómez-Ríos, M.N. Alam, E. Boyacl, B. Bojko, V. Singh, J. Grandy, J. Pawliszyn, Advances in Solid Phase Microextraction and Perspective on Future Directions, Anal. Chem. 90 (2018) 302–360. https://doi.org/10.1021/acs.analchem.7b04502.

[86] H. Lan, W. Zhang, J.-H. Smått, R.T. Koivula, K. Hartonen, M.-L. Riekkola, Selective extraction of aliphatic amines by functionalized mesoporous silica-coated solid phase microextraction Arrow, Microchim. Acta. 186 (2019) 412. https://doi.org/10.1007/s00604-019-3523-5.

[87] H. Lan, Development of Materials and Methodologies for Microextraction Techniques, University of Helsinki, 2019. http://hdl.handle.net/10138/303466.

[88] S.D. Supowit, I.B. Roll, V.D. Dang, K.J. Kroll, N.D. Denslow, R.U. Halden, Active sampling device for determining pollutants in surface and pore water - The in situ sampler for biphasic water monitoring, Sci. Rep. 6 (2016). https://doi.org/10.1038/srep21886.

[89] S.J. Hayward, T. Gouin, F. Wania, Comparison of four active and passive sampling techniques for pesticides in air, Environ. Sci. Technol. 44 (2010) 3410–3416. https://doi.org/10.1021/es902512h.

[90] N.A. Warner, V. Nikiforov, I.S. Krogseth, S.M. Bjørneby, A. Kierkegaard, P. Bohlin-Nizzetto, Reducing sampling artifacts in active air sampling methodology for remote monitoring and atmospheric fate assessment of cyclic volatile methylsiloxanes, Chemosphere. 255 (2020) 126967. https://doi.org/10.1016/j.chemosphere.2020.126967.

[91] W.A. Ockenden, F.M. Jaward, K.C. Jones, Atmospheric sampling of persistent organic pollutants: needs, applications and advances in passive air sampling techniques., ScientificWorldJournal. 1 (2001) 557–575. https://doi.org/10.1100/tsw.2001.255.

[92] J.A. Koziel, M. Odziemkowski, J. Pawliszyn, Sampling and analysis of airborne particulate matter and aerosols using in-needle trap and SPME fiber devices, Anal. Chem. 73 (2001) 47–54. https://doi.org/10.1021/ac000835s.

[93] J. Laaks, M.A. Jochmann, B. Schilling, T.C. Schmidt, Optimization strategies of in-tube extraction (ITEX) methods, Anal. Bioanal. Chem. 407 (2015) 6827–6838. https://doi.org/10.1007/s00216-015-8854-4.

[94] E.D. Pusfitasari, C. Youngren, J. Ruiz-Jimenez, S. Sirkiä, J.H. Smått, K. Hartonen, M.L. Riekkola, Selective and efficient sampling of nitrogen-containing compounds from air by in-tube extraction devices packed with zinc oxide-modified mesoporous silica microspheres, J. Chromatogr. Open. 3 (2023) 100081. https://doi.org/10.1016/j.jcoa.2023.100081.

[95] O. Appel, F. Köllner, A. Dragoneas, A. Hünig, S. Molleker, H. Schlager, C. Mahnke, R. Weigel, M. Port, C. Schulz, F. Drewnick, B. Vogel, F. Stroh, S. Borrmann, Chemical analysis of the Asian tropopause aerosol layer (ATAL) with emphasis on secondary aerosol particles using aircraft-based in situ aerosol mass spectrometry, Atmos. Chem. Phys. 22 (2022) 13607–13630. https://doi.org/10.5194/acp-22-13607-2022.

[96] C.A.M. Brenninkmeijer, P. Crutzen, F. Boumard, T. Dauer, B. Dix, R. Ebinghaus, D. Filippi, H. Fischer, H. Franke, U. Frieß, J. Heintzenberg, F. Helleis, M. Hermann, H.H. Kock, C. Koeppel, J. Lelieveld, M. Leuenberger, B.G. Martinsson, S. Miemczyk, H.P. Moret, H.N. Nguyen, P. Nyfeler, D. Oram, S. Penkett, U. Platt, M. Pupek, M. Ramonet, B. Randa, M. Reichelt, T.S. Rhee, J. Rohwer, K. Rosenfeld, D. Scharffe, H. Schlager, U. Schumann, F. Slemr, D. Sprung, P. Stock, R. Thaler, F. Valentino, P. Van Velthoven, A. Waibel, A. Wandel, K. Waschitschek, A. Wiedensohler, I. Xueref-Remy, A. Zahn, U. Zech, H. Ziereis, Atmospheric Chemistry and Physics Civil Aircraft for the regular investigation of the atmosphere based on an instrumented container: The new CARIBIC system, 2007. www.atmos-chem-phys.net/7/4953/2007/.

[97] M.M. Bela, M.C. Barth, O.B. Toon, A. Fried, C.R. Homeyer, H. Morrison, K.A. Cummings, Y. Li, K.E. Pickering, D.J. Allen, Q. Yang, P.O. Wennberg, J.D. Crounse, J.M. St. Clair, A.P. Teng, D. O'Sullivan, L.G. Huey, D. Chen, X. Liu, D.R. Blake, N.J. Blake, E.C. Apel, R.S. Hornbrook, F. Flocke, T. Campos, G. Diskin, Wet scavenging of soluble gases in DC3 deep convective storms using WRF-Chem simulations and aircraft observations, J. Geophys. Res. 121 (2016) 4233–4257. https://doi.org/10.1002/2015JD024623.

[98] T. Watanabe, Determination of dialkyl phthalates in high altitude atmosphere for validation of sampling method using a helicopter, Bull. Environ. Contam.

Toxicol. 66 (2001) 456–463. https://doi.org/10.1007/s00128-001-0028-8.

[99] M.O. Andreae, O.C. Acevedo, A. Araùjo, P. Artaxo, C.G.G. Barbosa, H.M.J. Barbosa, J. Brito, S. Carbone, X. Chi, B.B.L. Cintra, N.F. Da Silva, N.L. Dias, C.Q. Dias-Júnior, F. Ditas, R. Ditz, A.F.L. Godoi, R.H.M. Godoi, M. Heimann, T. Hoffmann, J. Kesselmeier, T. Könemann, M.L. Krüger, J. V. Lavric, A.O. Manzi, A.P. Lopes, D.L. Martins, E.F. Mikhailov, D. Moran-Zuloaga, B.W. Nelson, A.C. Nölscher, D. Santos Nogueira, M.T.F. Piedade, C. Pöhlker, U. Pöschl, C.A. Quesada, L. V. Rizzo, C.U. Ro, N. Ruckteschler, L.D.A. Sá, M. De Oliveira Sá, C.B. Sales, R.M.N. Dos Santos, J. Saturno, J. Schöngart, M. Sörgel, C.M. De Souza, R.A.F. De Souza, H. Su, N. Targhetta, J. Tóta, I. Trebs, S. Trumbore, A. Van Eijck, D. Walter, Z. Wang, B. Weber, J. Williams, J. Winderlich, F. Wittmann, S. Wolff, A.M. Yáñez-Serrano, The Amazon Tall Tower Observatory (ATTO): Overview of pilot measurements on ecosystem ecology, meteorology, trace gases, and aerosols, Atmos. Chem. Phys. 15 (2015) 10723–10776. https://doi.org/10.5194/acp-15-10723-2015.

[100] C. Yin, J. Xu, W. Gao, L. Pan, Y. Gu, Q. Fu, F. Yang, Characteristics of fine particle matter at the top of Shanghai Tower, Atmos. Chem. Phys. 23 (2023) 1329–1343. https://doi.org/10.5194/acp-23-1329-2023.

[101] J. Heintzenberg, W. Birmili, D. Theiss, Y. Kisilyakhov, The atmospheric aerosol over Siberia, as seen from the 300 m ZOTTO tower, Tellus, Ser. B Chem. Phys. Meteorol. 60 B (2008) 276–285. https://doi.org/10.1111/j.1600-0889.2007.00335.x.

[102] J.A. Armstrong, P.A. Russell, L.E. Sparks, D.C. Drehmel, Tethered balloon sampling systems for monitoring air pollution, J. Air Pollut. Control Assoc. 31 (1981) 735–743. https://doi.org/10.1080/00022470.1981.10465268.

[103] N.C. Bryan, M. Stewart, D. Granger, T.G. Guzik, B.C. Christner, A method for sampling microbial aerosols using high altitude balloons, J. Microbiol. Methods. 107 (2014) 161–168. https://doi.org/10.1016/j.mimet.2014.10.007.

[104] J. Lampilahti, H.E. Manninen, T. Nieminen, S. Mirme, M. Ehn, I. Pullinen, K. Leino, S. Schobesberger, J. Kangasluoma, J. Kontkanen, E. Järvinen, R. Väänänen, T. Yli-Juuti, R. Krejci, K. Lehtipalo, J. Levula, A. Mirme, S. Decesari, R. Tillmann, D.R. Worsnop, F. Rohrer, A. Kiendler-Scharr, T. Petäjä, V.M. Kerminen, T.F. Mentel, M. Kulmala, Zeppelin-led study on the onset of new particle formation in the planetary boundary layer, Atmos. Chem. Phys. 21 (2021) 12649–12663. https://doi.org/10.5194/acp-21-12649-2021.

[105] F. Rubach, Aerosol processes in the Planetary Boundary Layer: High resolution Aerosol Mass Spectrometry on a Zeppelin NT Airship, 2013.

[106] H. Kim, Y. Park, W. Kim, H. Eun, Vertical Aerosol Distribution and Flux Measurement in the Planetary Boundary Layer Using Drone, 14 (2018) 35–40.

[107] P. Bieber, T.M. Seifried, J. Burkart, J. Gratzl, A. Kasper-Giebl, D.G. Schmale, H. Grothe, A drone-based bioaerosol sampling system to monitor ice nucleation particles in the lower atmosphere, Remote Sens. 12 (2020). https://doi.org/10.3390/rs12030552.

[108] S. Lateran, M.F. Sedan, A.S.M. Harithuddin, S. Azrad, Development of unmanned aerial vehicle (UAV) based high altitude balloon (HAB) platform for active aerosol sampling, in: IOP Conf. Ser. Mater. Sci. Eng., Institute of Physics Publishing, 2016. https://doi.org/10.1088/1757-899X/152/1/012018.

[109] A. Kräuchi, R. Philipona, G. Romanens, D.F. Hurst, E.G. Hall, A.F. Jordan,

Controlled weather balloon ascents and descents for atmospheric research and climate monitoring, Atmos. Meas. Tech. 9 (2016) 929–938. https://doi.org/10.5194/amt-9-929-2016.

[110] J.A. Diaz, D. Pieri, K. Wright, P. Sorensen, R. Kline-Shoder, C.R. Arkin, M. Fladeland, G. Bland, M.F. Buongiorno, C. Ramirez, E. Corrales, A. Alan, O. Alegria, D. Diaz, J. Linick, Unmanned aerial mass spectrometer systems for in-situ volcanic plume analysis, J. Am. Soc. Mass Spectrom. 26 (2015) 292–304. https://doi.org/10.1007/s13361-014-1058-x.

[111] Y.C. Chen, C.C. Chang, W.N. Chen, Y.J. Tsai, S.Y. Chang, Determination of the vertical profile of aerosol chemical species in the microscale urban environment, Environ. Pollut. 243 (2018) 1360–1367. https://doi.org/10.1016/j.envpol.2018.09.081.

[112] C.C. Chang, J.L. Wang, C.Y. Chang, M.C. Liang, M.R. Lin, Development of a multicopter-carried whole air sampling apparatus and its applications in environmental studies, Chemosphere. 144 (2016) 484–492. https://doi.org/10.1016/j.chemosphere.2015.08.028.

[113] W. Chen, Y. Zou, W. Mo, D. Di, B. Wang, M. Wu, Z. Huang, B. Hu, Onsite Identification and Spatial Distribution of Air Pollutants Using a Drone-Based Solid-Phase Microextraction Array Coupled with Portable Gas Chromatography-Mass Spectrometry via Continuous-Airflow Sampling, Environ. Sci. Technol. 56 (2022) 17100–17107. https://doi.org/10.1021/acs.est.2c05259.

[114] O. Alvear, N.R. Zema, E. Natalizio, C.T. Calafate, Using UAV-based systems to monitor air pollution in areas with poor accessibility, J. Adv. Transp. 2017 (2017). https://doi.org/10.1155/2017/8204353.

[115] T.F. Villa, F. Salimi, K. Morton, L. Morawska, F. Gonzalez, Development and validation of a UAV based system for air pollution measurements, Sensors (Switzerland). 16 (2016). https://doi.org/10.3390/s16122202.

[116] F. Kleitz, S.H. Choi, R. Ryoo, Cubic Ia3d large mesoporous silica: Synthesis and replication to platinum nanowires, carbon nanorods and carbon nanotubes, Chem. Commun. 3 (2003) 2136–2137. https://doi.org/10.1039/b306504a.

[117] T. Martin, A. Galarneau, F. Di Renzo, F. Fajula, D. Plee, Morphological Control of MCM-41 by Pseudomorphic Synthesis, Angew. Chemie (International Ed.). 41 (2002) 2590–2592.

[118] A. Leitner, M. Sakeye, C.E. Zimmerli, J.H. Smått, Insights into chemoselectivity principles in metal oxide affinity chromatography using tailored nanocast metal oxide microspheres and mass spectrometry-based phosphoproteomics, Analyst. 142 (2017) 1993–2003. https://doi.org/10.1039/c7an00570a.

[119] A. Lind, C. du Fresne von Hohenesche, J.H. Smått, M. Lindén, K.K. Unger, Spherical silica agglomerates possessing hierarchical porosity prepared by spray drying of MCM-41 and MCM-48 nanospheres, Microporous Mesoporous Mater. 66 (2003) 219–227. https://doi.org/10.1016/j.micromeso.2003.09.011.

[120] Federal Register - Environmental Protection Agency, National ambient air quality standards for particulate matter, 62 (1997) 38651–38760.

[121] M. Kopperi, J. Ruiz-Jiménez, J.I. Hukkinen, M.L. Riekkola, New way to quantify multiple steroidal compounds in wastewater by comprehensive two-dimensional gas chromatography-time-of-flight mass spectrometry, Anal. Chim. Acta. 761 (2013) 217–226. https://doi.org/10.1016/j.aca.2012.11.059.

[122] Dassault Systèmes, Biovia COSMOconf 4.3, (2020). https://www.3ds.com/products-services/biovia/products/molecular-modeling-simulation/solvation-chemistry/biovia-cosmoconf/.

[123] K. Hartonen, J. Parshintsev, V.P. Vilja, H. Tiala, S. Knuuti, C.K. Lai, M.L. Riekkola, Gas chromatographic vapor pressure determination of atmospherically relevant oxidation products of β-caryophyllene and α-pinene, Atmos. Environ. 81 (2013) 330–338. https://doi.org/10.1016/j.atmosenv.2013.09.023.

[124] K. Ružicka, V. Majer, Simultaneous Treatment of Vapor Pressures and Related Thermal Data Between the Triple and Normal Boiling Temperatures for n-Alkanes C5–C20, J. Phys. Chem. Ref. Data. 23 (1994) 1–39. https://doi.org/10.1063/1.555942.

[125] B. Schröder, M. Fulem, M.A.R. Martins, Vapor pressure predictions of multi-functional oxygen-containing organic compounds with COSMO-RS, Atmos. Environ. 133 (2016) 135–144. https://doi.org/10.1016/j.atmosenv.2016.03.036.

[126] T. Kurtén, N. Hyttinen, E. Louise D'Ambro, J. Thornton, N.L. Prisle, Estimating the saturation vapor pressures of isoprene oxidation products C5H12O6 and C5H10O6 using COSMO-RS, Atmos. Chem. Phys. 18 (2018) 17589–17600. https://doi.org/10.5194/acp-18-17589-2018.

[127] V.P.P.S. Pragadheesh, A. Yadav, C.S. Chanotiya, P.K. Rout, G.C. Uniyal, Monitoring the emission of volatile organic compounds from flowers of Jasminum sambac using solid-phase micro-extraction fibers and gas chromatography with mass spectrometry detection, Nat. Prod. Commun. 6 (2011) 1333–1338. https://doi.org/10.1177/1934578x1100600929.

[128] I. Mokbel, A. Razzouk, T. Sawaya, J. Jose, Experimental vapor pressures of 2-phenylethylamine, benzylamine, triethylamine, and cis-2,6-dimethylpiperidine in the range between 0.2 Pa and 75kPa, J. Chem. Eng. Data. 54 (2009) 819–822. https://doi.org/10.1021/je800603z.

[129] C.L. Yaws, Handbook of Vapor Pressure. Vol 2: C5-C7 Compounds., Gulf Pub Co, Houston,TX, 1994.

[130] A.R.R.P. Almeida, M.J.S. Monte, Thermodynamic study of phase transitions of imidazoles and 1-methylimidazoles, J. Chem. Thermodyn. 44 (2012) 163–168. https://doi.org/10.1016/j.jct.2011.08.017.

[131] S. Warycha, J.H. Rytting, Vapor pressure studies of pyridine, picolines and 2,6-lutidine in isooctane, J. Solution Chem. 13 (1984) 589–598. https://doi.org/10.1007/BF00647227.

[132] T.E. Daubert, R.P. Danner, Physical and Thermodynamic Properties of Pure Chemicals (Data Compilation), Hemisphere Publishing Corporation, New York, 1989.

[133] F.C. Wu, R.L. Tseng, R.S. Juang, Characteristics of Elovich equation used for the analysis of adsorption kinetics in dye-chitosan systems, Chem. Eng. J. 150 (2009) 366–373. https://doi.org/10.1016/j.cej.2009.01.014.

[134] N. Yeddou, A. Bensmaili, Kinetic models for the sorption of dye from aqueous solution by clay-wood sawdust mixture, Desalination. 185 (2005) 499–508. https://doi.org/10.1016/j.desal.2005.04.053.

[135] I. Singh, R.K. Bedi, Studies and correlation among the structural, electrical and gas response properties of aerosol spray deposited self assembled

nanocrystalline CuO, Appl. Surf. Sci. 257 (2011) 7592–7599. https://doi.org/10.1016/j.apsusc.2011.03.133.

[136] C.W. Cheung, J.F. Porter, G. McKay, Sorption kinetics for the removal of copper and zinc from effluents using bone char, Sep. Purif. Technol. 19 (2000) 55–64. https://doi.org/10.1016/S1383-5866(99)00073-8.

[137] R. Absi, Concentration profiles for fine and coarse sediments suspended by waves over ripples: An analytical study with the 1-DV gradient diffusion model, Adv. Water Resour. 33 (2010) 411–418. https://doi.org/10.1016/j.advwatres.2010.01.006.

[138] G. Guiochon, A. Felinger, D.G. Shirazi, Fundamentals of Preparative and Nonlinear Chromatography, Academic Press, Boston, 2006.

[139] V.J. Inglezakis, S.G. Poulopoulos, H. Kazemian, Insights into the S-shaped sorption isotherms and their dimensionless forms, Microporous Mesoporous Mater. 272 (2018) 166–176. https://doi.org/10.1016/j.micromeso.2018.06.026.

[140] M.A. Al-Ghouti, D.A. Da'ana, Guidelines for the use and interpretation of adsorption isotherm models: A review, J. Hazard. Mater. 393 (2020) 122383. https://doi.org/10.1016/j.jhazmat.2020.122383.

[141] S.C. Tsai, T.H. Wang, Y.Y. Wei, W.C. Yeh, Y.L. Jan, S.P. Teng, Kinetics of Cs adsorption/desorption on granite by a pseudo first order reaction model, J. Radioanal. Nucl. Chem. 275 (2008) 555–562. https://doi.org/10.1007/s10967-007-7045-y.

[142] Z. Chang, L. Zeng, C. Sun, P. Zhao, J. Wang, L. Zhang, Y. Zhu, X. Qi, Adsorptive recovery of precious metals from aqueous solution using nanomaterials – A critical review, Coord. Chem. Rev. 445 (2021) 214072. https://doi.org/10.1016/j.ccr.2021.214072.

[143] X.S. Zhao, G.Q. Lu, A.K. Whittaker, G.J. Millar, H.Y. Zhu, Comprehensive study of surface chemistry of MCM-41 using 29Si CP/MAS NMR, FTIR, pyridine-TPD, and TGA, J. Phys. Chem. B. 101 (1997) 6525–6531. https://doi.org/10.1021/jp971366+.

[144] C.H. Nguyen, C.C. Fu, Z.H. Chen, T.T. Van Tran, S.H. Liu, R.S. Juang, Enhanced and selective adsorption of urea and creatinine on amine-functionalized mesoporous silica SBA-15 via hydrogen bonding, Microporous Mesoporous Mater. 311 (2021) 110733. https://doi.org/10.1016/j.micromeso.2020.110733.

[145] W.G. Cook, R.A. Ross, Heterogeneous Interactions of Methylamines on porous Adsorbents Part II. Interactions on Silica–Alumina and Silica Gel Surfaces of Di- and Tri-methylamine in the Region of their Boiling Points, Can. J. Chem. 50 (1972) 2451–2456. https://doi.org/10.1139/v72-395.

[146] Y.J. Jin, T. Aoki, G. Kwak, Control of Intramolecular Hydrogen Bonding in a Conformation-Switchable Helical-Spring Polymer by Solvent and Temperature, Angew. Chemie - Int. Ed. 59 (2020) 1837–1844. https://doi.org/10.1002/anie.201910269.

[147] A.S. Özen, F. De Proft, V. Aviyente, P. Geerlings, Interpretation of hydrogen bonding in the weak and strong regions using conceptual DFT descriptors, J. Phys. Chem. A. 110 (2006) 5860–5868. https://doi.org/10.1021/jp0568374.

[148] X. Cao, R.J. Hamers, Silicon surfaces as electron acceptors: Dative bonding of amines with Si(001) and Si(111) surfaces, J. Am. Chem. Soc. 123 (2001) 10988–10996. https://doi.org/10.1021/ja0100322.

[149] S.T. Pham, M.B. Nguyen, G.H. Le, T.D. Nguyen, C.D. Pham, T.S. Le, T.A. Vu, Influence of Brønsted and Lewis acidity of the modified Al-MCM-41 solid acid on cellulose conversion and 5-hydroxylmethylfurfuran selectivity, Chemosphere. 265 (2021). https://doi.org/10.1016/j.chemosphere.2020.129062.

[150] W. Guo, E.J.M. Hensen, W. Qi, H.J. Heeres, J. Yue, Titanium Phosphate Grafted on Mesoporous SBA-15 Silica as a Solid Acid Catalyst for the Synthesis of 5-Hydroxymethylfurfural from Glucose, ACS Sustain. Chem. Eng. 10 (2022) 10157–10168. https://doi.org/10.1021/acssuschemeng.2c01394.

[151] S. Liu, X.Y. Meng, J.M. Perez-Aguilar, R. Zhou, An in Silico study of TiO2 nanoparticles interaction with twenty standard amino acids in aqueous solution, Sci. Rep. 6 (2016). https://doi.org/10.1038/srep37761.

[152] Z. jie Tang, X. Hu, Y. jun Chen, J. qin Qiao, H. zhen Lian, Assessment of in vitro inhalation bioaccessibility of airborne particle–bound potentially toxic elements collected using quartz and PTFE filter, Atmos. Environ. 196 (2019) 118–124. https://doi.org/10.1016/j.atmosenv.2018.09.045.

[153] X. Hou, P.T. Deem, K.L. Choy, Hydrophobicity study of polytetrafluoroethylene nanocomposite films, Thin Solid Films. 520 (2012) 4916–4920. https://doi.org/10.1016/j.tsf.2012.02.074.

[154] G.E. Parsons, G. Buckton, S.M. Chatham B ', The use of surface energy and polarity determinations to predict physical stability of non-polar, non-aqueous suspensions, 1992.

[155] J. Parshintsev, J. Ruiz-Jimenez, T. Petäjä, K. Hartonen, M. Kulmala, M.L. Riekkola, Comparison of quartz and Teflon filters for simultaneous collection of size-separated ultrafine aerosol particles and gas-phase zero samples, Anal. Bioanal. Chem. 400 (2011) 3527–3535. https://doi.org/10.1007/s00216-011-5041-0.

[156] A. Galarneau, J. Iapichella, D. Brunel, F. Fajula, Z. Bayram-Hahn, K. Unger, G. Puy, C. Demesmay, J.L. Rocca, Spherical ordered mesoporous silicas and silica monoliths as stationary phases for liquid chromatography, J. Sep. Sci. 29 (2006) 844–855. https://doi.org/10.1002/jssc.200500511.

[157] G. Ballerini, K. Ogle, M.G. Barthés-Labrousse, The acid-base properties of the surface of native zinc oxide layers: An XPS study of adsorption of 1,2-diaminoethane, Appl. Surf. Sci. 253 (2007) 6860–6867. https://doi.org/10.1016/j.apsusc.2007.01.126.

[158] P. Houeto, J.R. Hoffman, P. Got, B. Dang Vu, F.J. Band, Acetonitrile as a possible marker of current cigarette smoking, Hum. Exp. Toxicol. 16 (1997) 658–661. https://doi.org/https://doi.org/10.1177/096032719701601105.

[159] M. Hemmilä, H. Hellén, A. Virkkula, U. Makkonen, A.P. Praplan, J. Kontkanen, L. Ahonen, M. Kulmala, H. Hakola, Amines in boreal forest air at SMEAR II station in Finland, Atmos. Chem. Phys. 18 (2018) 6367–6380. https://doi.org/10.5194/acp-18-6367-2018.

[160] Y. You, V.P. Kanawade, J.A. De Gouw, A.B. Guenther, S. Madronich, M.R. Sierra-Hernández, M. Lawler, J.N. Smith, S. Takahama, G. Ruggeri, A. Koss, K. Olson, K. Baumann, R.J. Weber, A. Nenes, H. Guo, E.S. Edgerton, L. Porcelli, W.H. Brune, A.H. Goldstein, S.H. Lee, Atmospheric amines and ammonia measured with a chemical ionization mass spectrometer (CIMS), Atmos. Chem. Phys. 14 (2014) 12181–12194. https://doi.org/10.5194/acp-14-12181-2014.

[161] A. Kieloaho, Alkyl Amines in Boreal Forest and Urban Area, University of

Helsinki, 2017. http://hdl.handle.net/10138/173284.

[162] D.S. Kosyakov, N. V. Ul'yanovskii, T.B. Latkin, S.A. Pokryshkin, V.R. Berzhonskis, O. V. Polyakova, A.T. Lebedev, Peat burning – An important source of pyridines in the earth atmosphere, Environ. Pollut. 266 (2020) 115109. https://doi.org/10.1016/j.envpol.2020.115109.

[163] Y. Ma, M.D. Hays, Thermal extraction-two-dimensional gas chromatography-mass spectrometry with heart-cutting for nitrogen heterocyclics in biomass burning aerosols, J. Chromatogr. A. 1200 (2008) 228–234. https://doi.org/10.1016/j.chroma.2008.05.078.

[164] K. Gao, Y. Zhang, Y. Liu, M. Yang, T. Zhu, Screening of imidazoles in atmospheric aerosol particles using a hybrid targeted and untargeted method based on ultra-performance liquid chromatography-quadrupole time-of-flight mass spectrometry, Anal. Chim. Acta. 1163 (2021) 338516. https://doi.org/10.1016/j.aca.2021.338516.

[165] C.J. Kampf, A. Filippi, C. Zuth, T. Hoffmann, T. Opatz, Secondary brown carbon formation: Via the dicarbonyl imine pathway: Nitrogen heterocycle formation and synergistic effects, Phys. Chem. Chem. Phys. 18 (2016) 18353–18364. https://doi.org/10.1039/c6cp03029g.

[166] Q. Li, D. Gong, H. Wang, Y. Wang, S. Han, G. Wu, S. Deng, P. Yu, W. Wang, B. Wang, Rapid increase in atmospheric glyoxal and methylglyoxal concentrations in Lhasa, Tibetan Plateau: Potential sources and implications, Sci. Total Environ. 824 (2022) 153782. https://doi.org/10.1016/j.scitotenv.2022.153782.

[167] P. Bonasoni, P. Laj, A. Marinoni, M. Sprenger, F. Angelini, J. Arduini, U. Bonafè, F. Calzolari, T. Colombo, S. Decesari, C. Di Biagio, A.G. Di Sarra, F. Evangelisti, R. Duchi, M.C. Facchini, S. Fuzzi, G.P. Gobbi, M. Maione, A. Panday, F. Roccato, K. Sellegri, H. Venzac, G.P. Verza, P. Villani, E. Vuillermoz, P. Cristofanelli, Atmospheric Brown Clouds in the Himalayas: First two years of continuous observations at the Nepal Climate Observatory-Pyramid (5079 m), Atmos. Chem. Phys. 10 (2010) 7515–7531. https://doi.org/10.5194/acp-10-7515-2010.

[168] K. Sandeep, A.S. Panicker, A.S. Gautam, G. Beig, N. Gandhi, S. Sanjeev, R. Shankar, H.C. Nainwal, Black carbon over a high altitude Central Himalayan Glacier: Variability, transport, and radiative impacts, Environ. Res. 204 (2022). https://doi.org/10.1016/j.envres.2021.112017.

[169] X.L. Pan, Y. Kanaya, Z.F. Wang, Y. Liu, P. Pochanart, H. Akimoto, Y.L. Sun, H.B. Dong, J. Li, H. Irie, M. Takigawa, Correlation of black carbon aerosol and carbon monoxide in the high-altitude environment of Mt. Huang in Eastern China, Atmos. Chem. Phys. 11 (2011) 9735–9747. https://doi.org/10.5194/acp-11-9735-2011.